# THE ROLE OF B1 METHYLATION, PHYSIOLOGIC REPLICATION INDEPENDENT ENDOGENOUS DNA DOUBLE STRAND BREAKS (PHY-RIND-EDSB) AND LAMININ 511 E8 PROTEINS IN RAT SECOND DEGREE BURN WOUND HEALING

Mr. Jiraroch Meevassana

จุฬาลงกรณ์มหาวิทยาลัย
CHULALONGKORN UNIVERSITY

A Dissertation Submitted in Partial Fulfillment of the Requirements
for the Degree of Doctor of Philosophy in Biomedical Sciences and
Biotechnology
FACULTY OF MEDICINE
Chulalongkorn University
Academic Year 2022
Copyright of Chulalongkorn University

บทบาทของบีวันเมทิลเลชั่น, การฉีกขาดของดีเอ็นเอสายคู่ที่เกิดขึ้นเองและโปรตีนส่วนอีแปดของ
โปรตีนลามินินห้าหนึ่งหนึ่งต่อการหายของแผลที่เกิดจากความร้อนลึกระดับที่สองในหนูทดลอง

นายจิระโรจน์ มีวาสนา

Thesis Title	THE ROLE OF B1 METHYLATION, PHYSIOLOGIC REPLICATION INDEPENDENT ENDOGENOUS DNA DOUBLE STRAND BREAKS (PHY-RIND-EDSB) AND LAMININ 511 E8 PROTEINS IN RAT SECOND DEGREE BURN WOUND HEALING
By	Mr. Jiraroch Meevassana
Field of Study	Biomedical Sciences and Biotechnology
Thesis Advisor	Professor Dr. APIWAT MUTIRANGURA
Thesis Co Advisor	Professor APICHAI ANGSPATT, M.D.
	Dr. Kevin J Hamill
	Dr. Carl Sheridan

Accepted by the FACULTY OF MEDICINE, Chulalongkorn University in Partial Fulfillment of the Requirement for the Doctor of Philosophy

--- Dean of the FACULTY OF MEDICINE

(Associate Professor CHANCHAI SITTIPUNT, M.D.)

DISSERTATION COMMITTEE

--- Chairman

(Professor Dr. SITHIPORN AGTHONG)

--- Thesis Advisor

(Professor Dr. APIWAT MUTIRANGURA)

--- Thesis Co-Advisor

(Professor APICHAI ANGSPATT, M.D.)

--- Thesis Co-Advisor

(Dr. Kevin J Hamill)

--- Thesis Co-Advisor

(Dr. Carl Sheridan)

--- Examiner

(Assistant Professor Dr. AMORNPUN SEREEMASPUN)

--- Examiner

(Professor PITHI CHANVORACHOTE, Ph.D.)

--- External Examiner

(Associate Professor Dr. Uraiwan Panich)

จิระโรจน์ มีวาสนา : บทบาทของบีวันเมทิลเลชั่น, การฉีกขาดของดีเอ็นเอสายคู่ที่เกิดขึ้นเองและโปรตีนส่วนอีแปดของ
โปรตีนลามินินห้าหนึ่งหนึ่งต่อการหายของแผลที่เกิดจากความร้อนลึกระดับที่สองในหนูทดลอง . (THE ROLE
OF B1 METHYLATION, PHYSIOLOGIC REPLICATION INDEPENDENT
ENDOGENOUS DNA DOUBLE STRAND BREAKS (PHY-RIND-EDSB)
AND LAMININ 511 E8 PROTEINS IN RAT SECOND DEGREE BURN
WOUND HEALING) อ.ที่ปรึกษาหลัก : ศ.ดร. นพ.อภิวัฒน์ มุทิรางกูร, อ.ที่ปรึกษาร่วม : ศ. นพ.อภิชัย อังส
พัทธ์,ดร.เควิน เจ แฮมิล,ดร.คาร์ล เชอริแดน

ความเป็นมา: ภาวะเหนือพันธุกรรม เมทิลเลชัน ของ DNA ผ่านองค์ประกอบดีเอ็นเอแบบกระจายสั้น (SINE) การ
สายอาร์เอ็นเอขนาดเล็ก siRNA สามารถช่วยป้องกันความเสียหายของดีเอ็นเอและส่งเสริมการเพิ่มจำนวนเซลล์ผิวหนัง นอกจากนี้ ลา
มินิน 511 (LM511) เป็นโปรตีนโครงสร้างภายนอกเซลล์ที่สามารถรองรับการยึดเกาะและการเคลื่อนที่ของเซลล์เยื่อบุผิว นอกจากนี้
โปรตีน ส่วน A ของโปรตีน HMGB1 ซึ่งเป็นส่วนประกอบของกลุ่มของโปรตีนที่ไม่ใช่ฮิสโตน ที่สามารถลดการตอบสนองความ
เสียหายของ DNA ต่อการบาดเจ็บจากการไหม้ ดังนั้น SINE siRNA, LM511 และ Box A ของ HMGB1 อาจสามารถ
ส่งเสริมการสมานแผลไหม้ได้

วัตถุประสงค์: เพื่อตรวจสอบว่าการรักษาแผลไฟไหม้โดยใช้ B1 siRNA, LM511 และ Box A ของ HMGB1
สามารถส่งเสริมการหายของแผลในแบบจำลองแผลไหม้ระดับที่สองในหนูทดลองหนู

วิธีการ: การศึกษาเชิงวิเคราะห์แบบตัดขวาง โดยใช้ตัวอย่างเนื้อเยื่อและเลือดจากผู้ป่วยไฟไหม้ 23 ราย เพื่อวัดระดับและ
รูปแบบของ อะลูเมทิลเลชัน ในการทดลองในสัตว์ทดลอง ได้มีการสร้างบาดแผลไฟไหม้ระดับที่สองที่หลังหนู จากนั้นหนูถูกแบ่งออกเป็น
กลุ่มควบคุมและกลุ่มทดลอง: ที่ได้รับสารทดลองด้วย B1 siRNA, LM511 และ Box A ของ HMGB1, กลุ่มควบคุมที่
ได้รับน้ำเกลือ และกลุ่มควบคุมที่ได้รับแคลเซียม ฟอสเฟต-อนุภาคนาโน (n = 15–20/กลุ่ม) ภาพบาดแผลในวันที่ 0, 7, 14, 21
และ 28 หลังการบาดเจ็บ ส่วนของเนื้อเยื่อได้รับการประมวลผลสำหรับการตรวจเมทิลเลชันและการตรวจเนื้อเยื่อวิทยาและอิมมูโนฮิสโต
เคมีและให้คะแนนโดยอิงจากการแสดงออกของฮิสโตน H2AX ฟอสโฟรีเลตบนซีรีน 139 (γH2AX), 8-ไฮดรอกซี-2′-ดีออก
ซีกัวโนซีน (8-OHdG) และการมีอยู่ของไซโตเคราติน 10 และ 14

ผลลัพธ์: ระดับ Alu methylation ในเนื้อเยื่อแผลเป็น ต่ำกว่าในผิวหนังปกติ (29.4 ± 2.5% เทียบกับ 35.6
± 3.2%, P = 0.0002) การหายของแผลไหม้ดีขึ้นในกลุ่มที่ได้รับ B1 siRNA เมื่อเทียบกับกลุ่มควบคุม (P < 0.001)
คะแนนทางพยาธิวิทยาโดยรวมและระดับของ B1 methylation ในกลุ่มที่ได้รับ B1 siRNA ดีขึ้นในวันที่ 14–28 วันหลังการ
บาดเจ็บ (P < 0.01) การย้อมสีอิมมูโนฮิสโตเคมีคอลเผยให้เห็นการแสดงออกที่ต่ำกว่าของ γH2AX และ 8-OHdG ในกลุ่มที่
ได้รับการรักษาด้วย B1 siRNA มากกว่าในกลุ่มควบคุมในวันที่ 14–28 หลังการบาดเจ็บ กล่อง A ของกลุ่มโปรตีน HMGB1
แสดงให้เห็นถึงอัตราการปิดบาดแผลที่เพิ่มขึ้นอย่างมีนัยสำคัญ โดยเริ่มตั้งแต่วันที่ 7 ถึงวันที่ 28 หลังจากได้รับบาดเจ็บ (P < 0.001)
นอกจากนี้ การแสดงออกของ γH2AX และ 8-OHdG ในกลุ่มที่บำบัดด้วยพลาสมิด HMGB1 นั้นต่ำกว่าในกลุ่มควบคุมตั้งแต่
วันที่ 7 ถึงวันที่ 21 (P < 0.05) การหายของแผลไฟไหม้ในกลุ่มที่บำบัดด้วย LM511-E8 นั้นเร็วกว่ากลุ่มควบคุมที่ 7–28 วัน
หลังการบาดเจ็บ (P < 0.001) คะแนนทางพยาธิวิทยาโดรวมของกลุ่มที่ได้รับการรักษาด้วย LM511-E8 นั้นสูงกว่าคะแนนของ
กลุ่มควบคุม

สาขาวิชา	ชีวเวชศาสตร์และชีวเทคโนโลยี	ลายมือชื่อนิสิต ....
ปีการศึกษา	2565	ลายมือชื่อ อ.ที่ปรึกษาหลัก ....
		ลายมือชื่อ อ.ที่ปรึกษาร่วม ....
		ลายมือชื่อ อ.ที่ปรึกษาร่วม ....

6074858030 : MAJOR BIOMEDICAL SCIENCES AND BIOTECHNOLOGY
KEYWORD: Second-degree burn, B1 siRNA, wound healing, B1 methylation, RNA-directed DNA methylation, LM511-E8, Box A of HMGB1 protein

Jiraroch Meevassana : THE ROLE OF B1 METHYLATION, PHYSIOLOGIC REPLICATION INDEPENDENT ENDOGENOUS DNA DOUBLE STRAND BREAKS (PHY-RIND-EDSB) AND LAMININ 511 E8 PROTEINS IN RAT SECOND DEGREE BURN WOUND HEALING. Advisor: Prof. Dr. APIWAT MUTIRANGURA Co-advisor: Prof. APICHAI ANGSPATT, M.D.,Dr. Kevin J Hamill,Dr. Carl Sheridan

Background: DNA methylation via short interspersed nuclear element (SINE) small interfering (si)RNA prevents DNA damage and promotes cell proliferation. Furthermore, laminin α5 β1 γ1(LM511) is an extracellular structural protein that can support epithelial cell adhesion and migration. Box A of high-mobility group box 1 protein (Box A of HMGB1) is a common nuclear protein in eukaryotic cells that can reduce DNA damage response toward burn injury.

Objective: To investigate whether treatment of burn wounds using B1 siRNA, Box A of HMGB1 and LM511-E8 fragment improved wound closure in a rat second-degree burn wound model.

Methods: I performed a cross-sectional analytical study using tissue and blood samples from post-burn and healthy patients (n = 23 each) to measure Alu methylation levels and patterns. In *in vivo* experiments, second-degree burn wounds were introduced on the backs of rats. The rats were then divided into control and experiment groups: a B1 siRNA-treated, Box A of HMGB1 protein and LM511-E8, saline-treated control, and calcium phosphate-nanoparticle-treated control group (n = 15–20/group). The wounds were imaged on days 0, 7, 14, 21, and 28 post-injuries. The tissue sections were processed for methylation and histological and immunohistochemical examination and scored based on the overall expression of histone H2AX phosphorylated on serine 139 (γH2AX), 8-hydroxy-2′-deoxyguanosine (8-OHdG), and presence of cytokeratin 10 and 14.

Results: Alu methylation levels were lower in hypertrophic scar tissues than in normal skin (29.4 ± 2.5% vs. 35.6± 3.2%, P = 0.0002). Burn wound closure improved in the B1 siRNA-treated group compared to that in the control group, especially from days 14 to 28 post-injury (P < 0.001). The overall pathological score and degree of B1 methylation in the B1 siRNA-treated group improved at days 14–28 days post-injury. The Box A of HMGB1 protein group demonstrated improvement in burn wound closure, starting from day 7th until day 28th after injury (P < 0.001). Furthermore, γH2AX and 8-OHdG expression in the HMGB1 plasmid-treated group was lower than that in the control group (P < 0.05). The re-epithelialisation in the LM511-E8-treated group was quicker than that of the control group at 7–28 days post-injury, with the largest improvement observed on days 7 and 14 (P < 0.001). The pathological score of the LM511-E8-treated group was higher than that of the control group at 14–28 days post-injury.

Conclusion: These results imply that LM511-E8 fragment, B1 siRNA, and Box A of High-mobility group box 1 protein (Box A of HMGB1) are promising therapeutic options for managing second-degree burns.

Field of Study:	Biomedical Sciences and Biotechnology	Student's Signature ....
Academic Year:	2022	Advisor's Signature ....
		Co-advisor's Signature ....
		Co-advisor's Signature ....

ACKNOWLEDGEMENTS

TABLE OF CONTENTS

Page

LIST OF TABLES

LIST OF FIGURES

จุฬาลงกรณ์มหาวิทยาลัย
CHULALONGKORN UNIVERSITY

Chapter 1. INTRODUCTION

Problem description

One of the most common causes of unintentional injuries and deaths is burn trauma. According to reports from the American Burn Association, more than 450,000 cases of burns require medical intervention in the United States every year. (H. Kim, Shin, & Han, 2022; Toussaint & Singer, 2014) In South Asia, the yearly incidence of burn injuries is estimated to be between 100,000 and 1,000,000. (Golshan, Patel, & Hyder, 2013) Major burn injuries are physically disabling traumas that can lead to serious morbidity and mortality. Burn wound infection, impaired wound healing, and keloid and hypertrophic scar complications remain major challenges in burn research. (Y. Wang et al., 2018)

Burn wounds are very difficult to heal. When high temperatures are directly applied to cells, proteins denature and DNA may be damaged, leading to genetic changes and/or the death of the cells and tissues. (Dos Santos-Silva, Trajano, Schanuel, & Monte-Alto-Costa, 2017) The contact of skin and tissue to heat increases matrix metalloproteinase, decreases type I procollagen, increases neo-angiogenesis, and results in the accumulation of inflammatory cells and DNA oxidative stress. (Shin et al., 2008) Heat stress not only halts DNA repair systems but also acts as a DNA-damaging agent. It is known that heat stress causes the accumulation of 8-hydroxy-2′-deoxyguanosine (8-OHdG), deaminated cytosine, and apurinic DNA sites (AP-sites) in cells. (Bruskov, Malakhova, Masalimov, & Chernikov, 2002) Other factors, such as an increase in free radicals and genomic instability, can impair wound healing. Moreover,

the increase in p53 and p21 protein levels due to heat can arrest the cell cycle (Fig. 1). (Nitta, Okamura, Aizawa, & Yamaizumi, 1997; Beomseok Son et al., 2019; Velichko, Petrova, Razin, & Kantidze, 2015) Oxidative stress caused by reactive oxygen species (ROS) is a crucial mechanism that accounts for local and remote pathophysiological processes during burns, causing lipid peroxidation, double-strand DNA breaks (DSBs), single-strand DNA breaks (SSBs), and apoptosis. (da Silva, Quintana, Bortolin, Ribeiro, & de Oliveira, 2015; Karni, Zidon, Polak, Zalevsky, & Shefi, 2013) Preventing DNA damage and genomic instability could speed wound maturation, improve scar quality, and decrease wound contraction. (Despa, Orgill, Neuwalder, & Lee, 2005; Purschke, Laubach, Anderson, & Manstein, 2010; Steinstraesser et al., 2001) Genomic instability has the worst effect on wound healing because it is a precursor to mutation, leading to cellular ageing and cell death. Therefore, the maintenance of genome stability is crucial for the survival and proper functioning of cells. Understanding the mechanisms underlying the maintenance of cell genome stability is critical. (Ermolaeva & Schumacher, 2014; Tubbs & Nussenzweig, 2017)

In 1983, McClintock received the Nobel Prize for the discovery of retrotransposons. At the time, transposons were described as useless and junk DNA because they are not transcribed and can move from one place to another in the DNA. In contrast, in recent years, many studies have reported their functions and benefits, such as gene regulation and chromatin organisation. Interspersed repetitive sequences are the main contributors to the genome (45%). (Natalia A. Veniaminova, Nikita S. Vassetzky, & Dmitri A. Kramerov, 2007) Consequently, the depletion of interspersed repetitive sequence (IRS) methylation was assumed to be the main cause of global hypomethylation. IRS comprises long interspersed elements (LINEs), short

2

interspersed elements (SINEs), long terminal repeat (LTR)-retrotransposons, and transposons. Alu is a SINE that is present in abundance in humans, equivalent to B1 in rats and rodents. Global hypomethylation during senescence is associated with the demethylation of repetitive DNA elements. (Barbot, Dupressoir, Lazar, & Heidmann, 2002; Mays-Hoopes, Brown, & Huang, 1983) DNA methyltransferases (DNMTs), responsible for the allocation of a methyl group from the general methyl donor to the 5-position of cytosine remains in DNA, are crucial for methylation processes. Recently, an experimental study reported an association between age and Alu hypomethylation; nevertheless, this association was not found in LINE1 hypomethylation. (Bollati et al., 2009) Moreover, positive associations were observed between Alu hypomethylation in blood cells and many ageing symptoms. The involvement of DNA methylation in the wound repair process was demonstrated in a rodent wound healing model. A large reduction in the wound area was accompanied by an increase in the expression levels of DNA methyltransferases 3a (Dnmt3a), suggesting that DNA methylation is an important molecular signalling process related to wound healing and that an increase in Dnmt3a levels could be related to the competence of the wound healing process. (Gomes et al., 2016) There is evidence that DNMT1 and DNMT3B levels were significantly increased through corneal epithelial healing, after global DNA hypermethylation. Moreover, decreased DNMT1 and genomic hypomethylation levels intensely delayed corneal epithelial wound healing and blocked human corneal epithelial cell proliferation and migration. (Luo et al., 2019)
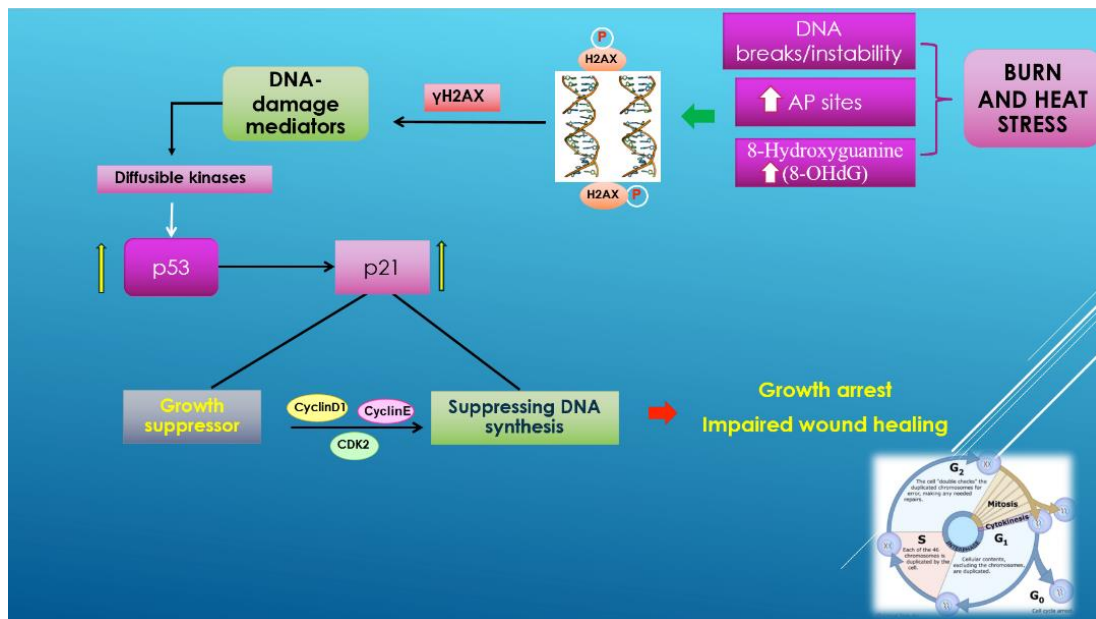
Figure 1. Mechanism of burn and heat stress that suppresses cell cycle and wound healing (Son et al., 2019a)

As a result, in this study, I focused on the role of B1 methylation in genomic instability and wound healing. I address the question of how to restore B1 methylation to reduce genomic instability and improve the rate and quality of wound healing and epithelialisation. It has recently been demonstrated that synthetic and expressed short interfering RNAs (siRNAs) and short hairpin RNAs (shRNAs), known as RNA-directed DNA methylation (RdDM), were able to generate DNA methylation in human cells. (Castanotto et al., 2005; Mathieu & Bender, 2004; M. A. Matzke & R. A. Mosher, 2014) Consequently, if we can identify the method to avoid loss of B1 methylation through the RdDM function, it may be possible to avoid genomic instability and improve wound healing.

Another noteworthy molecular mechanism underlying genomic instability is DNA DSBs and DSB repair. In non-replicative cells, there are two distinct types of endogenous DNA double strand breaks (EDSBs). The first type is pathologic DNA

lesions, pathologic-EDSBs. Pathologic-EDSBs, like replication or irradiation-induced DSBs, cause mutations and can lead to cell death. These EDSBs are quickly repaired and are detectable directly only when the DSB repair process is inhibited. (Kongruttanachok et al., 2010) Whereas the other, physiologic-EDSBs, without DSB repair inhibition, are detectable in yeast and all human cell types, are not related to γH2AX (histone H2AX phosphorylated at serine 139) and are retained in heterochromatin. Physiologic-EDSBs are located non-randomly. Most physiologic-EDSBs reside within hypermethylated genomes and occur right after an "ACGT" sequence. (Pongpanich, Patchsung, Thongsroy, & Mutirangura, 2014) They could be discovered in the G0 phase of the cell cycle, which is also known as the resting state. They have been termed Physiologic-Replication-Independent Endogenous DNA Double-Strand Breaks (PHY-RIND-EDSB).

Furthermore, re-epithelisation and angiogenesis play a crucial role in wound healing. (Pastar et al., 2014) Keratinocytes, the main cellular element of the epidermis, are not only essential as a barrier but also play an important role in regeneration after injury via epithelialisation. Laminins and associated extracellular matrix units play a crucial role in cell and tissue remodelling; moreover, during wound repair, laminins are a crucial component in re-epithelialisation and neovascularisation. (Iorio, Troughton, & Hamill, 2015a) Prolonged epithelialisation precipitates hypertrophic scar formation and leads to scar contracture and nerve compression. (van der Veer et al., 2009)

Considering the mechanisms by which molecules and proteins affect cell functions in various situations, this study aimed to develop a solid foundation to help establish new policies to improve wound healing or to treat burns and difficult-to-heal wounds.

Aims

To improve burn wound healing and ameliorate burn wound repair and epithelialisation to decrease the length of stay, scar complications, and improve quality of life.

Flow chart of experiment design and conceptual framework

The experimental plan was divided into three parts and three substances: Laminin511 E8 fragment protein, B1siRNA, and Box A of HMGB1 protein. B1 hypermethylation or an increase in the expression of Box A of the HMGB1 protein can reduce DNA damage and increase genomic stability, whereas laminin 511 E8 can improve burn wound healing and epithelialisation.

Figure 2. Flowchart of experiment design and conceptual framework

Does B1 methylation prevent genomic instability, improve cell proliferation and wound healing in second degree burn wound in rat?

Hypothesis: B1 methylation prevents genomic instability and improve cell proliferation and wound healing

To measure rate of rat burn wound healing and endogenous DNA damage markers levels in rat burn skin transfected with B1 siRNA, calculate wound contraction rate

Wound area and DNA damage markers levels are decreased in B1-siRNA treated cell

Wound area and DNA damage markers levels are increased in siRNA-B1 treated cell

Wound area and DNA damage markers levels are not changed in siRNA-B1 treated cell

The hypothesis is supported

Figure 3. Does B1 methylation prevent genomic instability and improve cell proliferation and wound healing in rat burn wound or rat cells?

Does B1-siRNA increase B1 methylation level in second degree burn wound in rat?

Hypothesis: B1-siRNA increases B1 methylation level in second degree burn wound in rat.

To measure B1 methylation level in rat burn treat with B1-siRNA in COBRA assay

B1 methylation levels are increased B1-siRNA treated group

B1 methylation levels are decreased siRNA-B1 treated cell

B1 methylation levels are not changed in siRNA-B1 treated cell

The hypothesis is supported

Figure 4. Does siRNA-B1 increase B1 methylation levels in treated second-degree burn wound in rats?

How are levels of RIND-EDSB in second degree burn wound in rat and do they correlate with genomic instability and improved wound healing?

Hypothesis: The levels of RIND-EDSB change and correlate with the healing of second degree burns

To quantify RIND-EDSBs in rat burn wound using EDSB PCR and wound contraction rate

Wound healing rate and levels of RIND-EDSB are increased, DNA damage markers levels are decreased in rat burn wound

The levels of RIND-EDSB are not changed in rat burn wound

The hypothesis is supported

Figure 5. How are levels of PHY-RIND-EDSB in rat burn wound related to genomic instability and improving wound healing?

Does Laminin 511 E 8 fragments protein improve healing rate of second degree burn wound?

Hypothesis: Laminin 511 E 8 fragments protein can improve healing rate of second degree burn wound in rat.

To measure wound healing rate and epithelialization rate in rat burn wound using pathological and immunohistochemistry.

The wound healing rate, pathological and IHC are better in rat burn wound treated group

The wound healing rate, pathological and IHC are decreased or not changed in rat burn wound treated group

The hypothesis is supported

Figure 6. Does Laminin 511 E 8 fragments protein improve the rate of second-degree burn wounds in rat and rat cells?

Research questions

1. Does B1-siRNA increase B1 methylation levels in second-degree burn wounds in rats?

2. Does B1 methylation prevent genomic instability and improve cell proliferation and wound healing in second-degree burn wounds in rats?

3. How are levels of PHY-RIND-EDSB related to genomic instability and wound healing in second-degree burn wounds in rats?

4. Does Laminin 511 E 8 fragments protein improve the healing rate of second-degree burn wounds in rats?

Hypotheses

1. B1-siRNA increases B1 methylation levels in second-degree burn wounds in rats.

2. B1 methylation prevents genomic instability and improves cell proliferation and wound healing in second-degree burn wounds in rats.

3. The levels of PHY-RIND-EDSB change and are correlated with the healing of second-degree burn wounds in rats.

4. Laminin 511 E 8 fragments protein improves the healing rate of second-degree burn wounds in rats.

Objectives

1. To examine if B1-siRNA can increase B1 methylation levels.

2. To examine if B1 methylation can prevent genomic instability, improve cell proliferation, and improve wound healing in second-degree burn wounds in rats.

3. To quantify PHY-RIND-EDSB and their correlation with the healing of second-degree burn wounds in rats.

4. To examine if Laminin 511 E 8 fragments protein can improve the healing rate of second-degree burn wounds in rats.

Chapter 2. BACKGROUND AND LITERATURE REVIEW

Burn injuries cause a high mortality rate and increased complications, which are caused by many factors, such as heat, scald, electrical, radiation, and chemical burns. Burns are one of the most common major public health problems that occur around the world, and they are prevalent among every age group. According to the World Health Organisation, the estimated annual burn mortality rate in the world is 180,000 deaths. (Van Lieshout et al., 2018) The consequences of burn wound repair include inflammation, oedema, hypertrophy, and scar formation. Burn wound treatment is crucial to regenerating tissues and accelerating wound healing. Burn wounds require treatment based on the depth of injury. First and superficial second-degree burns require dressing with topical antibiotics, while deep second and third-degree burns require immediate medical treatment and/or surgery and removal of the dead tissue. Unsuitable treatment may interrupt epithelialisation, leading to wound infection and nonhealing, chronic wounds. Treatment may require prolonged hospital stays, many surgeries, dressings, and long-term follow-up.

How to approach the burn wound studies

Clinical studies

It is necessary to conduct a medical assessment and analyse patient symptoms for diagnosing a burn wound or accident, which depends on the wound evaluation and the medical history. (Cancio, 2020) During these examinations, several resuscitation procedures, immediate wound care, diagnostic laboratory tests, or physical procedures (e.g., electrocardiogram, computed tomography, blood test) may also be conducted to

evaluate the complications and consequences of burn injuries, as well as prompt interventions such as resuscitation and debridement. (Ladhani et al., 2020)

A detailed inquiry is typically required to determine the underlying incident, illness, environmental exposure, or metabolic malfunction that is responsible for the symptoms of the condition after burn injury. Patients' vital signs or fluid levels in their bodies, for example, may be measured in the case of haematological or sepsis complications. (Chen et al., 2021) Isolated blood, tissue, or urine samples could be investigated in other situations, such as shock and cardiopulmonary resuscitation. The *ex vivo* culture of tissue samples collected from affected areas may indicate a possible cause of wounds or systemic infections. As a result of these approaches, a large number of human (and animal) cell lines have been developed, and they can be used as sample models of the affected organ from which the cell or tissue was isolated, as well as to better understand the biochemical effects that cause burn progression and complications in *in vitro* experiments. Furthermore, such cell lines may be employed in burn models to identify possible novel therapeutic agents before they are produced for clinical usage as new medications and then commercialised.

Explant cells and cell lines are used in research studies

Explant cells and cell lines have resulted in valuable advancements in the fields of burns and heat stress at the molecular level, as well as a foundation for drug development programs, many of which have proven to be beneficial in the treatment of burn wounds in clinical settings: (1) these cells can be distributed among research communities, creating different teams to study the same cells and tissue samples; (2) there are few ethical considerations when starting to work with cell lines derived from

12

isolated somatic cells, whether collected through blood samples, biopsy, or surgery; (3) the toxic effects of exploratory medicine are of minor concern; and (4) specific genes can be transformed into cell lines to test for specific diseases.

Explant cells and cell lines currently used in research, as well as their limitations

Using such cell lines has various disadvantages, one of which is that the longer they are cultured after being taken from patients or donors, the more they lose their distinct pathogenicity or features. Their utility as burn models might be affected as a result of changes in their morphology. (Schneider et al., 2021) Furthermore, their practical application in pharmacology and drug discovery research findings is limited because it is impossible to draw conclusions regarding the effects of a given drug concentration on a single cell population and correlate them to the effects of the same molecule on target cells or tissues or after physiochemical modifications in the body.

Certain cells cannot be cultured and do not multiply in the laboratory setting. (Holzer et al., 2020) Human epithelial tissue and fibroblasts, for example, lose their proliferative properties *in vitro* and have a short half-life *ex vivo*, even when grown under survival-enhancing circumstances. The lack of proliferation and short half-life of the cells limit genetic manipulation. Aside from that, the two-dimensional nature of *ex vivo* cells cannot accurately represent a real wound, which has a larger expression level and more diversity.

Models based on animals

Several model systems have been established and investigated to avoid many of the limits related to the use of human cell lines or *ex vivo* cells collected from patients with particular diseases. Among the models available are those of animals, insects, nonvertebrate, and microbes. Cell lines as well as three dimensions skin model are

seldom utilised in the testing of novel medications, and animal testing is necessary to establish the wound healing cascade and the phase of wound healing to evaluate the effectiveness of a new drug. Burn wound studies may be conducted on a wide range of species, each with a different level of appropriateness for the procedure. Drug and dosage testing on people is the only conclusive way of assessing the harmful effects and efficacy of novel treatments, even though genetic variability might result in varied reactions among individuals. This diversity serves as the foundation for emerging precision medicine techniques that attempt to identify the most effective treatment for each patient. (Abdullahi, Amini-Nik, & Jeschke, 2014; Malinda, Wysocki, Koblinski, Kleinman, & Ponce, 2008; Mao, Wu, Dong, & Wu, 2016)

Current techniques in animal modelling as well as their limitations

Animal models, such as mice, rats, rabbits, and monkeys, are beneficial for studying the genetic and molecular foundation of burn wounds and the systemic reactions that result from burn injury. Their use has led to significant discoveries since such models can be used to mimic human illnesses or disorders to facilitate the investigation of their underlying processes and modulate the effects of treatment.

There are some limitations to using these animal models in research. Research using mice or other vertebrates involves highly specialised and strictly controlled animal facilities, which are expensive to operate as per local regulatory standards (requiring appropriate project- and personal-licences). Given the ethical issues associated with animal studies, there is a major focus on methods that reduce the use of animals and/or reduce their pain and suffering. Finally, there is a growing disagreement concerning whether or not some animal models are acceptable for investigating diseases

that affect humans. For example, many experimental studies presume that gene function in mice adequately represents human gene function. Although many genes, particularly those related to the immune system, are now considered to display substantial structural and functional differences between mice and humans, there are still some questions about whether this is true. This means that findings in mice may not always be an accurate reflection of the results in humans.

Burn wound treatment

Burn depth

In general, the deeper the burn, the more difficult it is to achieve appropriate therapeutic and healing outcomes. First-degree burns to the epidermis are normally painless, heal without scars, and do not require surgery. Second-degree burns penetrate the dermal layer under the skin, resulting in painful wounds. Furthermore, second-degree burns vary in severity, ranging from superficial second-degree burns, which are homogenous, moist, and hyperemic, to deep second-degree burns, which are less sensate, drier, and have less erythema. Surgery is required for third- and fourth-degree burns, which are commonly accompanied by no or minimal pain as nerve endings are destroyed (Fig. 7). (Jeschke et al., 2020)
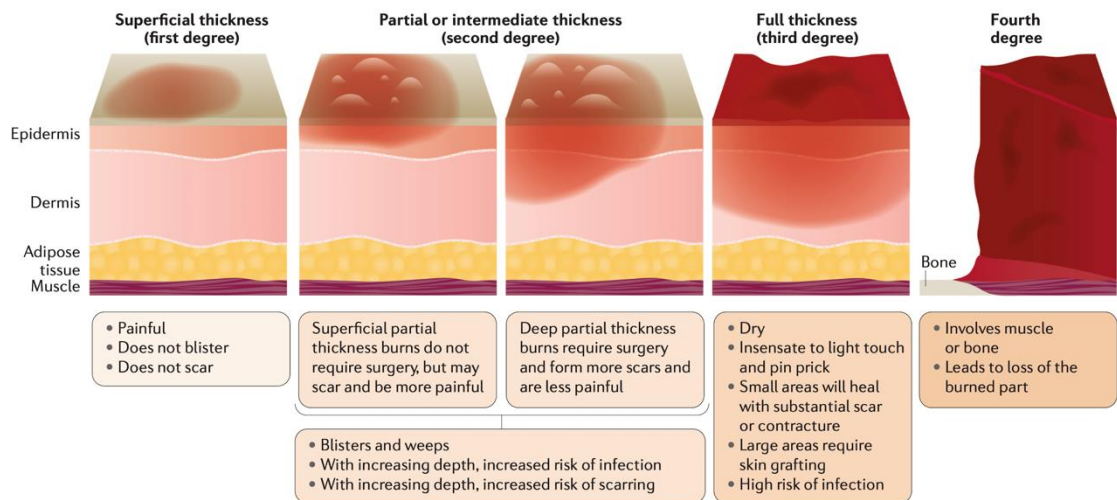
Figure 7. Depth of the burn: the depth of a burn is a significant consideration
when evaluating a patient's treatment
(Jeschke et al., 2020)

Burn area

The Lund and Browder diagram, the Rule of Palms, and the Rule of Nines seem
to be the most commonly used approaches for calculating total body surface area
(TBSA) in burn victims. (Amirsheybani et al., 2001; Murari, 2017) Studies have shown
that the burn surface area is frequently underestimated when using these three
conventional methods, particularly the first two. Studies have also revealed that there
is a large inter-rater variance in the estimation of burn area when using these techniques.
Because children's body proportions change with age, as opposed to their adult
counterparts, it is much more difficult to accurately estimate the TBSA burned in
children using these conventional methods (Fig. 8). (Wachtel, Berry, Wachtel, & Frank,
2000)
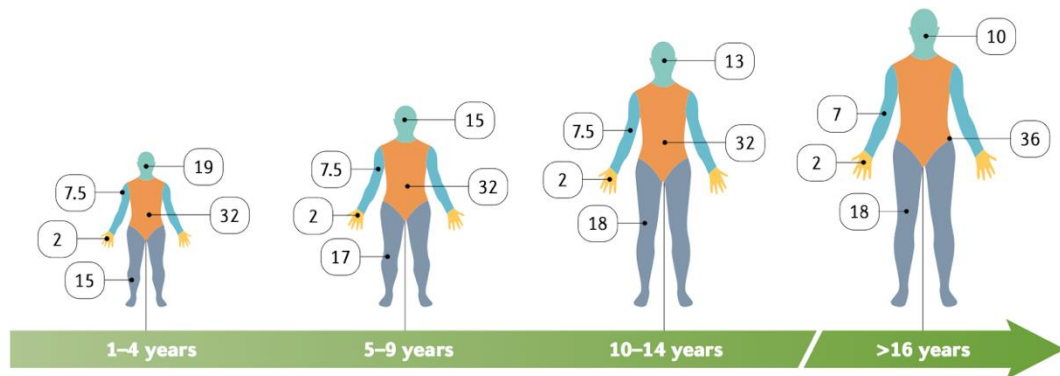
Figure 8. Burn area estimation
(Wachtel et al., 2000)

The most critical burn management decisions are based on an accurate assessment of the burn location, TBSA, and depth. The calculation of burn area is critical for estimating severity and assessing fluid resuscitation in burn patients. Most fluid resuscitation formulas used in emergency burn treatments are based on the total surface area burned. The most important factor in each resuscitation formula is an accurate estimation of the TBSA burned. In burn patients, inadequate or excessive resuscitation can result in increased complications and mortality. (Jiraroch Meevassana et al., 2022)

Phases of burn care and treatment

Burn wound healing is a complex process with many treatment phases. The first phase is a primary survey, which includes checking for airway, breathing, and circulation after injury, calculating the percent burn area, and beginning fluid resuscitation. (Lindley, Stojadinovic, Pastar, & Tomic-Canic, 2016) The second phase involves monitoring vital signs and urine output after adequate fluid resuscitation has been completed. The third phase involves the application of antimicrobial dressings to deep burn wounds in order to prevent infection and the debridement of these wounds.

The fourth phase is wound infection prevention and providing nutritional support to improve burn wound healing, and the final phase is rehabilitation to ensure the patient's proper recovery (Fig. 9). (Lang et al., 2019)

Phase I
Initial assessment and triage
• Stop the burning process
• Remove patient and providers from harm
• Primary survey (airway, breathing and circulation)
• Secondary survey (assess other injuries, estimate percentage TBSA affected)
• Begin resuscitation (calculate initial fluid rate using either 2–4 ml/kg per 24 hours to estimate 24-hour volume or calculate initial fluid rate using Rule of Tens)

Phase II
Fluid resuscitation (0–48 hours)
• Titrate IV fluid rate hourly based on urine output (0.5 ml/kg per hour for adults, 1 ml/kg per hour for children)
• Albumin early for 'runaway' resuscitation
• Consider other adjuncts such as plasma, high-dose vitamin C and plasmapheresis
• Serial evaluation for resuscitation morbidity

Phase III
Burn wound coverage
• Use of topical antimicrobial creams or dressings to prevent infection
• Surgical debridement, burn wound excision and autografting or temporary coverage with skin substitute
• Optimize conditions for wound healing (haemodynamics, organ support and nutritional support)

Phase IV
Supportive and critical care
• Prevent and treat infectious complications
• Treat hospital complications and provide organ support
• Nutritional support

Phase V
Rehabilitation
• Proper limb positioning to prevent contractures
• Aggressive rehabilitation — active range of motion and exercise
• Anabolic agents (oxandrolone) and catabolism-reducing agents (propranolol)
• Psychosocial support
• Return to work and work strengthening programmes

Hours / Days to weeks / Months to years

Burn injury / Hospital discharge

Figure 9. Phases of burn treatment
(Lang et al., 2019)

Burn and heat stress cause DNA damages and IRS methylation changes

Burns may have local and systemic consequences. Skin burns cause inflammation, immune suppression, and a hypermetabolic state. Inflammation could induce pain, and various cytokines such as tumour necrosis factor (TNF) and

18

interleukins (IL) can induce hyperthermia. **(Lootens, Brusselaers, Beele, & Monstrey, 2013)** Moreover, tissue damage after a thermal injury is associated with raised ROS, contributing to the cause of triggered neutrophils and macrophages, leading to the necessitating of wound dressing with materials that can inhibit inflammation and antioxidants. **(Kantidze, Velichko, Luzhin, & Razin, 2016; Petrova, Velichko, Razin, & Kantidze, 2016)**

Burn injury results in oxidative stress, which develops as a result of the incredible production of ROS. This stress is the most important cause of local and systemic responses. Previous research has suggested that ROS causes lipid, membrane, nucleic acid, and protein damage, which can result in DNA breaks (SSB and DSB), lipid peroxidation, and cell apoptosis. **(da Silva et al., 2015; Karni et al., 2013)** (Fig. 10)
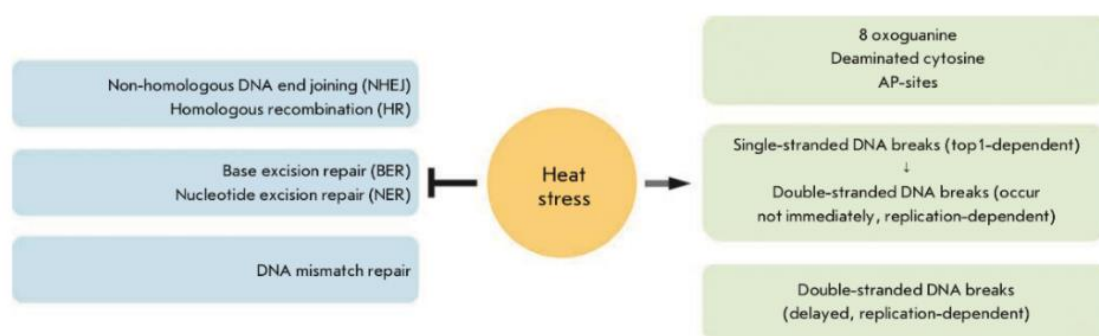
Figure 10. Consequences of burn and heat stress in DNA and DNA repair systems
(Kantidze et al., 2016; Petrova et al., 2016)

Heat stress not only reduces the rate of the DNA repair process but also forces the body to produce DNA-damaging response chemicals. The DNA damage repair signal (DDR) is activated by the accumulation of DNA damage products, which is throughout the situation of DNA and base modification, base loss, and DNA breakage.

The DDR stimulates cells to repair DNA damage. (Kantidze et al., 2016) However, inhibiting DDR signals, repressing cellular metabolism, and encouraging cell senescence result in programmed cell death. Then, an excessive amount of DDR signals can result in the onset of cellular instability. Thus, DNA damage is an important molecular pathogenic mechanism in the senescence-inducing process. However, it is necessary to investigate the underlying cause of DNA damage that occurs spontaneously during genome instability. **(Petrova et al., 2016; Velichko et al., 2015)**

In burn wounds, heat stress can result in the accumulation of 8-OHdG, apurinic DNA sites (AP-sites), and deaminated cytosine. It may be inferred that heat stress-induced suppression of excision repair mechanisms causes such DNA damage responses, including single-stranded DNA breaks (SSBs), to accumulate slowly in the cell. Double stranded DNA breaks (DSBs) are caused by heat stress-induced SSB. These DSBs share a few key features: they occur 2 to 5 h after heat exposure, rather than immediately and are S-phase specific. Following topoisomerase-1 suppression, replication forks that are re-started following heat stress-induced arrest collide with SSBs, resulting in late DSBs. (Velichko et al., 2015) Furthermore, burns and heat stress can cause DNA damage in various cells and animals (Apiwat, 2019; Korkmaz, Butuner, & Roggenbuck, 2018; Mah, El-Osta, & Karagiannis, 2010; Mataix et al., 2020; Reis, Vargas, & Lemos, 2016; Takahashi et al., 2004) and result in DNA damage responses. (Purschke et al., 2010) For example, in heated germline cells, an increase in 8-OHdG levels was observed in response to DNA damage. (Houston et al., 2018) Keratinocytes experience DNA damage and exhibit delayed proliferation and apoptosis after exposure to temperatures > 42°C for 24 h. (Hintzsche, Riese, & Stopper, 2012) Furthermore, an increase in histone H2AX phosphorylation on serine 139 (γH2AX) occurs in response

to ROS-induced DNA double strand breaks, which have multiple causes, including irradiation, burns, and laser exposure. (Firsanov, Solovjeva, & Svetlova, 2011; Kaneko, Igarashi, Kataoka, & Miura, 2005; Kinner, Wu, Staudt, & Iliakis, 2008) There is a positive correlation between increasing the temperature from 41.5˚C to 45.5˚C and the expression levels of γH2AX in H1299 (human non–small-cell lung carcinoma p53-deficient) cells. (Takahashi et al., 2004) Moreover, high temperature-induced formation of γ-H2AX foci may result in carcinogenesis. (Dewhirst, Lora-Michiels, Viglianti, Dewey, & Repacholi, 2003)

The relationship between heat, burns, and methylation has been studied previously. (M. C. Bind et al., 2016; Hao, Cui, & Gu, 2016; R. Xu et al., 2020) There is evidence that heat stress and high temperatures lower DNA methylation levels in pig muscles and fish tissues, specifically in the promoter regions of heat shock protein genes. (M.-A. Bind et al., 2014; Varriale & Bernardi, 2006; Vinoth et al., 2018) An increase in the ambient temperature can affect Alu methylation in humans. (Dridi, 2012) However, to the best of our knowledge, no study has investigated the relationship between burn wound healing and Alu methylation with markers of genomic instability, as has been done for 8-OHdG and γH2AX.

In addition to growth arrest, some markers are used to identify senescent cells. The most common characteristics are cell and nucleus enlargement. (Velichko et al., 2015) Furthermore, p53 normally occurs in an inactive state that is non-action at binding to DNA, which causes transcription. Stimulation of p53 during DNA damage is related to increased levels and the ability of p53 to bind to DNA and mediate transcriptional initiation. This then causes the activation of several genes that stop cell cycles, DNA repair, and cell apoptosis. (Lakin & Jackson, 1999; Nicolai et al., 2015)

(Fig. 11) Moreover, p21 is a p53 transcriptional target involved in the cell's response to DNA damage. p21 has multiple functions in mammalian cells depending on its subcellular location. To stop G1/S and G2/M cell cycle progression, nuclear p21 can inhibit CDK1 and CDK2 kinase activities.

(Bedelbaeva et al., 2010; Jiang et al., 2020; Kulaberoglu, Gundogdu, & Hergovich, 2016)
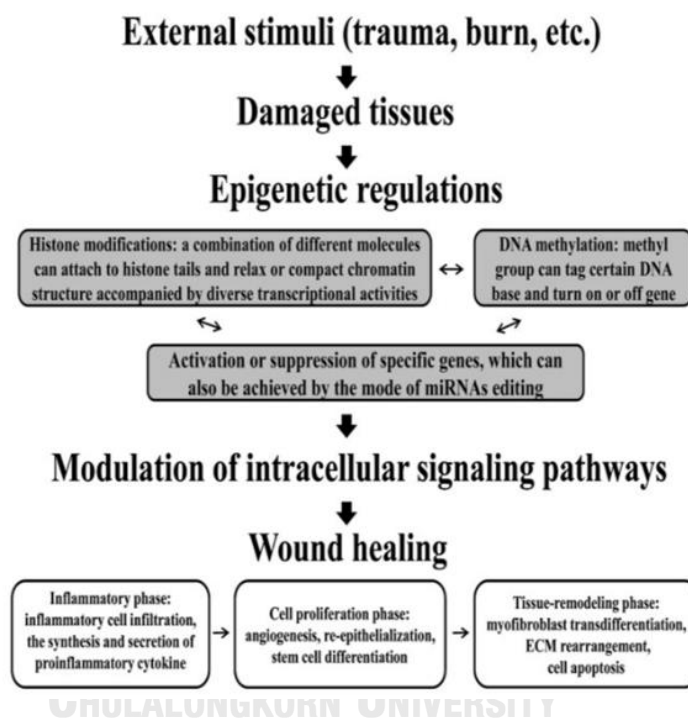
Figure 11. Epigenetic changes in chromatin organisation facilitate transcription machinery and promote wound repair (Ti, Li, Fu, & Han, 2014)

As a result, severe burns and heat stress can cause DNA damage, increased activity of H2AX, 8-OHdG, p53, and p21, and cell cycle arrest, among other effects. Cell cycle arrest causes cell proliferation, wound healing, and epithelialisation to slow down, as well as the formation of new cells. By preventing or improving the cell cycle arrest process caused by heat stress, we can improve the rate of wound healing and

epithelialisation, as well as reduce the duration of time that patients spend in the hospital. (Jeschke et al., 2020; Rennekampff & Alharbi, 2021)

Heat stress affects epithelialisation

Tests on keratinocytes *in vitro* have been conducted to assess the effect of heat. Apoptosis was identified using ultrastructural microscopy and was characterised by cell shrinkage, cytoplasmatic budding, and changes in the nuclear morphology, among other features, in the cells studied. In the presence of heat stress, the proliferation of keratinocytes is slowed, perhaps as a result of decreased keratinocyte adhesion. (Rennekampff & Alharbi, 2021) It is well recognised that the *in vitro* proliferation and expansion of keratinocytes rely on the adherence of the cells to a substrate via the action of integrins. Therefore, detachment of cells from an extracellular matrix, particularly the basement membrane due to integrin breakdown, triggers the activation of this apoptosis pathway in the cell. (Manohar et al., 2004)

Part A: B1siRNA

B1 elements

Transposable elements (TEs) or mobile genes are fragments of DNA that can move from their genomic sites to other genomic locations. These account for roughly 45% of the total length of the entire genome. In general, transposons are separated into two main groups: retrotransposons and DNA transposons. (Cordaux & Batzer, 2009) DNA transposons are transported through a cut-and-paste process, in which they are removed from their original locations and reinserted into new ones. Although there are currently no active DNA transposons in the human genome, they were active over 37 million years ago during the primate evolution period. (Han, Szak, & Boeke, 2004) In

contrast, retrotransposons move using a mechanism whereby the element is duplicated and inserted at target locations via an RNA-intermediate, which is created by a reverse transcriptase enzyme. Retrotransposons are classified into two subgroups: retrotransposons with LTRs and retrotransposons without long terminal repeats (non-LTR). LTR elements are endogenous retroviruses that are currently inactive. However, the majority of TEs are non-LTR retrotransposons, accounting for 34% of the human genome. The main elements of non-LTR retrotransposons are autonomous long interspersed element-1 (LINE-1; 17%), SINEs (Alu, 11%), and non-autonomous long interspersed elements (SVA, 0.2%). (Chisholm et al., 2012) These elements are the only TEs that are currently active and affect the human genome, causing genomic instability and mutations. (Apiwat, 2019)

SINE retrotransposons are one of the repetitive elements, approximate 85–500 bp sequences in length. Though, two SINE families, first-B1 of mouse, rat, and hamster genomes and Alu of human genome. (Batzer & Deininger, 2002; Gebhard, Meitinger, Hochtl, & Zachau, 1982) Rodents are a very huge order totalling over 30 families; however, B1 elements are well recognised in mice and rats (Muridae) and closely related to those in hamsters. (Zhang et al., 2009) Each short retrotransposon (SINE) expresses sequence differences (5–35%). Generally, individual SINE families are found in creatures of one or several families or orders. (Gogolevskaya, Veniaminova, & Kramerov, 2010; N. A. Veniaminova, N. S. Vassetzky, & D. A. Kramerov, 2007) IRS methylation levels are crucial for preserving the stability of the genome. (Natalia A. Veniaminova et al., 2007) Mutation rates are increased in cells with IRS hypomethylation. (Gaudet et al., 2003; Slimen et al., 2014) A SINE retrotransposon is a repetitive element that is 85–500 bp in length. Two SINE families exist, namely the

24

B1 (in mice, rats and hamsters) and Alu (in humans) families. (Batzer & Deininger, 2002; Gebhard et al., 1982)

Similar to the Alu element, the B1 element in rodents originate from 7SL RNA, which is cytoplasmic RNA; it facilitates protein excretion as a part of the signal recognition particle. (Tsirigos & Rigoutsos, 2009) The B1 element assists in transcriptional regulation and DNA stability by binding to the Aryl hydrocarbon (dioxin) receptor, which is a ligand-activated transcription factor (Roman, Benitez, Carvajal-Gonzalez, & Fernandez-Salguero, 2008; Román, González-Rico, & Fernández-Salguero, 2011). A link between B1 element methylation, wound healing, and epithelialisation has not yet been documented (Fig. 12).

Figure 12. Components of B1 repetitive elements in rodents

Epigenetic changes associated with chromatin re-organisation can facilitate the transcription machinery and promote wound repair. (Ti et al., 2014) Genomic hypomethylation is characterised by reduced methylation of the methyl groups at the 5′ position of cytosine and plays crucial roles in important events such as ageing, cancer, and various skin diseases. (Apiwat, 2019; Bollati et al., 2009; Li, Sawalha, & Lu, 2009; Ti et al., 2014) Furthermore, current research shows that global hypomethylation is associated with delayed proliferation; in contrast, following increased Alu methylation, cells can tolerate toxic substances and decreased DNA damage responses and exhibit an enhanced proliferation rate. (Patchsung et al., 2018) Regarding corneal ulcers, the expression levels of DNA methyltransferase 1 (Dnmt1) and Dnmt3a, which participate

in the methylation process, are upregulated during corneal epithelial healing. (Luo et al., 2019) Therefore, decreased Dnmt1 expression and genomic hypomethylation defer corneal epithelial wound healing and block human corneal epithelial cell proliferation and migration. The roles of DNA methylation in rodents include considerably reducing the wound area and increasing the wound healing rate by increasing DNA Dnmt3a expression. (Luo et al., 2019) Moreover, decreased DNMT1 expression is associated with a low rate of squamous skin cell proliferation, whereas increased DNMT1 expression is associated with rapid limb bud generation. (Aguilar & Gardiner, 2015; Plikus, Guerrero-Juarez, Treffeisen, & Gay, 2015) A previous study revealed an association between age and Alu hypomethylation. (Mutirangura, 2019a) Positive associations have also been observed between Alu hypomethylation in blood cells and several ageing phenotypes. (Erichsen et al., 2018; Mutirangura, 2019b) The use of Alu short interference RNA (siRNA) enhanced Alu methylation, which allows cells to better withstand harmful substances and proliferate at a greater rate. (Mutirangura, 2019b)

RNA-directed DNA methylation (RdDM)

RNA interference (RNAi) is a post-transcriptional gene regulation process that causes RNA degradation of complementary RNA sequences. Moreover, siRNAs can join other pathways through which a different argonaut-family protein leads to inhibition of the beginning transcripts that are still bound to RNA polymerase II and the DNA strands. This alternative pathway arises in the nucleus on an area of chromatin for modification via induction of protein complexes to incorporate methylation of the histones and cytosine bases in DNA. This alteration contributes to the condensation of

mRNA making it unavailable for transcription (Fig. 13). (Slotkin & Martienssen, 2007) Each strand of siRNA has a 3' hydroxyl (OH) group and a 5' phosphate group, as is typical of RNA. Dicer, an enzyme that also transforms long dsRNAs or hairpin RNAs into siRNAs, creates this RNA type. Exogenous siRNAs may also be delivered into cells via a number of transfection procedures, resulting in the precise silencing of a gene. Principally, if we know the sequence of genes then we can target them with a matching custom-made siRNA.
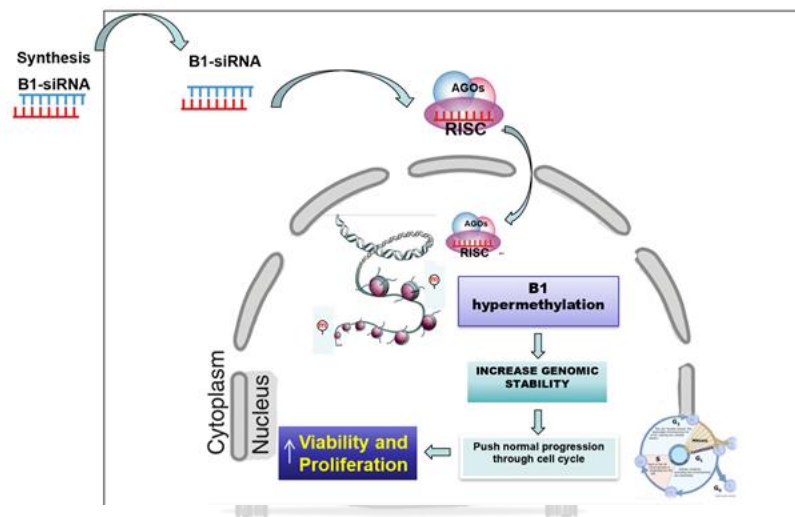
Figure 13. Mechanism of RNAi induces chromatin and DNA modification and increases methylation

RdDM is a natural process through which RNA molecules, which are not translated into any proteins, direct the accumulation of methyl groups at the 5′ position of cytosine specific to the RNA in CpG islands. These islands are genomic regions where CpG sites, DNA regions in which a cytosine nucleotide is followed by a guanine nucleotide, occur at a high frequency. The CpG islands are predominantly found in SINE repetitive DNA, such as B1 and Alu. (Batzer & Deininger, 2002; Mathieu & Bender, 2004) RdDM process is facilitated by a cascade of enzymes, Dicer, RNA-induced silencing complex, and argonaut proteins. (Castanotto et al., 2005) This

alternative pathway is initiated in chromatin within the nucleus and leads to epigenetic modifications, including DNA cytosine methylation and histone methylation. (Marjori A. Matzke & Rebecca A. Mosher, 2014)

Further evidence showed that siRNA generated in plants consists of short (21–22 bp) and long (24–26 bp) classes, while those from endogenous retroelements only consist of the long class. (Katiyar-Agarwal et al., 2006) These classes of siRNAs have different effects. The long siRNA is associated with general silencing and direct DNA methylation. (Castanotto et al., 2005; M. A. Matzke & R. A. Mosher, 2014)

Interspersed repetitive sequences methylation

One important task of DNA methylation is to avoid DNA damage caused by both endogenous and exogenous factors. DNA methylation and DNA damage are inversely correlated in white blood cell DNA. Moreover, adding Alu methylation by Alu siRNA reduces DNA lesions. (Patchsung et al., 2018) In the elderly, DNA shows reduced methylation, leading to global hypomethylation; therefore, the senescence genome is unstable and exhibits DNA damage. (Yanting Luo, Xuemei Lu, & Hehuang Xie, 2014) Global hypomethylation and accumulation of DNA lesions have been identified in ageing people and those with noncommunicable diseases, such as individuals with osteoporosis, diabetes mellitus, and high blood pressure or hypertension. (Salameh, Bejaoui, & El Hajj, 2020) Excessive DDR during intracellular DNA lesion repair prevents cell growth, promotes death, causes cellular metabolic response, and aggravates senescence. As a result, global hypomethylation is an unfavourable epigenetic alteration that contributes to genomic instability and the onset of senescence-associated disease phenotypes. (Thongsroy & Mutirangura, 2022)

DNA lesions, which are caused by either endogenous or exogenous sources, are naturally found in a common cellular fate and are repaired through various DNA repair mechanisms. According to several studies investigating ROS, cell proliferation, senescence, and epigenetic modification, Alu hypomethylation plays a critical role in mechanisms underlying genomic instability, eventually resulting in cellular senescence. (Guillaumet-Adkins et al., 2017; Pal & Tyler, 2016)

Recently, an experimental study found an important correlation between age and Alu hypomethylation, but this association was not found in LINE1 hypomethylation. Further evidence confirming this finding was obtained in volunteers aged 20–88 years, that age was negatively correlated with Alu methylation levels but not LINE-1. Moreover, positive correlations between Alu hypomethylation in blood cells and many senescence diseases have also been identified. (Guillaumet-Adkins et al., 2017; Jintaridth & Mutirangura, 2010; Jintaridth, Tungtrongchitr, Preutthipan, & Mutirangura, 2013; Y. Luo, X. Lu, & H. Xie, 2014; Perez, Tejedor, Bayon, Fernandez, & Fraga, 2018; Thongsroy, Patchsung, & Mutirangura, 2017) These findings emphasised that Alu methylation levels obviously play specific roles in senescence phenotypes. Additionally, it has been observed that hypermethylated Alu elements induced by Alu siRNA could prevent genomic instability. Specifically, a study aimed to specifically enhance the methylation levels of Alu elements using Alu siRNA transfection in HeLa cells and human embryonic kidney (HEK) cells. They reported that Alu siRNA transfection system significantly increased Alu methylation compared to the Lipofectamine-negative control. Consequently, similar results were observed in both HeLa cells and HEK293 cells on Alu siRNA transfection compared to negative controls, and the methylated Alu elements sustainably increased in 7 days after Alu

siRNA transfection. Alu siRNA transfection specifically promoted methylation levels of Alu sequences due to no significant conversions in LINE-1 levels of methylation in both cell lines. Similarly, Alu siRNA transfection increased the ratio of methylation of Alu repetitive sequences in periodontal ligament fibroblasts (PDL) when compared to lipofectamine transfection control (Fig. 14). (Patchsung et al., 2018)
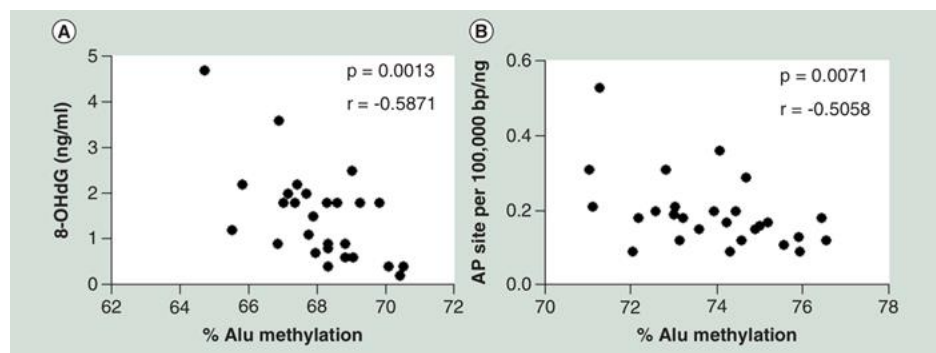
Figure 14. Univariate investigation of association between the
levels of 8-OHdG and Alu methylation (Patchsung et al., 2018)

In addition to specific methylated Alu enhancement, Patchsung M and colleagues investigated the association between increased cell proliferation after Alu siRNA transfection using 3-[4,5-dimethylthiazol-2-yl]-2,5 diphenyl tetrazolium bromide (MTT assay) and methylation levels of Alu repetitive sequences, absolute cell count, and population doublings. Interestingly, Alu siRNA transfection enhanced cell proliferation of HEK293 and periodontal ligament cells. Consistently, the absolute cell count of HEK293 cells was enumerated for three days after Alu siRNA transfection and the result showed a higher cell number when compared to the control. Expectedly, the replication of Alu siRNA transfected periodontal ligament cells was inspected at the 13th and 14th passages and an increase in population doublings was observed. (Patchsung et al., 2018)

The preceding study showed that Alu hypermethylation contributed to the prevention of *in vitro* DNA damage. Interestingly, Alu hypermethylation significantly reduced the susceptibility to DNA damage and enhanced the percentage of cell survival in both HEK293 and PDL cells when exposed to methyl methane sulphonate and H_2O_2 at the higher concentrations (1.0 to 2.0 mM and 100 to 150 µM, respectively) compared to control cells. Moreover, the levels of AP site and 8-OHdG were reduced in siRNA-treated cells when compared with control cells (Fig. 15). (Patchsung et al., 2018)
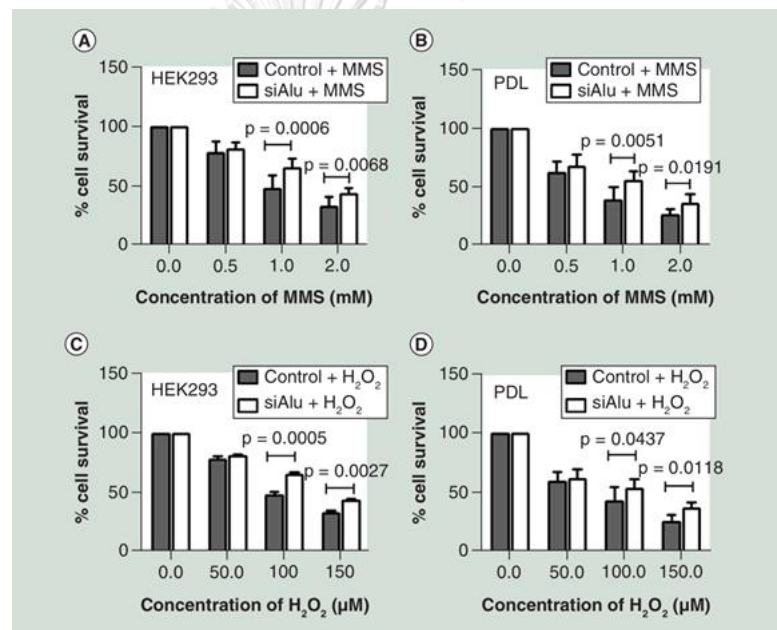
Figure 15. When exposed to DNA-damaging substances, cells that were hypermethylated were less susceptible (Patchsung et al., 2018)

Accordingly, it might be determined that an increase in DNA methylation, particularly Alu elements in humans or B1 in rodents, is associated with strengthening the genome and could recover senescence phenotypes as genomic instability in many previous studies. (Guillaumet-Adkins et al., 2017; Pal & Tyler, 2016; Patchsung et al., 2018; P. Sen, Shah, Nativio, & Berger, 2016) More than in intact skin, DNA methylation occurs at the 5′ end of the CpG dinucleotide of the cytosine ring and is

31

frequently a transcriptional silencing presentation. DNA methyltransferases (DNMTs) catalyse this activity through S-adenosyl-methionine as a methyl donor; inactivation of DNMT1 results in epidermal hypoplasia and suppression of proliferation-associated genes. (S. Kang, Chovatiya, & Tumbar, 2019; G. L. Sen, Reuter, Webster, Zhu, & Khavari, 2010; Ti et al., 2014) Although the Alu methylation status is apparently linked to senescence phenotypes *in vitro*, whether an increased Alu methylation status or B1 methylation in rats also improves proliferation phenotypes and restores the physiological functions of wound healing had not been further investigated using an animal burn wound model.

Therefore, it was hypothesised that DNA methylation in IRSs can prevent DNA damage and accelerate burn wound healing in rats. In the present study, the role of B1 methylation in genomic instability in relation to wound healing was studied. The following questions were addressed: How can B1 methylation be restored to reduce genomic instability caused by heat, and how can the rate and quality of wound healing and epithelialisation be accelerated and improved?

Burn Scars and Alu hypomethylation

A hypertrophic scar is the most common complication of burn wounds and is defined by an elevated border of the scar confined in the wound area, for which erythematous and clinical presentation might improve with time. (Finnerty et al., 2016) The prevalence of hypertrophic scars in post-burn patients was reported to be more than 60% and 75% in white and non-white races, respectively. (Bombaro et al., 2003; Lawrence, Mason, Schomer, & Klein, 2012) Hypertrophic scars have both physical and psychological consequences in post-burn patients, leading to poor function and cosmetic outcomes, including pain, discomfort, itching, hyper/hypopigmentation,

temperature sensitivity, and scar contracture, limited range of motion, changed rotational axis of the joint, and nerve compression. (Chiang et al., 2016)

Hypertrophic scars are fibroproliferative disorders and common complications of burn injuries. The risk factors for hypertrophic scar formation are sex, age, race, genetics, and wound location; however, post-burn hypertrophic scars are often found in full-thickness burn wounds because of prolonged inflammation and slow wound healing. (Xiao et al., 2018) Current treatments for post-burn hypertrophic scars include medical and surgical therapy, such as silicone gel sheet, corticosteroids, botulinum toxin, pulsed dye laser, Nd-YAG, non-ablative and ablative fractional laser, lipofilling, and surgical excision; however, current therapies have poor outcomes. (Deflorin et al., 2020; Klifto, Asif, & Hultman, 2020; Tredget, Levi, & Donelan, 2014) Understanding post-burn injury scar formation and finding new therapies remain challenging in the treatment of such injuries.

The epigenetic phenomenon refers to the modulation of gene expression that occurs without a change in the DNA sequence itself. It is possible that it is involved in the complexity of the illness that cannot be described just through hereditary and environmental variables. Methylation is the most prevalent type of epigenetic modification and is associated with genomic instability. (Mutirangura, 2019b) Methylation is a chemical modification process in which a methyl group from adenosyl methionine is inserted onto a carbon atom of the cytosine ring of the DNA. Methylation mostly occurs at CpG dinucleotides and depends on DNA methyltransferase enzymes. Two patterns of methylation have been described: hypermethylation, which silences genes, and hypomethylation, which activates genes. (Jones et al., 2017) Alterations in the methylation of Alu and LINE-1 have been shown to be associated with many cancer

33

types, genetic, and autoimmune diseases, such as haemophilia, Behçet's disease, Dent's disease, cystic fibrosis, Walker–Warburg syndrome, Apert syndrome, X-linked dilated cardiomyopathy, neurofibromatosis, Duchenne muscular dystrophy, von Hippel-Lindau disease, β-thalassemia, familial hypercholesterolemia, rheumatoid arthritis, lichen simplex chronicus, hepatoma, breast cancer, ovarian cancer, acute myeloid leukaemia, T-cell lymphoblastic leukaemia, Ewing sarcoma, and colorectal cancer. (Belancio, Deininger, & Roy-Engel, 2009; Chenais, 2015; Jordà et al., 2017; Park et al., 2014; Yooyongsatit et al., 2013; Yüksel et al., 2016) Hypertrophic scar is a benign proliferative disorder. (Tsou et al., 2000) Previous research has demonstrated that the expression of multiple genes is altered in hypertrophic scars in Bama mini pigs and human skin, including the downregulation of apoptotic genes and upregulation of tumour suppressor genes and proto-oncogenes. However, no specific genes have been identified yet. (Liu, Liu, Wang, Hou, & An, 2018; Paddock et al., 2003; Tsou et al., 2000) Recent studies have emphasised the role of epigenetics in the pathophysiology of scars and wound healing, and histone modification is differentially acetylated in histone H4 at lysine K12 compared with normal skin. (Nascimento-Filho et al., 2020) Moreover, methylation changes exist in multiple genes in hypertrophic scars, such as TNKS2, CAMKK1, and GAS7. (Alghamdi et al., 2020) To date, however, no studies are available on Alu methylation in hypertrophic scars.

Here, I examined whether the pathophysiology of hypertrophic scars may be associated with epigenetic changes. Dissimilar to genetic mutation, epigenetic processes are reversible. Thus, research on epigenetic processes could result in treatments and interventions, such as Alu siRNA, that can increase methylation, cell proliferation, and well tolerate DNA-damaging agents and toxic substances. (Patchsung

et al., 2018) To this end, I compared Alu methylation levels and patterns between normal skin and hypertrophic scars. I anticipate that the findings of this study will contribute to the understanding of the pathophysiology of hypertrophic scars and development of new treatments for burn injuries.

Part B: Box A of HMGB1 protein

BOX A OF HMGB1 PROTEIN

Protein with high mobility group box 1 (HMGB1) is a nuclear protein that is present in all eukaryotic cells and is a member of the high mobility group (HMG) family of proteins. The human HMGB1 protein contains 215 amino acids and is composed of three functional domains, including nucleotide-binding boxes (A and B boxes) and a C-terminal that is rich in anionic residues (Box-A (aa 9-79) and Box-B (aa 89-162), as well as a terminal acidic tail (186-215). While the A and B boxes are capable of binding DNA, the C-terminal area is capable of binding histones. The C-terminal section can also interact with the A and B boxes, modifying the three-dimensional structure and complex interactions of HMGB1 in the process. The A and B boxes are two homologous nucleic-acid-binding and function as DNA-binding protein and a sirtuin-1 (SIRT-1) binding domain, (SIRT-1, a protein is bound to the DNA and responsible for histone deacetylation involved in DNA repair and DNA stability). According to its preference for certain DNA structures, also including bending, HMGB1 is reported to be responsible for the modification of the nucleosomal structure to control transcription, repair, and recombination of DNA (Fig. 16). (Magna & Pisetsky, 2014; Ugrinova & Pasheva, 2017)
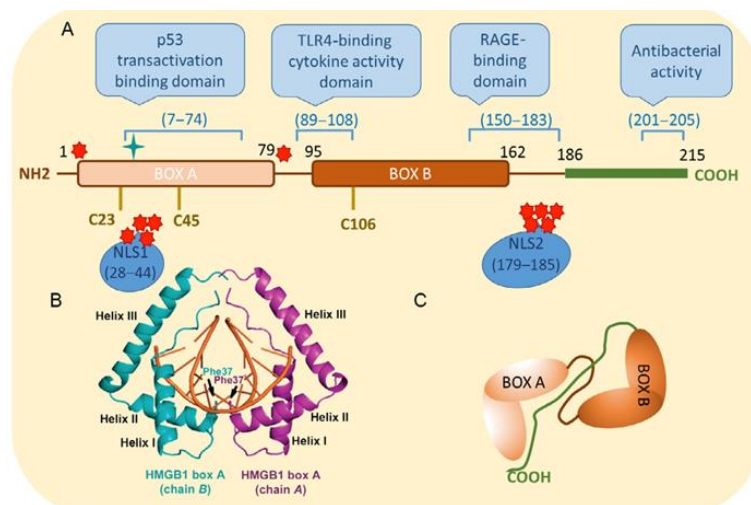
Figure 16. The HMGB1 protein structure is shown in this diagram.
A and B boxes, which are helical DNA-binding sites (Ugrinova & Pasheva, 2017)

HMGB1 protein has distinctively different dual functions. The function of HMGB1 depends on its location. A protein HMGB1 attaches to the minor groove of DNA in the nucleus, causing the DNA to be curved into helical form. HMGB1 stabilises nucleosomes and helps DNA replication, V(D)J recombination and DNA repair. Moreover, evidence shows that HMGB1 in mammals and Nhp6A/B HMGB1 homolog in yeast can protect DNA from damaging agents. (Giavara et al., 2005; Thongsroy, Patchsung, Pongpanich, Settayanon, & Mutirangura, 2018) So, nucleus HMGB1 serves a crucial role in maintaining nuclear homeostasis and genomic stability. (Giavara et al., 2005; R. Kang, Zhang, Zeh, Lotze, & Tang, 2013) Loss of HMGB1 in nuclease results in telomere shortening by its requirement for chromosomal stability. (Polanská, Dobšáková, Dvořáčková, Fajkus, & Štros, 2012) In contrast, extra nucleus HMGB1 plays a role in many diseases, especially inflammatory and cancer. (Magna & Pisetsky, 2014; Ugrinova & Pasheva, 2017; Yang, Wang, Chavan, & Andersson, 2015)

Box A of HMGB1, the first part of HMGB1 protein (Fig. 17) overexpression cells, showed lowered endogenous DNA damage and increased cell proliferation. In HMGB1 and Box A overexpression, cells exhibited lower level of endogenous DNA damage; AP- site and 8-OHdG and cell viability of overexpressed cells was increased after exposure to DNA-damaging agents; H_2O_2, and rapamycin. (Patchsang M. and Settayanon S, unpublished data) Sepsis in mice exposed to a peritonitis model is prevented by Box A of the HMGB1 protein, and hepatitis B in mice exposed to an HBV infection model is also prevented by Box A of the HMGB1 protein. (Sitia, Iannacone, Müller, Bianchi, & Guidotti, 2007; H. Yang et al., 2004)
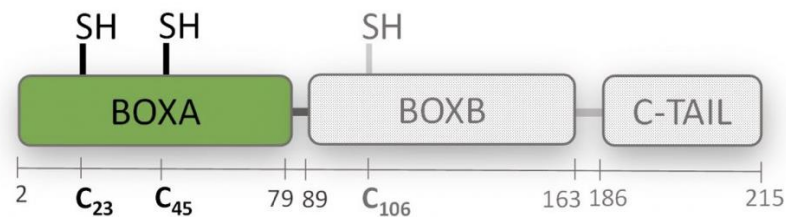
Figure 17. Box A of Hmgb1 protein

Physiologic Replication-Independent Endogenous DNA Double-Strand Breaks (PHY-RIND-EDSB)

Global DNA hypomethylation promotes genomic instability though the damage to DNA is accumulated over time and resulted in an increasing rate of mutation. To stabilise the genome, cells possess an epigenetic mechanism to reduce DNA tension that causes DNA damage, named Physiologic-Replication-Independent Endogenous DNA Double-Strand Breaks (PHY-RIND-EDSBs). They are localised within methylated genome and maintained by non-histone HMGB1 and SIRT1 proteins. (Mutirangura, 2019a) Furthermore, PHY-RIND-EDSBs can be found in yeast cells

(Thongsroy et al., 2018), and a reduction in PHY-RIND-EDSBs was observed in hypomethylated genome including cancer and ageing. (Perez et al., 2018)

According to a recent study, a novel form of physiologic endogenous DNA double strand break that occurs without the influence of DNA replication has been discovered. They could be discovered in the G0 phase of the cell cycle, which is also known as the resting state. In human cells, DSBs caused by hypermethylation of PHY-RIND-EDSBs were repaired more precisely by an ataxia telangiectasia mutated-dependent and non-homologous end-joining (NHEJ), whereas pathogenic DSBs were more commonly repaired by an error-prone Ku-mediated NHEJ. (Kongruttanachok et al., 2010; Pongpanich et al., 2014; Thongsroy et al., 2013; Thongsroy et al., 2018) It's interesting to note that PHY-RIND-EDSB in yeast decrease as the age of the yeast cells increases. (Thongsroy et al., 2018)

Hypermethylated DNA regions and deacetylated histones contain human PHY-RIND-EDSBs. (Kongruttanachok et al., 2010; Pornthanakasem et al., 2008) Cells deficient in HMGB proteins and Sir2 have a decreased ability to produce PHY-RIND-EDSBs. (Shore, 2000; Thongsroy et al., 2013) Sirtuin 1 (SIRT1), a human Sir2 homolog, binds to the HMGB1 and deacetylates DNA methyl transferase 1. (DNMT1). (Hwang et al., 2015; L. Peng et al., 2011) Deoxyribophosphate lyase activity is also observed in HMGB1 protein. It does this by acting on DNA, which results in the production of PHY-RIND-EDSB. Histones are deacetylated by the SIRT1-bound HMGB1 protein, which prevents DNA damage response from affecting PHY-RIND-EDSBs. SIRT1-DNMT1 cooperation or deacetylation of histones and DNA methylation may be responsible for the hypermethylation of regions around human PHY-RIND-EDSB (Fig. 18). (Prasad et al., 2007)
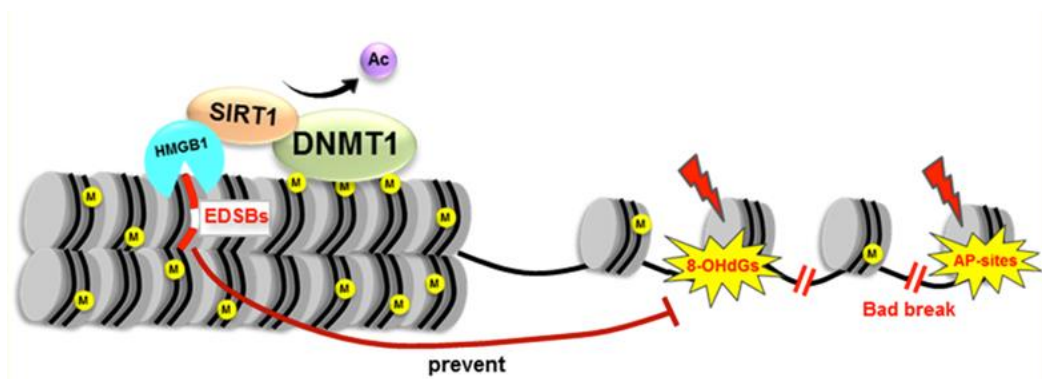
Figure 18. Appropriate epigenetic changes make structural alterations in chromatin organisation

It has been purposed that Box A of HMGB1 protein might become a hopeful nuclear protein that might be able to effectively reduce the genomic instability and enhance the levels of PHY-RIND-EDSBs in cellular damage. Finally, the less genomic instability in the heat stress cells, along with more PHY-RIND-EDSBs by enhancing Box A of HMGB1 protein expression might potentially improve or reverse damaging phenotypes by restoring impaired wound healing in burn wounds. Moreover, HMGB1 has been identified to prevent genomic instability by retaining PHY-RIND-EDSBs.

Furthermore, it has been shown that HMGB1 is capable of preventing genomic instability by preserving PHY-RIND-EDSBs. The amount of PHY-RIND-EDSBs was lowered in yeast that did not contain the Nhp6A/B genes, which are identical to the HMGB1 gene in humans, and a similar result was obtained in HeLa cells that had the HMGB1 gene knocked out or downregulated. (Thongsroy et al., 2013) As a whole, our data show that HMGB1 preserves these physiologic-EDSBs, and that each of these EDSB types may play a particular role in preserving genomic integrity. Additional evidence supports the role of HMGB1, which has been linked to PHY-RIND-EDSBs, and there are multiple lines of evidence to support this function. The V(D)J cleavage reaction, which is a kind of physiologic EDSB, is mediated by HMGB1, which plays a

role. It has a mild 5-deoxyribose phosphate lyase activity, which allows it to cleave DNA strands. (Ugrinova & Pasheva, 2017) It is interesting to note that both HMGB1 and HMG Box A possess nuclease activity. It has been discovered that the Box A domain of HMGB1 interacts with SIRT1, a histone deacetylase that is reliant on nicotinamide dinucleotide (NAD+) and is involved in the development of heterochromatin. It is believed that SIRT1 is connected with ageing, and its lowering results in increased DNA damage. Therefore, this study aimed to explore the role of Box A of HMGB1-mediated DNA methylation in genomic instability prevention and to improve burn wound healing.

In addition to direct DNA damage by heat, the burn may cause a reduction of DNA protection epigenetic marks, Box A of HMGB1 produced PHY-RIND-EDSBs. Recently, we demonstrated a new type of epigenetic marks playing a role in genomic instability prevention. PHY-RIND-EDSBs are produced by Box A, part of the HMGB1 gene. Lack of HMGB1 led to PHY-RIND-EDSBs reduction and consequently spontaneous DNA shearing. (Thongsroy et al., 2018) On the contrary, introducing new DNA gaps by Box A expression plasmid transfection increased DNA durability and reduced endogenous DNA damage. (Yasom et al., 2022b) Burn ignites HMGB1 release, resulting in intranuclear HMGB1 depletion. (Lantos et al., 2010) In addition, introducing a DNA break promoted global DNA gap repair. Both events cause PHY-RIND-EDSBs reduction. (Thongsroy et al., 2018) DNA sequences around PHY-RIND-EDSBs are hypermethylated, and depleting intranuclear HMGB1 reduces PHY-RIND-EDSBs and global DNA methylation. (Thongsroy et al., 2018; Watcharanurak & Mutirangura, 2022) Recently, we reported global hypomethylation in burn scars. (J. Meevassana et al., 2021) This evidence supported the reduction in HMGB1 produced

PHY-RIND-EDSBs in burn wounds. So I hypothesized here that Box A of HMGB1 plasmid transfection should produce new PHY-RIND-EDSBs to compensate PHY-RIND-EDSBs reduction promoting DNA damage mechanism and consequently facilitating burn wound healing.

As a result, I postulated that PHY-RIND-EDSBs, which is produced by the HMGB1 protein Box A, may protect DNA and speed up the healing of burn wounds in rats. The involvement of BoxA of the HMGB1 protein in genomic instability in connection to wound healing was investigated in this work. The following concerns were addressed: how can the BoxA of the HMGB1 protein be restored to minimise genomic stability induced by heat, and how can wound healing and epithelialization be accelerated at a greater rate and with better wound quality.

Part C: Laminin 511 E8

The rate at which burns heal following injury is a primary determinant of the likelihood of infection, and slow healing is associated with prolonged hospital stays and severe patient morbidity. The development of new methods to improve the rate of wound repair and thereby improve outcomes would substantially benefit patients. (Kusu-Orkar, Islam, Hall, Araia, & Allorto, 2019) One approach is the direct application of biologically derived proteins, peptides or compounds to the wound bed, where the applied material is known to be involved in the native wound healing response. (Finlay et al., 2017) Keratinocytes, the primary cells of the epidermis, are important not only for their role as physical barriers to the body but also for rebuilding the injured layer via re-epithelialisation. (Pastar et al., 2014) This process involves

41

keratinocyte proliferation and interaction with a provisional extracellular substrate to migrate to the wound bed, thereby closing the wound. (Rowan et al., 2015) In this study, I hypothesised that an extracellular matrix component that is known to promote keratinocyte adhesion and migration could aid the re-epithelialisation process, thereby improving the rate of wound healing. Laminins (LMs) are proteins that are present in abundance in the extracellular matrix (ECM), mostly in basement membranes. Eighteen different isoforms of laminin have been found based on the unique trimeric components of the alpha (α), beta (β), and gamma (γ) chains. Laminins are extracellular proteins that provide a role in the organization of several vital cellular pathways, including cell proliferation, adhesion, and migration. Different LM isoforms display distinct distribution profiles and differ in terms of their structure and their specificity and affinity for cell surface receptors. (Fig. 19) LMs 511 is the most common type of LMs found in mammalian skin. (Iriyama et al., 2020; Koivisto, Heino, Häkkinen, & Larjava, 2014; K. Sugawara, Tsuruta, Ishii, Jones, & Kobayashi, 2008; Yap, Tay, Nguyen, Tjin, & Tryggvason, 2019) LMs have been shown in numerous studies to improve keratinocyte and fibroblast function and differentiation. (Domogatskaya, Rodin, & Tryggvason, 2012; Hohenester & Yurchenco, 2013; Longmate & Dipersio, 2014)

Laminin and extra cellular matrix

Laminins (LMs) are extracellular macromolecules that play key roles in the regulation of a plethora of core cell and tissue functions, including regulation of cell proliferation, adhesion, and migration. (Hamill, Kligys, Hopkinson, & Jones, 2009) The extracellular matrix's primary components, laminin and collagen. When other proteins come into contact with laminin proteins via their C-terminal regions, they operate as

42

scaffolds. Integrin, syndecan and dystroglycans are the protein receptors for laminin proteins, which are responsible for the formation of the hemidesmosome and the focal adhesion complex in the basement membrane, and they aid in the process of cell migration. (Hopkinson et al., 2014; Iorio, Troughton, & Hamill, 2015b; Longmate & Dipersio, 2014; Tsuruta, Hashimoto, Hamill, & Jones, 2011)

Several different laminin isoforms bind to a range of different receptors on the cell surface. Indeed, LMs are involved in most tissue remodelling processes, including neovascularisation processes during wound repair, (Iorio et al., 2015b) Laminin-511 and the α6β1 integrin receptor have a very strong affinity towards one another. Researchers identified that the integrin α6β1 binding site is required for laminin to function properly throughout the epithelialisation process. It is known that LM 511 interacts with the α6β1 integrin receptor and increases the synthesis of focal adhesion kinase (FAK) (Essayem et al., 2006) (Gates, King, Hanks, & Nanney, 1994; Januszyk et al., 2017; Renshaw, Price, & Schwartz, 1999; B. Son et al., 2019), which is required for the migration of both keratinocytes and fibroblasts. On the other hand, when anti-α6β1 antibodies are utilised, cell proliferation and migration are significantly inhibited.
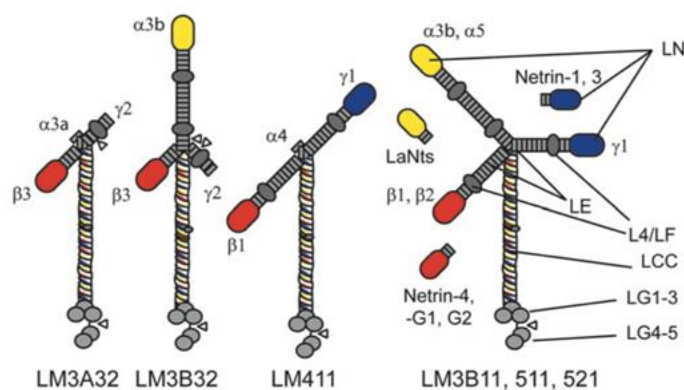
Figure 19 Laminin proteins components (Iorio et al., 2015b)

Furthermore, laminins and associated extracellular matrix components are responsible for a specific function in tissue regeneration. In the wound repair process, laminins play an important role in re-epithelialisation and neovascularisation. The understanding of how laminin protein manages cell function in these different situations will increase the probability of producing a new method to improve wound closure or treat chronic or nonhealing wounds (Fig. 20).
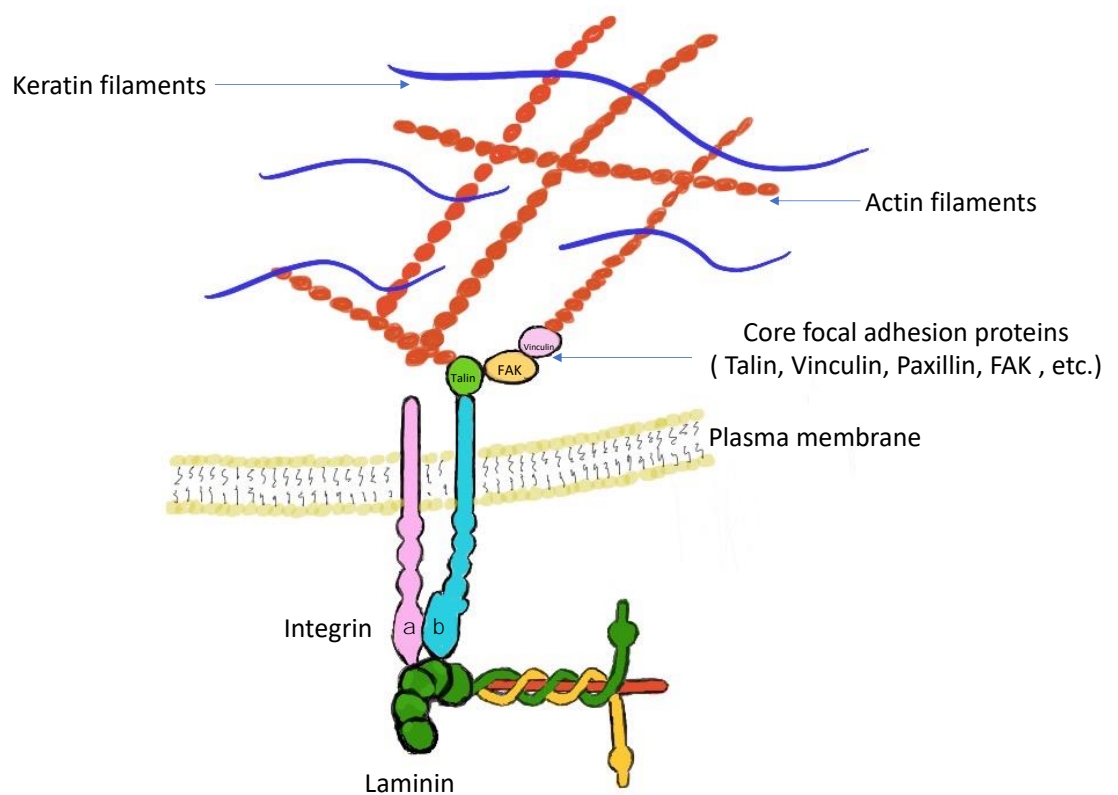
Figure 20. Focal adhesion formation

The laminin 511 isoforms enhanced adherence in cells and increased the cell growth and differentiation of human corneal endothelial cells (HCEC). (Okumura et al., 2015) In addition, using both *in vitro* and *in vivo* characterisations, Tjin MS and colleagues revealed that the laminin 511 protein provides a reliable culture substrate that can be used to replace the usual co-culture approach without compromising the quality of the cells. (Tjin et al., 2018) Moreover, laminin α5β1γ1 (LM511) potently

enhances keratinocyte migration in *in vitro* wound healing assays, and *in vitro* and *in vivo* assays have demonstrated that LM511 provides a robust culture platform for the expansion of epidermal keratinocytes. (Tjin et al., 2018) LM511 is also located in the endothelial basement membrane and supports faster migration of cultured endothelial cells. (Doi et al., 2002; Hallmann et al., 2005; Simon-Assmann, Orend, Mammadova-Bach, Spenle, & Lefebvre, 2011) As each of these activities is associated with the native wound response, supplying recombinant LM511 at wound sites may promote re-epithelialisation and angiogenesis. (Durbeej, 2010; Pouliot, Saunders, & Kaur, 2002) Human embryonic stem cells (hESCs) are proven to proliferate in an undifferentiated phase when they are given recombinant laminin isoforms (laminin-511). The production of recombinant laminins utilising mammalian expression systems is now in progress. However, the process of extracting naturally purified laminin protein from these is time-consuming and labour-intensive. (T. Miyazaki et al., 2012; Pouliot & Kusuma, 2013; Pouliot et al., 2002) With the intention of overcoming this task, Laminin-511 proteins were fragmented to identify the smallest integrin-binding component.

Laminin E8 fragments are truncated proteins that combine the C-terminal portions of the alpha (α), beta (β), and gamma (γ) chains to form a single shorter protein. However, these simplified proteins still contain the integrin-binding facility, which includes the laminin-globular 1-3 domains of the alpha (α) chain and the glutamate residue in the gamma (γ) chain's C-terminal tail, but they lack the other functions, such as the heparin-and-heparan sulphate binding activity. (Deutzmann et al., 1990; Taniguchi et al., 2009) Thus, although LM511-E8 is substantially smaller (~150 kDa) than the full-length protein (~800 kDa), it serves as a functionally minimal form of

LM511 and retains the key characteristics of the full-length protein including integrin-binding and dystroglycan binding sites that support adhesion and migration. (Doi et al., 2002; Kumai et al., 2019; T. Miyazaki et al., 2012; Y. Sugawara et al., 2019) Recent studies demonstrated that in biosynthetic scaffold-based approaches for corneal epithelial tissue engineering, LM511-E8 supported human corneal epithelial keratinocyte regeneration with an efficacy similar to that of full-length LM511 and LM521. (Aumailley, Nurcombe, Edgar, Paulsson, & Timpl, 1987; Okumura et al., 2015; N. Polisetti et al., 2017). Furthermore, laminin 511 E8s play an important in HCEC growth with the same results that have been treated with full-length laminin. (Okumura et al., 2015)

Laminin proteins interact with integrin proteins to activate key focal adhesion proteins like Talin, Vinculin, Paxillin, and FAK. These mechanisms will next activate actin and keratin organisation, which will promote cell motility and epithelialisation. (Hohenester & Yurchenco, 2013; T. Miyazaki et al., 2012) The most LM- integrins binding receptors are α3β1, α6β1 or α6β4, different in cell type and function of those cells (Koivisto et al., 2014; Yazlovitskaya et al., 2019) LM511 has been widely studied, and the E8 portion in particular contains high-affinity cell surface receptor binding sites, including that for integrin α6β1, enhances the human pluripotent stem cell adhesion, and accelerates the migration of human limbal melanocyte via FAK. (DiPersio, Zheng, Kenney, & Van De Water, 2016; Januszyk et al., 2017; Takamichi Miyazaki et al., 2012; Y. Sugawara et al., 2019; Takizawa et al., 2017) As a result, laminin E8 components serve as a small form that performs the function of interacting with integrin α6β1 (Fig. 21).
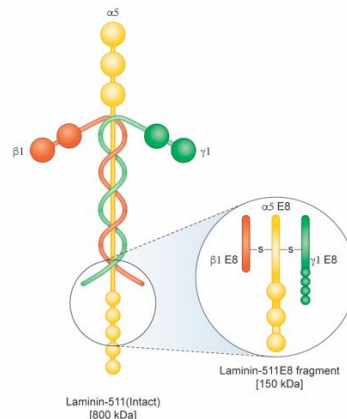
Figure 21. Structure of Laminin 511 E8 fragment

Thus, LM-E8s serve as a functionally reduced form of the LM 511 while retaining its full integrin-binding capacity. Therefore, using this smaller fragment may be sufficient for the effective treatment of burn wounds and have benefits over the full-sized protein in terms of future manufacturing scale-up and therapeutic delivery.

Keratin or cytokeratin plays the role of a skeleton of cells that are used as a support framework and help in cell migration and proliferation. (Coulombe & Lee, 2012; P. Xu et al., 2020) Keratin 10 is essential in increasing the migration of keratinocytes cell in the upper layer. (Fuchs, Esteves, & Coulombe, 1992; Laskin et al., 2020) Furthermore, Keratin 14 is important for increasing basal keratinocyte migration and proliferation. (Y. Chan et al., 1994; Coulombe et al., 1991; Rouabhia et al., 2020; Velez-delValle, Marsch-Moreno, Castro-Muñozledo, Galván-Mendoza, & Kuri-Harcuch, 2016) These keratins are then used to monitor the progress in wound healing and epithelialisation. (T. Chan et al., 2002; Liovic et al., 2009; Watt, 2002; Yoon & Leube, 2019)

Consequently, I proposed that recombinant LM511-E8 repairs tissues in burn wounds and possesses the ability to promote wound closure and epithelialization at the
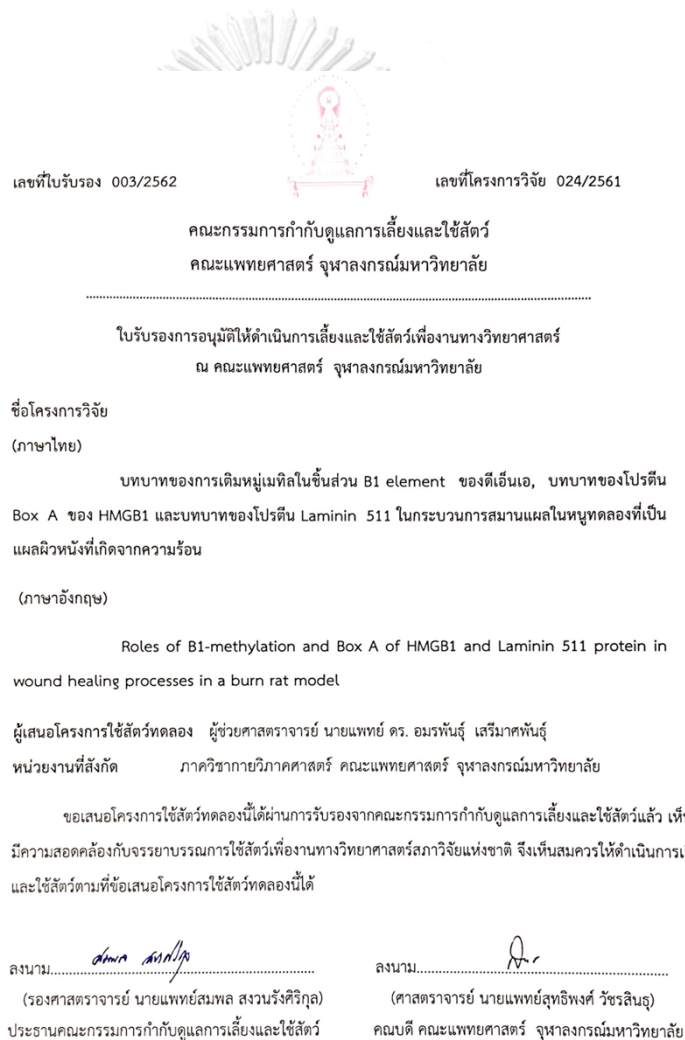
wound edge. Furthermore, this knowledge can be applied to tissue engineering and clinical trials.

Chapter 3. MATERIALS AND METHODS

Ethics

The thesis was focused on bio-specimens and animal studies. As a result, this study proposal was submitted to the Institutional Review Board from the Faculty of Medicine of the Chulalongkorn University, Thailand. The proposals, which were marked 003/62 and 753/62, were approved by the Ethics Committee. All procedures were carried out in accordance with the Declaration of Helsinki's principles (7th version) (Fig. 22-23).

เลขที่ใบรับรอง 003/2562   เลขที่โครงการวิจัย 024/2561

คณะกรรมการกำกับดูแลการเลี้ยงและใช้สัตว์
คณะแพทยศาสตร์ จุฬาลงกรณ์มหาวิทยาลัย

ใบรับรองการอนุมัติให้ดำเนินการเลี้ยงและใช้สัตว์เพื่องานทางวิทยาศาสตร์
ณ คณะแพทยศาสตร์ จุฬาลงกรณ์มหาวิทยาลัย

ชื่อโครงการวิจัย
(ภาษาไทย)

บทบาทของการเติมหมู่เมทิลในชิ้นส่วน B1 element ของดีเอ็นเอ, บทบาทของโปรตีน Box A ของ HMGB1 และบทบาทของโปรตีน Laminin 511 ในกระบวนการสมานแผลในหนูทดลองที่เป็นแผลผิวหนังที่เกิดจากความร้อน

(ภาษาอังกฤษ)

Roles of B1-methylation and Box A of HMGB1 and Laminin 511 protein in wound healing processes in a burn rat model

ผู้เสนอโครงการใช้สัตว์ทดลอง   ผู้ช่วยศาสตราจารย์ นายแพทย์ ดร. อมรพันธุ์ เสรีมาศพันธุ์
หน่วยงานที่สังกัด   ภาควิชากายวิภาคศาสตร์ คณะแพทยศาสตร์ จุฬาลงกรณ์มหาวิทยาลัย

ขอเสนอโครงการใช้สัตว์ทดลองนี้ได้ผ่านการรับรองจากคณะกรรมการกำกับดูแลการเลี้ยงและใช้สัตว์แล้ว เห็นว่ามีความสอดคล้องกับจรรยาบรรณการใช้สัตว์เพื่องานทางวิทยาศาสตร์สภาวิจัยแห่งชาติ จึงเห็นสมควรให้ดำเนินการเลี้ยงและใช้สัตว์ตามที่ข้อเสนอโครงการใช้สัตว์ทดลองนี้ได้

ลงนาม...................................   ลงนาม...................................
(รองศาสตราจารย์ นายแพทย์สมพล สงวนรังศิริกุล)   (ศาสตราจารย์ นายแพทย์สุทธิพงศ์ วัชรสินธุ)
ประธานคณะกรรมการกำกับดูแลการเลี้ยงและใช้สัตว์   คณบดี คณะแพทยศาสตร์ จุฬาลงกรณ์มหาวิทยาลัย

Figure 22. Animal ethics approval certification

COA No. 170/2020

IRB No. 753/62

INSTITUTIONAL REVIEW BOARD

Faculty of Medicine, Chulalongkorn University

1873 Rama 4 Road, Patumwan, Bangkok 10330, Thailand, Tel 662-256-4493

Certificate of Approval

The Institutional Review Board of the Faculty of Medicine, Chulalongkorn University, Bangkok, Thailand, has approved the following study which is to be carried out in compliance with the International guidelines for human research protection as Declaration of Helsinki, The Belmont Report, CIOMS Guideline and International Conference on Harmonization in Good Clinical Practice (ICH-GCP)

Study Title	: Alterations in the Alu methylation pattern in burn scar.
Study Code	: -
Principal Investigator	: Jiraroch Meevassana, M.D.
Affiliation of PI	: Department of Anatomy, Faculty of Medicine, Chulalongkorn University.
Review Method	: Expedited
Continuing Report	: At least once annually or submit the final report if finished.

Document Reviewed :

1. Research Proposal Version 2.0 Date 20/1/2020
2. Protocol Synopsis Version 2.0 Date 20/1/2020
3. Information sheet for research participant Version 2.0 Date 20/1/2020
4. Informed consent for participating volunteers Version 3.0 Date 6/2/2020
5. Case Record Form (CRF) Version 1.0 Date 3/11/2019

Figure 23. Human ethics approval certification

Part A: B1 siRNA

Alu methylation in burn scar: study design, sample size, and population

This study was an analytical cross-sectional study. The G*Power 3.1 program was used with an independent sample t-test to calculate the sample size. (Franz Faul, Erdfelder, Buchner, & Lang, 2009; F. Faul, Erdfelder, Lang, & Buchner, 2007) The 46 Thai participants were patients who required surgical treatment and visited the plastic and reconstructive surgery clinic at King Chulalongkorn Memorial Hospital from 2019 to 2021. The complete medical record was examined by the surgeon before excision, and physical examination was performed to make a diagnosis and evaluate hypertrophic scars. The research only included patients who met the following criteria: age >18 years, surgery needed to correct scar contracture, and no previous surgery at the biopsy sites. Exclusion criteria for both groups were low quality or quantity of DNA from the tissue or blood samples or other (chronic) diseases. The 23 patients in the control group were healthy and required surgical excisions of the skin, such as upper and lower blepharoplasty, mastectomy, and abdominoplasty. The 23 patients in the hypertrophic scar group were post-burn patients who required surgical correction of scar complications, such as scar contracture, joint contracture, or nerve compression. Table 1 shows the demographics of patients with hypertrophic scars and healthy controls.

Sample group	Sex	Age (years)
	(Male/Female)	(Mean ± SD)
Normal controls (n = 23)	5/18	42 ± 21
Burn scar (n = 23)	18/5	36± 14
Burn type	No	Percent
Flame burn	17	74
Scald burn	2	8.6
Chemical burn	2	8.6
Electrical burn	2	8.6
Percent burn	No	Percent
1–20%	5	21.7%
21–40%	8	34.7%
61–80%	3	13.0%
Time to injury	No	Percent
1–6 months	6	26.1%
7-12 months	14	60.9%
13-18 months	2	8.7%
19-24 months	1	4.3%

Table 1. Patient demographic data; SD: standard deviation

Blood and tissue samples

Ethylenediaminetetraacetic acid (EDTA) blood samples (23 samples each from healthy normal controls and patients with hypertrophic scars) and tissue samples (23 samples each from normal skin and from hypertrophic scars) were obtained. None of the patients received systemic or topical therapies for at least one month before the collection of the tissue samples. Three milliliters of peripheral blood was collected and stored in an EDTA tube at 4°C. The biopsy skin was cut to roughly 0.5–1 cm^2 and maintained in Dulbecco's Modified Eagle Medium (10 mg/mL gentamycin and 10,000 U/mL penicillin) to preserve the tissues before extraction of DNA.

DNA preparation

The QIAamp® DNA Mini Kit was used to extract DNA from tissue samples after the tissues were washed with 1X PBS (Qiagen, Germany). The tissue samples

were diced into tiny pieces and lysed by mixing ATL buffer with proteinase K, vortexing, and incubating at 60°C until lysis occurred. The DNA was precipitated by adding 200 µL of AL buffer, mixing for 15 s followed by incubation at 70°C for 10 min. Before transferring the mixture to the QIAamp Mini spin column, 200 µL of ethanol (96–100%) was added and vortexed for 18000 rpm for 1 min. After washing spin column twice and eluting it with buffer AE, the eluate was moved to a 1.5 mL tube. The extracted DNA was stored at 4°C until combined bisulfite restriction analysis (COBRA) was performed.

White blood cells (WBCs) were isolated from whole blood. The blood in EDTA tubes (Nipro, Japan) was centrifuged at $700 \times g$ for 15 min to separate the layers. The buffy coat layer was collected from the interface layer. Red blood cells (RBC) were discarded with RBC lysis solution (Qiagen, Germany) at a ratio of 1:20 and centrifuged at $700 \times g$ for 20 min. The upper part fluid was then removed, rinsed with 1X PBS and centrifuged twice at $700 \times g$ for 20 min at room temperature. Then, 20 µL of proteinase K (20 ng/mL) (USB, OH, USA) and 500 µL of lysis buffer II (0.75 M NaCl, 0.024 M EDTA at pH 8, and 10% SDS) were mixed. WBCs were maintained overnight at 50°C. DNA was extracted from WBCs with QIAamp® DNA Mini Kit.

Alu COBRA

COBRA analysis was used to determine the amounts of methylation present in DNA isolated from tissue and blood samples. An EZ DNA methylation-gold kit was used to execute the bisulfite conversion process (Zymo Research, Orange, CA, USA). The bisulfite transforms DNA using Alu primers in a polymerase chain reaction (PCR) (Table. 2).

Forward primer	5′-GGYGRGGTGGTTTAYGTTTGTAAA-3′
Reverse primer	5′-CTAACTTTTTATATTTTTAATAAAAACRAAATTTCACCA-3′

Table 2. Alu repetitive sequence primer

For the PCR, the following conditions were used: initial denaturation at 95°C for 15 min, 35 cycles of denaturation at 95°C for 45 s, annealing and extension at 57°C for 45 s and at 72°C for 45 s for extension PCR process, and at 72°C for 7 min for the final extension. The digest TaqI and TasI enzymes (Thermo Scientific, MA, USA) were used to digest the PCR products and were maintained at 65°C for 16 h. Subsequently, 8% polyacrylamide gel electrophoresis was used to determine the amount of methylation in the samples. The bands were determined utilising the Azure300 Gel Imaging System in conjunction with the AzureSpot 2.0 software (Azure Biosystem Inc., Dublin, CA, USA).

Methylation analysis

The results of the COBRA were allocated into four groups via the methylation status of two (cytosine-phosphate-guanine) CpG sites from the 5′ to the 3′ ends of the Alu DNA: methylation at both CpGs (mCmC), unmethylation at both CpGs (uCuC), 5′ methylated and 3′ unmethylated CpGs (mCuC), and 5′ unmethylated (uCmC). The DNA parts after enzymatic digestion were quantified and consisted of 43, 32, and 58 bp parts for the $^mC^mC$ group, a 133 bp part for the $^uC^uC$ group, 43 and 90 bp parts for the $^mC^uC$ group, and 75 and 58 bp parts for the $^uC^mC$ group (Fig 24).
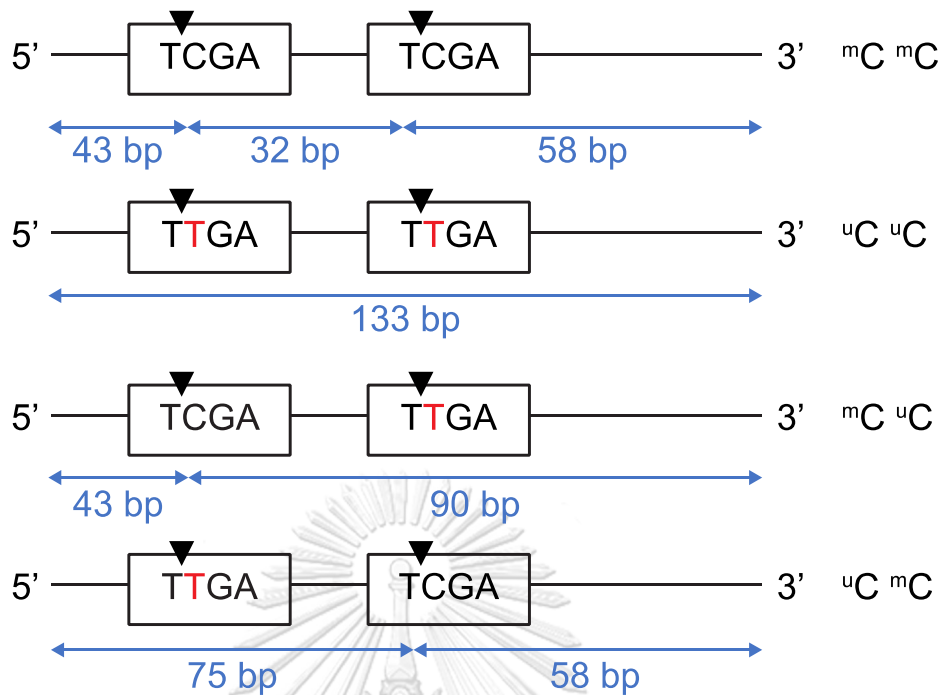
Figure 24. The patterns of Alu parts of methylation

To conduct Alu methylation analysis, the band intensities of the six Alu product sizes were calculated according to the following DNA length: (133 bp, 90 bp, 75 bp, 58 bp, 43 bp, and 32 bp). A = band intensity of 133 bp/133; B = band intensity of 58 bp/58; C = band intensity of 75 bp/75; D = band intensity of 90 bp/90; E = band intensity of 43 bp/43; and F = band intensity of 32 bp/32. Alu methylation was calculated as follows:

Alu total methylation level (%mC) (Equation 1) = ([B + E]/[2A + B + C + D + E]) × 100

$\%\,^{m}C^{m}C = (F/[A + B + C + D + F]) \times 100$

$\%\,^{m}C^{u}C = (D/[A + B + C + D + F]) \times 100$

$\%\,^{u}C^{m}C = (C/[A + B + C + D + F]) \times 100$

$\%\,^{u}C^{u}C = (A/[A + B + C + D + F]) \times 100$

$$\text{Alu total methylation level (\%mC)} = \frac{(B + E) \times 100}{2A + B + C + D + E}$$

Equation 1. Alu total methylation level (%mC)

Cells and cell culture

Rat epidermal keratinocytes (REKs) and rat dermal fibroblast (RDF) (Cell Applications) were cultured in Dulbecco Modified Eagle's Medium (DMEM) with 10% FBS. Cells were kept at 37°C in an incubator supplied with 95% air and 5% CO_2. The cells were cultured in T-75 Corning™ U-shaped cell culture flasks and harvested at a confluency of ~80% using 0.05% Trypsin-EDTA (Thermo Fisher Scientific, Inc.). Cells were then cultured in 12 wells plate at a density of 1×10^4 cells. The cells at 80–90% confluency were subjected to induce burns by boiling in digital water bath at various temperatures. The cells at 80–90% confluency were divided into four groups and transfected to measure the methylation level: normal saline solution (NSS; 100 µL), calcium phosphate (Ca-P) nanoparticles, 150 nM scramble siRNA in 100 µL of a solution containing Ca-P nanoparticles, or 150 nM B1 siRNA in 100 µL of a solution containing Ca-P nanoparticles. (Fernandes et al., 2014; Kerschbaum, Wegrostek, Riegel, & Czerny, 2021; Mahmood, 2016)

Quantitative combined bisulfite restriction analysis for B1 element (COBRA B1)

A total of 1 µL bisulfited DNA by EZ DNA methylation-gold™ kit was subjected to 45 cycles with the PCR mastermix™ (Thermo Scientific, MA, USA) under

the following thermocycling conditions: 95˚C for 15 min; 40 cycles at 95˚C for 45 sec, 53˚C for 45 sec and 72˚C for 45 sec; 72˚C for 10 min for final extension steps using the primer as Table 3.

Forward primer	5'-YGYAYGYYTTTAATYYYAGYAAT-3'
Reverse primer	5'- CCCTRRCTRTCCTRRAACTCAC-3'

Table 3. B1 repetitive sequence primer

Primers were designed using Primer 3 version 4.1.0 (Untergasser et al., 2012; Natalia A. Veniaminova et al., 2007) (Fig. 25). The amplified PCR DNA was separated with two units of Taq1 and Tas1 enzyme in NE buffer II (Thermo Fisher Scientific, Inc.) at 37˚C 24 h (Fig. 26). Then PCR results were separated using 8% gel non-denaturing polyacrylamide, stained with SYBR (Sigma-Aldrich; Merck KGaA). After enzyme digestion, six products of different lengths were detected after COBRA B1 (98, 78, 54, 44, 34 and 20 bp). The band intensities of the COBRA B1 products were determined using Image Quant version 8.2 (Molecular Dynamics; GE Healthcare).
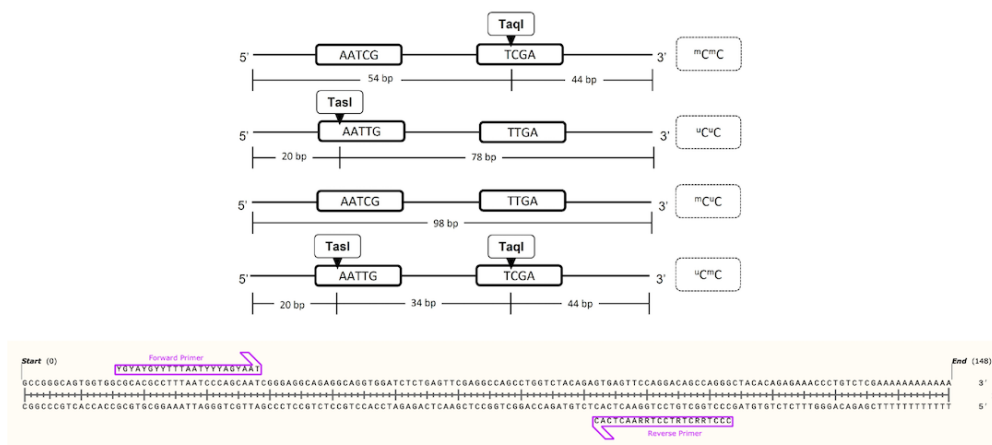
Figure 25. The methylation patterns of B1 detected by COBRA-B1, and the restriction enzyme digest sites
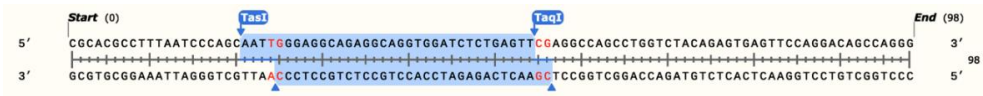
Figure 26. Sequences of B1 repetitive elements in rat and restriction enzymes cutting point (TasI, TaqI)

Sequences of B1 repetitive elements in rats and locations of the Taq1 and Tas1 restriction enzyme sites

According to the B1 analysis and calculations, two types of COBRA B1 products could be classified based on the methylated CpG dinucleotides, namely methylated loci (mC) and unmethylated loci (uC). The percentage of B1 methylation was measured. The B1 sequence has two CpG dinucleotide at 5′ and 3′ ends. B1 loci consisted of two-methylated CpG of B1 sequence ($^{m}C^{m}C$), two-unmethylated CpG of B1 sequence (^{u}C ^{u}C), 5′ methylated and 3′ unmethylated CpG of B1 sequence ($^{m}C^{u}C$) and 5′ unmethylated and 3′ methylated CpGs ($^{u}C^{m}C$). The intensity of each part was divided by the amplicon length in terms of bp, resulting in the following scores: %98/98 = A, %78/74 = B, %54/54 = C, %44/42 = D, %34/34 = E, and %20/20 = F (Fig 27).

Subsequently, the %methylation was measured using the following formula:

% total methylation (%mC) = $100 \times (A + C + D)/2A + 2B + 2D$ (Equation 2). As an internal control, 25% methylated rat genomic DNA (EpigenDX) was used for the experiments and inter-assay adjustment (Fig. 28).
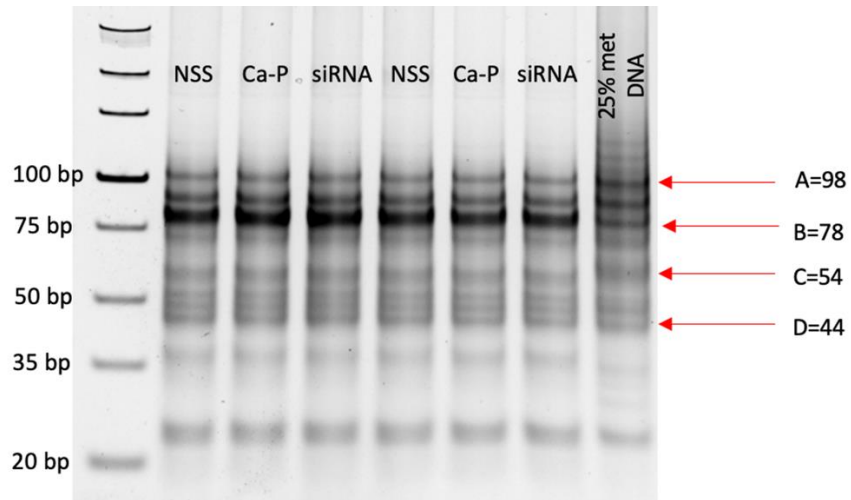
Figure 27. Polyacrylamide gel electrophoresis after cleavage with Taq1 and Tas1 restriction enzyme
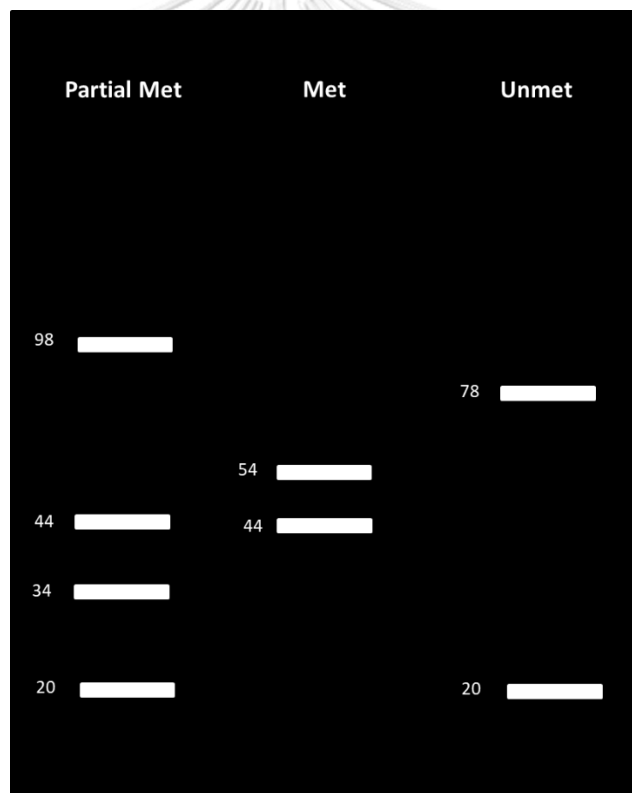
Figure 28. Simulated polyacrylamide gel electrophoresis after cleavage with Taq1 and Tas1 restriction enzyme

$$\text{B1 total methylation level (\%mC)} = \frac{(A+C+D) \times 100}{(2A) + (2B) + (2D)}$$

Equation 2. The level of B1 methylation

Animal Study and Experimental Design

A total of 45 eight-week-old male Wistar rats were obtained from Namura Animal Company (Bangkok, Thailand). Rats were acclimated for 7 days under a controlled normal light/dark cycle, standard fed and provided *ad libitum* access to water. To create second-degree burns, the rats were anaesthetised with 2% isoflurane (Sigma-Aldrich; Merck KGaA) (Marquardt et al., 2018), and the dorsal skin was shaved. Two burn wounds were created on the back of each rat using a 10-mm-diameter aluminium rod, which was heated to 100˚C and placed on the skin for 10 s. (Cai et al., 2014) The rats were allocated to three groups. NSS (100 µL), Ca-P nanoparticles, or 150 nM B1 siRNA in 100 µL of a solution containing Ca-P nanoparticles was applied daily to each wound on the rats in the control and treatment groups.

The wounds of three animals in each group (a total of six) were imaged on days 0, 7, 14, 21, and 28 after injury, and the wound areas were calculated using ImageJ program 1.52t with a freehand selection tool. Wound areas are reported as a percentage of the initial wounded area (Equation 3).

$$\% \text{ Wound contraction rate} = \frac{(\text{Wound area day 0} - \text{Wound area day n})}{\text{Wound area day 0}} * 100$$

Equation 3. Formular to calculate wound contraction rate

On day 28, the rats were euthanised by exposing them to 5% isoflurane for 5–10 min until respiration ceased, and they were confirmed dead. (Cai et al., 2014) For 12 animals in each group (a total of 24 wounds), three rats (a total of six wounds) were euthanised with 5% isoflurane on days 3, 7, 14, and 21. On each of the specified euthanasia days, wound tissues were excised, and three of these samples (from the initial six wounds) were subjected to the DNA extraction process and measured to determine the methylation levels. The remaining three wound samples were subjected to 10% neutral-buffered formalin for fixation at room temperature (28–30ºC) for at least 48 h and subsequent embedding in paraffin for pathological examination (Fig. 29).

In this study use of one-way analysis of variance (ANOVA) by program G*Power 3.1 was used to calculate sample size, power = 0.95, effect size f = 0.8, alpha error = 0.05 number of groups = 3. The results revealed 90 wounds; 45 rats were used for this experiment. (F. Faul et al., 2007)
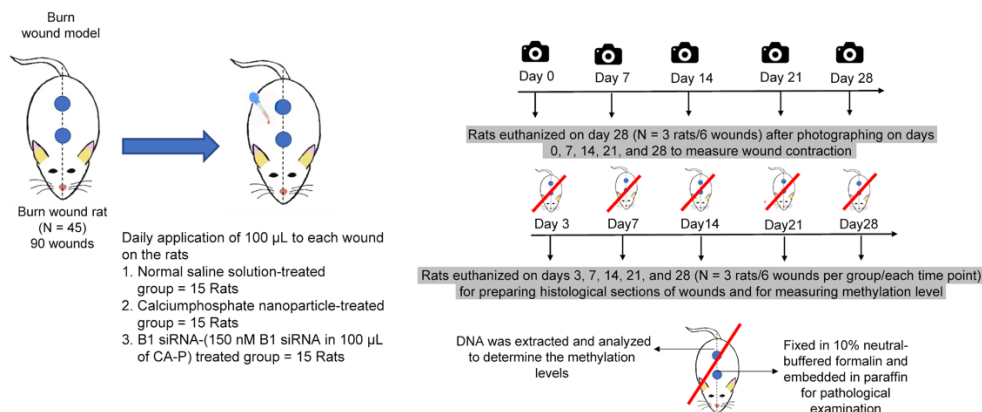
Figure 29. Integrated experimental design. siRNA, small interfering RNA

Two wounds of the second-degree burns were produced on the back using a 10 mm aluminium rod heated to 100°C (Fig. 30-31). (Cai et al., 2014). They were further divided into three groups and treated with

1. NSS-treated group (negative control) = 30 wounds

2. Ca-P nanoparticle-treated group (control group) = 30 wounds

3. B1siRNA-B1-treated group = 30 wounds
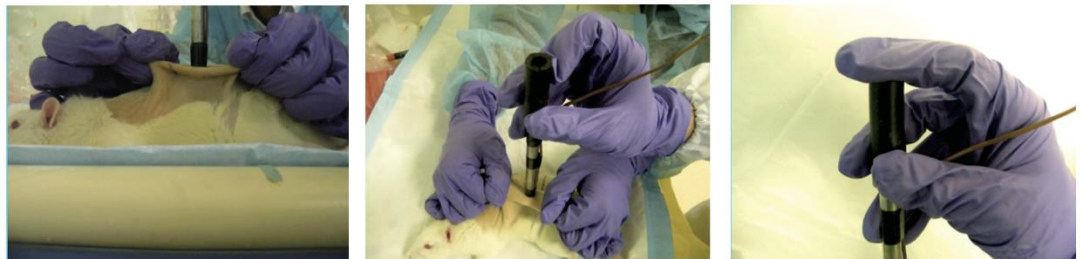
Figure 30. Creation of second-degree burn wounds at the dorsum of rats
using a 10 mm aluminium rod heated to 100°C (Cai et al., 2014)
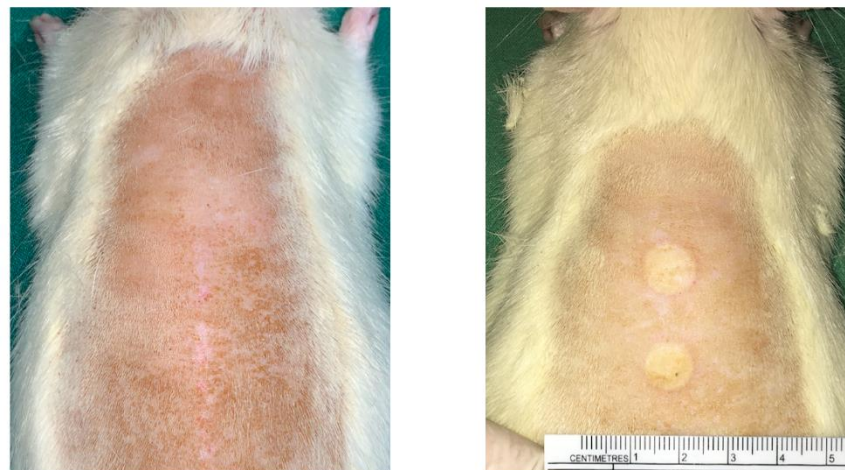
Figure 31. Before and after creation of second-degree burn wound

siRNA delivery system

The B1 siRNAs—5′-CGCACGCCUUUAAUCCCAGCACUCGUU-3′ and 5′-CGAGUGCUGGGAUUAAAGGCGUGCGUU-3′—and scrambled siRNA were

purchased from Bioneer, Inc. The siRNA sequences were designed using siRNA wizard software version 3.1 (InvivoGen).

The day before transfection, 5×10^4 REK cells/well were growth in a 24-well plate. Then the medium from each well in the control and experiment groups was replaced with 150 nM of B1 siRNA in 100 µL CA-P nanoparticles, 150 nM of scramble siRNA in 100 µL CA-P nanoparticles, 100 µL of Ca-P nanoparticles, and 100 µL of NSS and incubated for 48 h at 37˚C.

To deliver siRNAs to target cells, the siRNAs were coated with a nanoparticle solution before topical administration on the burn wounds. The most effective siRNA: nanoparticle solution ratio was 150 nM B1 siRNA in 100 µL Ca-P nanoparticles. (Patchsung et al., 2018; Wu et al., 2015; D. Zhao, Wang, Zhuo, & Cheng, 2014)

First, B1 siRNA was mixed with an appropriate proportion and concentration of calcium solution (MilliporeSigma). Next, the B1 siRNA-calcium complex was added to a mixture of sodium carbonate (Na_2CO_3; MilliporeSigma) and sodium dihydrogen phosphate monohydrate ($NaH_2PO_4 \cdot H_2O$; MilliporeSigma). After the B1 siRNA-coating process, the nanoparticle-coated B1 siRNAs were stored at room temperature (28–30˚C) until use. The media was composed of 50 µL of a mixture containing 0.5 M calcium chloride ($CaCl_2$) solution (MilliporeSigma) and 150 nM B1 siRNA + 50 µL of a mixture of 0.01 M Na_2CO_3 solution (MilliporeSigma) and 0.01 M $NaH_2PO_4 \cdot H_2O$ solution (MilliporeSigma). A 31:1 molar ratio of CO_3^{2-}:PO_4^{3-} was used. The B1 siRNA was mixed with 16 µL of 0.5 M $CaCl_2$ solution and adjusted to a final volume of 50 µL using sterile dH_2O. Thereafter, the B1 siRNA-calcium complex was added to 50 µL of a mixture of Na_2CO_3 solution and $NaH_2PO_4 \cdot H_2O$ solution (16 µL) and 34 µL sterile dH_2O. (D. Zhao et al., 2014) All steps in the preparation of the nanoparticle solution

were performed under sterile conditions. Each nanoparticle solution preparation was used to confirm the transfection efficiency with rat dermal keratinocytes (Cell Applications) prior to each experiment. (Mostaghaci, Loretz, & Lehr, 2016; Wu et al., 2015; Xie, Chen, Sun, & Ping, 2013; X. Xu, Li, Zhao, Keen, & Kong, 2016)

Histopathology and immunohistochemistry

Formalin-fixed wound tissues were dehydrated and embedded in paraffin; subsequently, 3-µm-thick sections were prepared using a microtome. Hematoxylin and eosin (H&E) staining was performed for scoring. Immunohistochemical staining of the tissue sections was performed using monoclonal antibodies against γH2AX (dilution 1:100, Ab2893; Abcam, Cambridge, MA, USA) and 8-OHdG (dilution 1:100, Ab48508; Abcam). (F. Wang, Zieman, & Coulombe, 2016)

The histological sections of the wounds were graded using a histopathological scoring system, following a previously published method, with some modifications. (Edraki et al., 2014; Tanideh et al., 2014) Three dermatopathologists who were blinded to the treatment regime independently performed H&E scoring, based on five criteria: epithelialization, polymorphonuclear leukocyte (PMNL) infiltration, collagen formation, number of fibroblasts, and presence of new blood vessels. A score of zero was assigned for no evident epithelialisation and no increase in the number of fibroblasts, PMNLs, or new blood vessel formation. A score of one demonstrated a raised thickness of the epithelial tissue sections, or the few fibroblasts present, PMNLs, and blood vessel formation. A score of two showed epithelisation, or the presence of a moderate number of fibroblasts, PMNLs, and blood vessels. A score of three demonstrated epithelial movement to the centre of the wound and the presence of many fibroblasts, PMNLs, and blood vessels. A score of four was assigned to sections

showing complete regeneration of the epithelium, or the presence of excessive fibroblasts, PMNLs, and blood vessels. The mean of the scores provided by the three scorers were determined and combined to obtain an overall pathology score. Sections positive for anti-cytokeratin immunohistochemical staining were scored similarly by three dermatopathologists, scoring the sections on a scale of 0 to 4, starting from no staining to strong staining.

Statistical analysis

The Shapiro–Wilk test was used to identify how the data was distributed. The methylation status of the two independent groups (two-tailed t-test) was compared. The mean and standard deviation are presented for the data. An examination of the receiver operating characteristic (ROC) of Alu methylation status was carried out in order to determine if it was capable of distinguishing between hypertrophic scar and normal control. To compare the groups where the data was normally distributed, a one-way ANOVA and Bonferroni post-hoc corrections were applied. When data was not normally distributed, a Kruskal–Wallis followed by a Dunn's post-hoc test was performed to determine the differences between groups. In order to conduct the statistical analyses, GraphPad Prism version 9.0.0 (GraphPad Software, Inc.) was utilised. A statistically significant difference was determined to exist when the P value was less than 0.05.

Part B: Box A of HMGB1 protein

Construction of HMGB1-BOXA plasmids

The Box A of HMGB1 plasmid was customised by Addgene (Cambridge, MA, USA) containing a FLAG sequence driven by cytomegalovirus (CMV) promoter. The 350 nucleotides of Box A of the HMGB1 sequence were inserted into pcDNA 3.1(+) plasmid backbone vector (plasmid size 5.4 kb) which contained the ampicillin-resistant gene as an antibiotic selective marker. The Box A of HMGB1 sequence (350 nucleotides) was inserted into the pLenti-C-mGFP-P2A-Puro backbone vector (plasmid size 7.5 kb). The Box A-GFP plasmid consists of a chloramphenicol-resistant gene providing a potential selective marker in a plasmid preparation process. Each plasmid was amplified in *Escherichia coli* (DH5) cells (Invitrogen, USA). The plasmid was extracted with Plasmid Maxiprep Kit (Thermo Scientific, MA, USA) following the manual. Then the plasmids were determined the purity and the absorption using the Thermo Scientific™ NanoDrop 2000 spectrophotometer. The HMGB1-BOXA plasmids were proved sequences before the experimental studies.

Plasmid preparation

Each type of plasmid (Box A of HMGB1 plasmid and pcDNA 3.1(+) plasmid control) was transformed into *E. coli* competent cell DH5-α (Invitrogen, USA) following a conventional chemical transformation protocol (Sambrook JF. et al, 2002). The transformant *E. coli* were cultured on the Luria-Bertani (LB) agar with ampicillin-containing. After overnight incubation at 37℃, a single isolated colony of transformant was selected and transferred to 5 mL of LB broth with appropriate antibiotics as a starter culture. Then, a starter culture of a single colony was maintained by shaking at 37℃ at 220 rpm for 8 h. After incubation, the starter culture was inoculated into 250 mL of LB

broth containing ampicillin (ratio 1:1,000) and further maintained in a shaker at 220 rpm for 16–18 h at 37℃. The optical density was measured using the Asys UVM 340 spectrophotometer (Biochrom, MA, USA) to estimate the rate of bacterial growth until the optical density reached 2–3.

To harvest the transformant *E. coli*, culture media was centrifuged at $6,000 \times g$ for 10 min, and the supernatant was discarded. The plasmid was extracted using Plasmid Maxiprep Kit (Thermo Scientific, MA, USA) as per the manufacturer's instructions. The amount of plasmid was determined using the Thermo Scientific™ NanoDrop 2000 spectrophotometer. The plasmid in each preparation was sequenced and aligned with each original plasmid sequence to confirm the accuracy of the plasmid sequence. After plasmid sequencing, plasmids were pooled and stored at -20℃ until further use.

Plasmid delivery by nanoparticle coating system

The plasmids were coated with Ca-P nanoparticles before the topical administration to the wound burn model. The most effective ratio is 5% concentration of plasmid in Ca-P nanoparticle solution. (Cao et al., 2011; Mostaghaci et al., 2016; X. Xu et al., 2016)

First, plasmid DNA was mixed in an appropriate proportion and concentration of 0.5 M $CaCl_2$ solution (Merck Millipore, USA), a plasmid DNA-binding reagent. Second, the plasmid DNA-calcium complex was further added to the solution of 0.01 M sodium carbonate (Na_2CO_3, Merck Millipore, USA) and 0.01 M sodium dihydrogen phosphate monohydrate ($NaH_2PO_4 \cdot H_2O$, Merck Millipore, USA). After the coating process, nanoparticle-coated plasmid DNA was stored at 25℃ until further use. (D. Zhao et al., 2014)

All steps of nanoparticle solution preparation were performed under sterile conditions. Each preparation of nanoparticle solution was validated using the transfection efficiency of nanoparticle solution after coating transfection into the rat 3T3 cell line.

High-molecular-weight (HMW) DNA preparation for EDSB-LMPCR

HMW DNA was prepared for the initial step with 1% low-melting-point agarose, lysed and digested in 400 µL of 1 mg/mL protein kinase K, 50 mM Tris, pH 8.0, 20 mM EDTA, and 1% sodium lauryl sarcosine. Then, the agarose plugs were washed with PBS buffer for 40 min. To polish cohesive-end EDSBs, T4 DNA polymerase (New England Biolabs) was added, and the modified ligation-mediated PCR (EDSBLMPCR LONG and SHORT) linkers were ligated to HMW DNA (Table 4). Then DNA was extracted from the agarose plugs using a QIA quick gel extraction kit.

EDSBLMPCR LONG	5′-AGGTAACGAGTCAGACCACCGATCGCTCGGAAGCTTACCTCGTGGACG-3′
EDSBLMPCR SHORT	5′-ACGTCCACGAG-3′

Table 4. EDSBLMPCR linker sequence

B1 element primer	5′-AATCCGCCTGCCTCTGCCTCC-3′
The linker primer	5′-AGGTAACGAGTCAGACCACCGA-3′
Taq man probe (6FAM)	(6FAM) ACGTCCACGAGGTAAGCTTCCGAGCGA(TAM)

Table 5. EDSBLMPCR primer

Real-time PCR was performed using two PCR primers The B1 element primer was binding to the B1 repetitive sequence, and the linker primer was binding with the sequence as the 5′ end of the ligation linker (Table 5). The number of EDSBs could be measured by TaqMan probe homology to the 3′ end of the linker sequence. The dark blue and vertical dashed lines show genomic DNA with EDSB end. The red parallel line shows the linker sequences. The light blue line shows the B1 elements that are B1 repetitive sequences. The green and red arrows show the forward and reverse primers. The purple line is TaqMan probe (Fig. 32). The PCR components were composed of 1X of TaqMan^{TM} Fast Advance Master Mix (Applied Biosystems, CA, USA), 0.5 U of HotStarTaq DNA polymerase (Quigen, Hilden, Germany), 0.3 mM of probe homologous   with   3′-linker sequence(6FAM)ACGTCCACGAGGTAAGCTTCCGAGCGA   (TAM)(phosphate), 0.5 mM of rat B1 repetitive sequences primer, 5′-AATCCGCCTGCCTCTGCCTCC-3′. Control DNA was cut by EcoRV (New England Biolab) and ligated with linkers to build the standard curve. The PCR cycles were set as follows: 1 cycle of 50°C for 2 min followed by 95°C for 10 min and 60 cycles of 95°C for 15 sec along with 60°C for 2 mins. The amount of DNA-GAP PCR in each test was compared to the digested ligated control DNA and reported as the percentage of DNA-GAP PCR amplicons of control DNA. (Schlissel, 1998; Steen, Gomelsky, Speidel, & Roth, 1997)
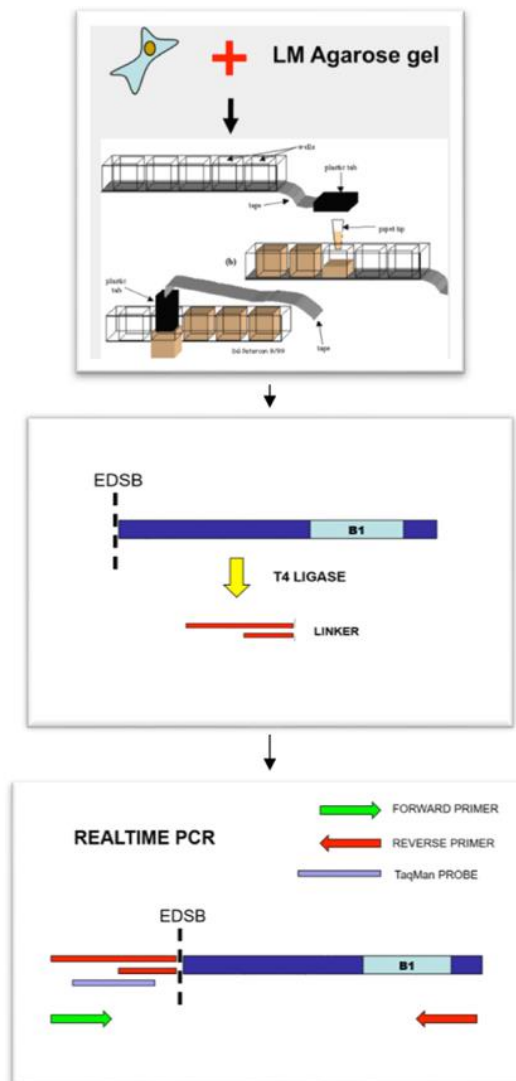
Figure 32. Demonstration of the PHY-RIND-EDSB -detection using real-time PCR

Cells and cell culture

REK (Cell Applications) was cultured in DMEM with 10% FBS. Cells were kept at 37˚C in an incubator supplied with 95% air and 5% CO_2. The cells were cultured in T-75 Corning™ U-shaped cell culture flasks and harvested at a confluency of ~80% using 0.05% Trypsin-EDTA (Thermo Fisher Scientific, Inc.). Cells were then cultured in a 35 mm culture plate at a density of 1×10^4 cells. The cells at 80–90% confluency were subjected to induce burns by boiling in digital water bath at various temperatures. Briefly, cell culture plates were wrapped with paraffin film and placed in a water bath for 10 min when the desired after the required temperature was reached; 37 degrees Celsius, 45 degrees

Celsius, 60 degrees Celsius, 75 degrees Celsius, and 90 degrees Celsius. (Fernandes et al., 2014; Kerschbaum et al., 2021; Mahmood, 2016; Schneider et al., 2021)

Animal Study and Experimental Design

Twenty-four male Wistar rats were purchased from the Namura Animal Center, Thailand. Animals were acclimatised for 1 week before being subjected to second degree burn wounds.

In this study use one-way ANOVA by program G*Power 3.1 was used to calculate the sample size with effect size f = 0.8, alpha error = 0.05, power = 0.95, number of groups = 3. This resulted in 90 wounds on 45 rats used for this experiment. (F. Faul et al., 2007) (Fig. 33)
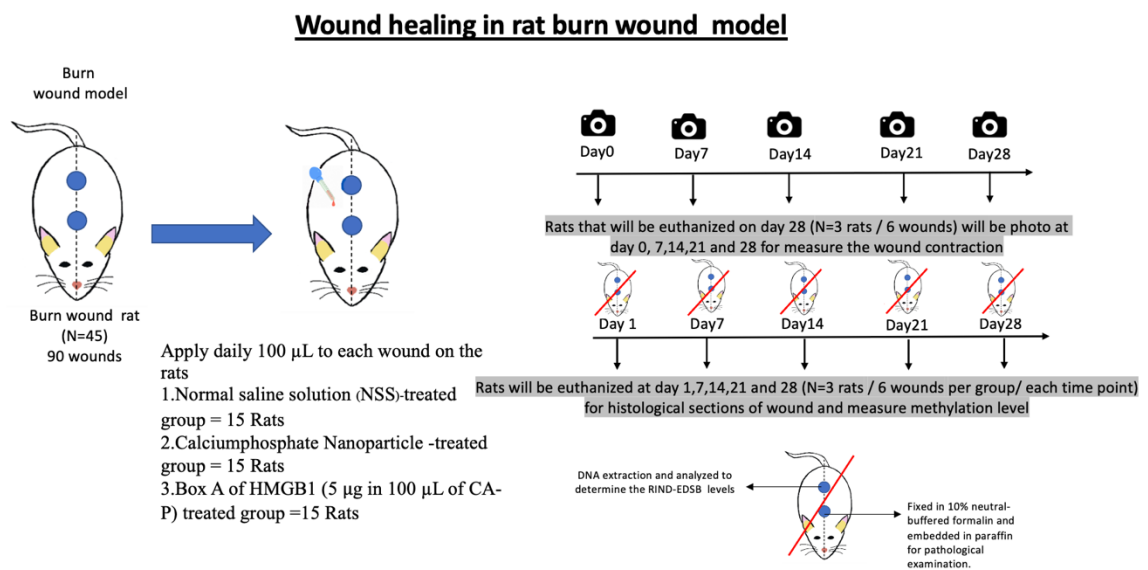
Figure 33. Rats burn wound experiment

Two second degree burn wounds were produced on the rats' dorsum using a 10 mm aluminium rod heated to 100°C (Cai et al., 2014). Rats were further divided into three groups and treated with

1. NSS-treated group (negative control) = 30 wounds

2. Ca-P nanoparticle-treated group (control group) = 30 wounds

3. Box A plasmid-treated group = 30 wounds

Histopathology and immunohistochemistry

Formalin-fixed wound tissues were dehydrated and embedded in paraffin, after which 3-µm-thick sections were prepared using a microtome. H&E staining was performed for scoring. Immunohistochemical staining of the tissue sections was performed using monoclonal antibodies against γH2AX (dilution 1:100, Ab2893; Abcam, Cambridge, MA, USA) and 8-OHdG (dilution 1:100, Ab48508; Abcam). (F. Wang et al., 2016)

The histological sections of the wounds were graded using a histopathological scoring system, following a previously published method, with some modifications. (Edraki et al., 2014) Three dermatopathologists who were blinded to the treatment regime independently performed H&E scoring, based on five criteria: epithelialization, polymorphonuclear leukocyte (PMNL) infiltration, collagen formation, number of fibroblasts, and presence of new blood vessels. A score of zero was assigned when there was no evident epithelialisation and no increase in the number of fibroblasts, PMNLs, or new blood vessel formation. A score of one demonstrated a raised thickness of the epithelial tissue sections, or the few fibroblasts present, PMNLs, and blood vessel formation. A score of two showed epithelisation, or the presence of a moderate number of fibroblasts, PMNLs, and blood vessels. A score of three demonstrated epithelial movement to the centre of the wound and the presence of many fibroblasts, PMNLs, and blood vessels. A score of four was assigned to sections showing complete regeneration of the epithelium, or the presence of excessive fibroblasts, PMNLs, and blood vessels. The mean of the scores provided by the three scorers was determined and combined to obtain an overall pathology score. Sections positive for anti-

cytokeratin immunohistochemical staining were scored similarly by three dermatopathologists, scoring the sections on a scale of 0 to 4, starting from no staining to strong staining. (Edraki et al., 2014; Farghali, AbdElKader, Khattab, & AbuBakr, 2017; Haghdoost et al., 2013; Tavares Pereira Ddos, Lima-Ribeiro, de Pontes-Filho, Carneiro-Leao, & Correia, 2012)

Statistical analysis

The data were expressed as mean ± standard deviation (SD). A one-way ANOVA was performed to test the difference between the groups with normally distributed data, and Kruskal–Wallis test was used with non-normal distribution data. SPSS version 25.0 (SSPS Inc., IL, USA) was used for all statistical analyses. P-value < 0.05 was considered as significant.

Part C: Laminin 511 E8

LAMININ 511 E8

Recombinant laminin-511 E8 fragments are available as iMatrix-511. This product was purchased form Takara Bio Inc. and Nippi, Inc. In this experiment, 2.5 μg of this product was applied per wound every day. (Araki et al., 2009; Malinda et al., 2008)

Cells and cell culture

RDF cells (Cell Applications, San Diego, CA, USA) and REK cells (Cell Biologics, Inc., Chicago, IL, USA) were cultured in DMEM with 10% FBS at 37°C in a humidified atmosphere (95% air: 5% CO_2). The cell lines were grown in 75 cc culture flasks and were harvested at 90% confluence with 0.05% trypsin. The cells were washed with sterile PBS. RDF cells were seeded in 24-well culture plates (5×10^4

73

cells/well), which were then filled with medium and incubated in a CO$_2$ incubator at 37°C.

Wound migration assays

Cells were grown to confluence in 24-well culture plates. Two parallel wounds were made in the monolayer with a 200 µL pipette tip and debris was removed by washing with sterile 1X PBS. Fresh medium with 1.0, 2.5, 5.0, 10, and 25 µg/µL of laminin were added for the experimental groups, and fresh medium without laminin was added for the control group. The wound size after 0, 6, and 24 h in RDF cells and REK cells of the experimental groups and the control group were photographed under a light microscope with 200× magnification.

Experiment on the interaction between laminin and integrin *in vitro*

HaCaT spontaneously transformed human epidermal keratinocytes and REK cells were cultured using DMEM with 10% fetal bovine serum (LabTech, East Sussex, UK).

Fluorescence Microscopy

The following procedure was used to culture REK cells on coverslips prior to their labelling with an immunofluorescent dye: Once the cells were rinsed with PBS, they were fixed with 3.7% paraformaldehyde for 20 min before being permeabilised with 0.5% Triton X-100/PBS for 7 min on a shaker at 25°C to identify integrin receptors. Then, for 2 h at 25°C, non-specific binding was blocked with 5% goat serum in PBS. Subsequently, the coverslips were stained with anti-integrin α6 and β1 primary antibodies at a concentration of 1:200 for 30 min, followed by a secondary antibody at a concentration of 1:500 incubated for 30 min. The coverslips were then washed with

Vectashield with DAPI, sealed with nail varnish, and stored at -20°C for analysis with a confocal microscope (Zeiss LSM 800). (Horzum, Ozdil, & Pesen-Okvur, 2014)

Real-time PCR

Total RNA was extracted using the RNeasy Mini Kit according to the manufacturers' instructions (Qiagen, Hilden, Germany), and concentration was measured using a NanoDrop-1000 spectrophotometer (Peq Lab Biotechnologie, Erlangen, Germany).

Real-time qPCR was performed on the Roche 96 using the SYBR green detection method (New England Biolabs, UK). The PCR reaction was performed in a 100-ng volume containing the Luna® Universal One-Step RT-qPCR Kit (New England Biolabs, UK) and 1 μL of primer mix (10 μM forward primer, 10 μM reverse primer). Primer sequences (IDT DNA) are given in Table 6. (Dingemans et al., 2010; T. Miyazaki et al., 2012) The PCR profile with 40 cycles of 15 s at 95°C and 30 s at 60°C was performed; a melting curve analysis was performed, which consisted of 70 cycles of 10 s with a temperature increment of 0.5 °C/cycle starting from 60 °C. For normalisation of gene expression levels, ratios relative to the housekeeping gene were calculated by the comparative CT method ($\Delta\Delta$CT). (Livak & Schmittgen, 2001) Genes were considered as differentially expressed when their expression levels exceeded a two-fold difference in all specimens analysed. The normalised data uses an average of two housekeeping genes, GAPDH and HPRT1. All experiments were performed in triplicate, and the results were expressed as the means fold change ± SD.

Flow cytometric analysis

Cells were washed with PBS for 2–5 min then detached by 0.05% trypsin/EDTA solution for 5 min. After three washes with blocking buffer (0.1% BSA/PBS), 1×10^5 cells were incubated for 45 min

at 25°C with primary antibodies at 1:100 diluted in blocking buffer. Cells were then rinsed twice with blocking buffer and incubated for 30 min at 25°C with secondary antibodies at 1:500 diluted in blocking buffer. Cells were then rinsed twice with blocking buffer and resuspended in 200 µL of blocking buffer for measurement. Fluorescence intensities were analysed on an Accuri 6™ flow cytometer (Becton Dickinson). The following primary antibodies were used: 1:100; integrin alpha 3 polyclonal antibody (Thermo Fisher), 1:100; integrin alpha 6 (CD49f) monoclonal antibody (Mab-5A) (Thermo Fisher), 1:100; integrin alpha 7 polyclonal antibody (Thermo Fisher), 1:100; integrin beta 1 (CD29) recombinant rabbit monoclonal antibody (SR30-03) (Thermo Fisher), 1:100; rabbit integrin beta-4 polyclonal antibody (Mybiosources), 1:100; goat anti-rabbit IgG (H+L) cross-adsorbed secondary antibody, 1:500; Alexa Fluor 647 (Thermo Fisher) and goat anti-mouse IgG1 cross-adsorbed secondary antibody, 1:500 ; Alexa Fluor 488 were used as secondary antibodies. Mouse IgG1 kappa isotype control (P3.6.2.8.1), eBioscience™ (Thermo Fisher) and rabbit IgG isotype control (31235) (Thermo Fisher) were used as isotype control.

Animal Study and Experimental Design

In the preliminary experiment, eighteen eight-week-old male Wistar rats were purchased from the Namura Animal Center (Thailand). The rats were acclimatised for 7 d under a controlled cycle and fed chow with access to water. To create second-degree burns, rats were anaesthetised using isoflurane and the dorsal skin was shaved. Two burn wounds were created on the rats' dorsum using a 10 mm diameter aluminium rod heated to 100°C and applied to the skin for 10 s. The rats were allocated into two groups of nine rats/group. NSS (100 µL) or 2.5 µg LM511-E8 (commercially available as iMatrix-511; Takara Bio Inc., Nippi, Tokyo, Japan) in 100 µL PBS was applied daily to each wound on the rats in the control and treatment groups, respectively.

In the complete *in vivo* experiment consisting of four animals/group (eight wounds), the wounds were imaged on days 0, 7, 14, 21, and 28 after injury, and the wound areas were analysed using the ImageJ software version 1.52t (NIH, MA, USA) using the freehand selection tool. Wound areas were reported as a percentage area relative to day 0. For twenty animals/group, four rats (eight wounds) were

euthanised after 3, 7, 14, 21, and 28 days, the wound tissues were excised and immediately fixed in 10% neutral-buffered formaldehyde for at least 48 h followed by a paraffin-embedding.

In this study the program G*Power 3.1 was used for calculating sample size, alpha error = 0.05, power = 0.95, effect size f = 0.6, number of groups = 2. This resulted in 80 wounds from 40 rats used in this experiment. (F. Faul et al., 2007) (Fig. 34)
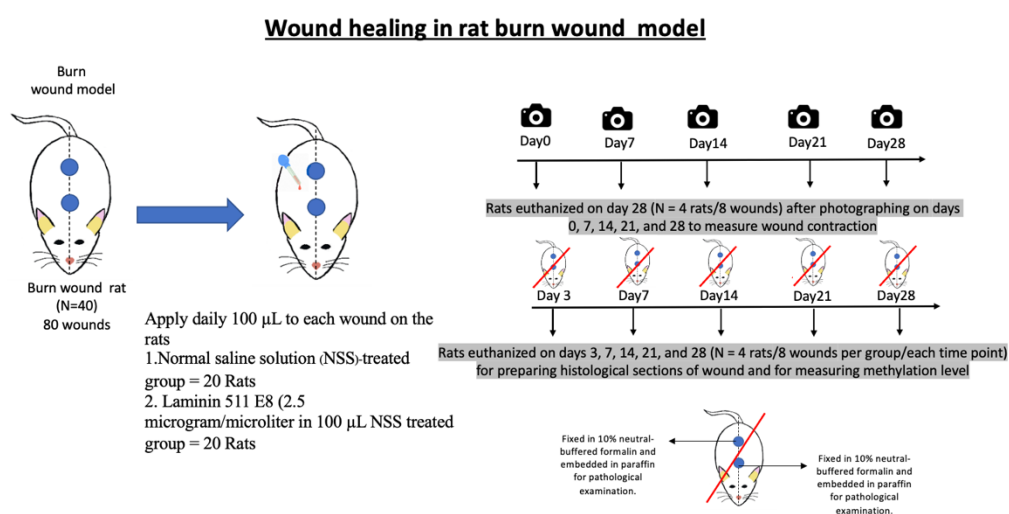
Figure 34. Sample size and allocation of rat burn wound experiment

Then, two second-degree burn wounds were produced on the back of rats. They were further divided into two groups and treated with

1. NSS-treated group (negative control) = 20 rats/40 wounds

2. Laminin 511 E8-treated group = 20 rats/40 wounds

Histopathology and Immunohistochemistry

The formalin-fixed paraffin-embedded tissues were cut into 3 µm sections using a Leica RM 2125 microtome (Leica, Heidelberg, Germany). H&E staining was performed; in addition, immunohistochemistry of the tissue sections was performed using monoclonal antibodies against cytokeratin 10 (Dako Corp., Carpinteria, CA, USA) and cytokeratin 14 (Neomarkers, Inc., Fremont, CA, USA).

The histological sections of the wounds were graded using a histopathological scoring system, following a previously published method, with some modifications. (Edraki et al., 2014)

Statistical Analysis

Data were determined for normal distribution using the Shapiro–Wilk test ($P > 0.05$). For normally distributed data, one-way ANOVA followed by Bonferroni's post-hoc test were used to compare groups, or two-way mixed ANOVA was used to determine the difference between groups and times. For non-normally-distributed data, the Kruskal–Wallis followed by a Dunn's post-hoc was used to test the difference between groups. P-values < 0.05 were considered statistically significant.
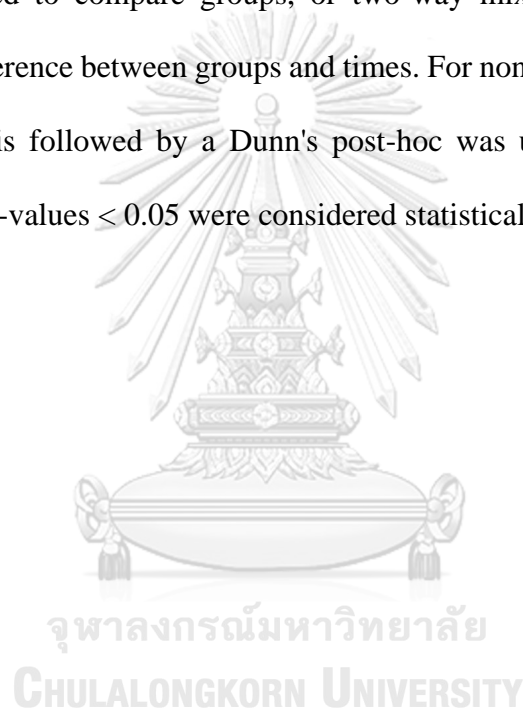
Chapter 4. RESULTS

Part A: B1 siRNA

Methylation levels of Alu in hypertrophic scars and normal skin

Alu-combined bisulfite restriction analysis (COBRA-Alu) was used to quantify Alu methylation levels (mC) in either control or hypertrophic scar tissue sample groups. The results showed that the levels were significantly lower in hypertrophic scars than in normal tissues ($35.6 \pm 3.2\%$ and $29.4 \pm 2.5\%$, respectively; $p < 0.001$) (Fig. 35-36).
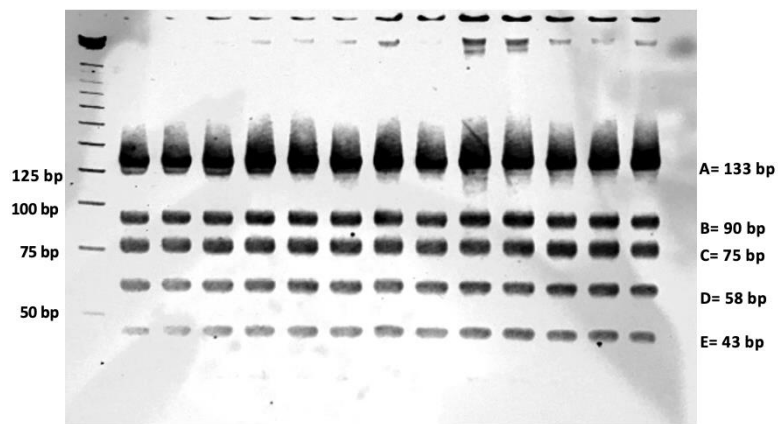
Figure 35. Polyacrylamide gel of DNA from human skin bisulfite
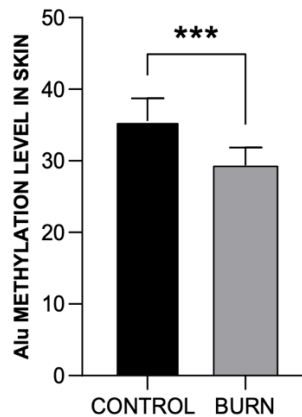
Figure 36. Alu methylation levels in control and burn scar tissue samples, 35.6 ± 3.2% and 29.4 ±
2.5%, respectively; t-test
(*P 0.05, **P 0.01 and ***P 0.001; N = 23 per group)

Methylation levels of Alu in WBCs from hypertrophic scar and normal control groups

WBCs were isolated from the blood of 46 patients and Alu methylation levels were analysed by COBRA-Alu. The results revealed that the total methylation levels (mC) were slightly higher but significant in WBCs from hypertrophic scars than in those from the normal control group (27.0 ± 4.0% and 24.6 ± 3.3%, respectively; $p < 0.05$) (Fig. 37). Remarkably, the trend was different from that observed in tissue samples.
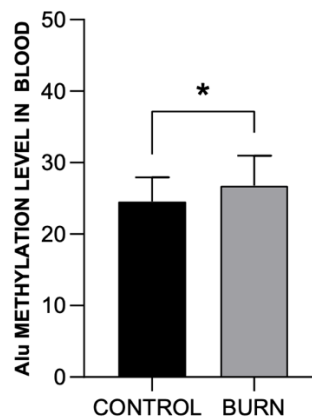
Figure 37. Alu methylation levels in white blood cells (WBCs) from burn scar

and normal control groups, 27.0 ± 4.0% and 24.6 ± 3.3%, respectively; t-test
(*P 0.05, **P 0.01 and ***P 0.001; N = 23 per group)

Alu methylation patterns in tissue samples and ROC analysis

The uCmC pattern was significantly lower, whereas the uCuC pattern was significantly higher, in the hypertrophic scar tissue (p < 0.0001; Fig. 38A). Thus, this method showed the potential for using ROC analysis to distinguish between normal skin and hypertrophic scar tissue. The ROC values of the uCmC and uCuC patterns verified the screening reliability. The area under the curve for the uCmC pattern was 0.95, and the cut-off value, sensitivity, and specificity were 27.87%, 91.30%, and 96.23%, respectively (Fig. 38B). Furthermore, the AUC of the uCuC pattern was 0.98, and the cut-off value, sensitivity, and specificity were 42.34%, 100%, and 94.23%, respectively (Fig. 38C). Therefore, the most effective method for identification of hypertrophic scar tissue was the analysis of the Alu uCmC and uCuC patterns.
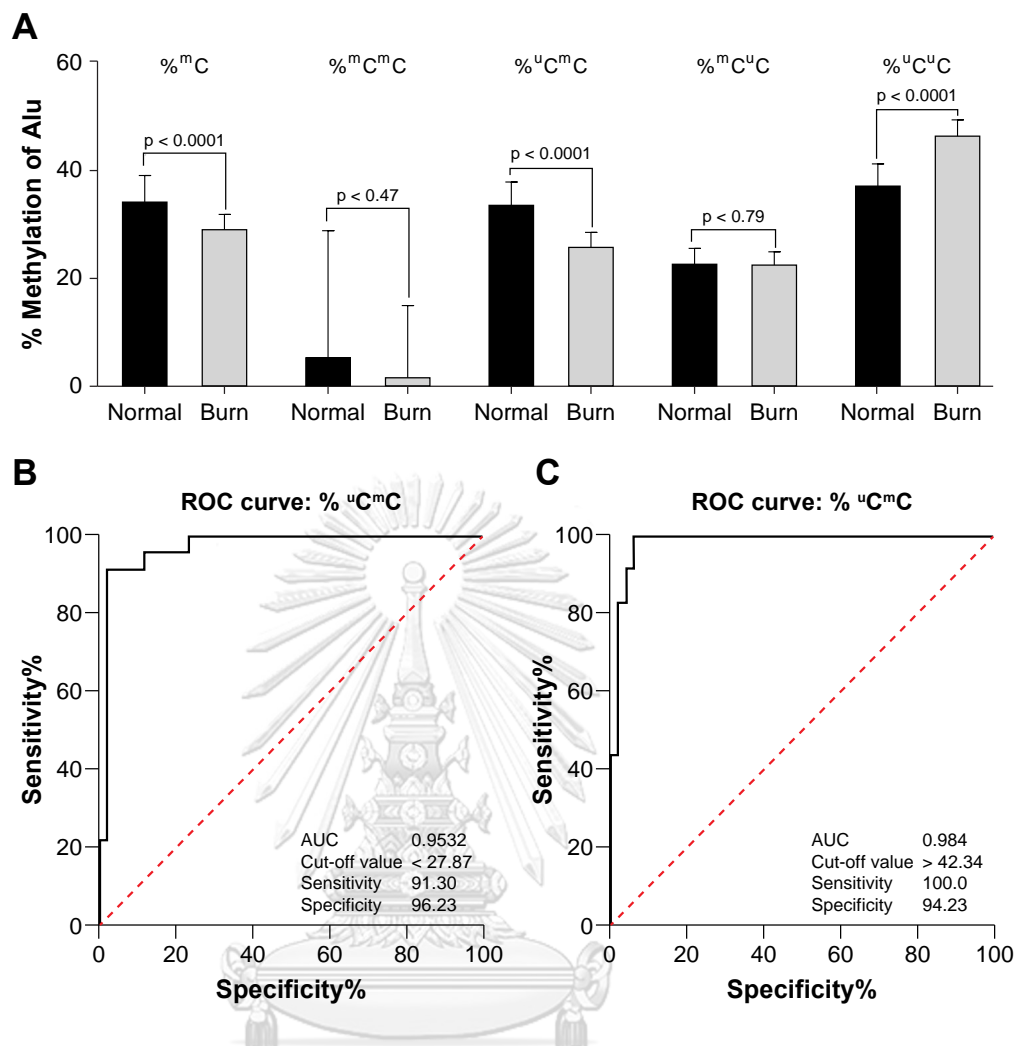
Figure 38. (A) Alu methylation patterns in burn scar and normal skin tissue samples.
(B) ROC analysis of the uCmC pattern. (C) ROC analysis of uCuC pattern; t-test, ROC test
(*P 0.05, **P 0.01 and ***P 0.001; t-test, N = 23 per group)

Invitro B1 siRNA result: the B1 methylation levels in rat epidermal keratinocytes cells

B1 methylation in REK cells was increased in the B1 siRNA-treated group compared to the control and scramble siRNA groups: i) control, $28.83 \pm 0.86\%$; ii) Ca-P, $29.0 \pm 0.70\%$; iii) scramble siRNA, 29.22 ± 1.09; iv) B1 siRNA, $43.72 \pm 1.25\%$ (Fig. 39).
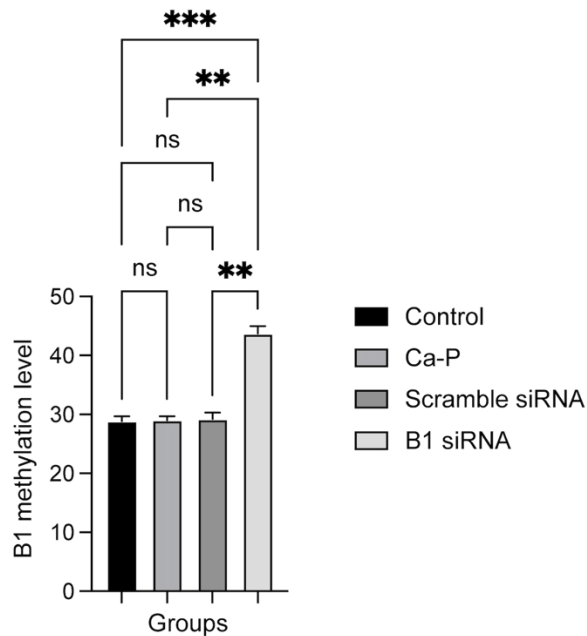
Figure 39. The B1 methylation levels in rat epidermal keratinocytes cells; Kruskal–Wallis followed by a Dunn's post-hoc (*P 0.05, **P 0.01 and ***P 0.001; N = 3 per group)

Treatment with B1 siRNA increases the percent wounds contracture as well as the methylation levels in the wounds

Second-degree burn wounds were treated each day with 150 nM B1 siRNA, and the wound areas were measured using photographs taken on days 0, 7, 14, 21, and 28 post-injury (Fig. 40).
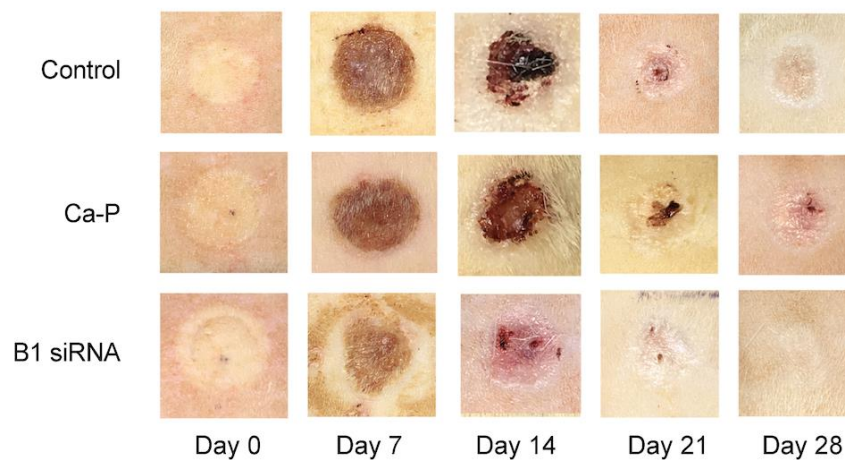
Figure 40. Images of wounds that were treated daily with a saline control, Ca-P nanoparticles or B1 siRNA

Statistically significant improvements in wound healing were observed in the NSS and Ca-P nanoparticle groups compared with the wounds in the B1 siRNA-treated group. The respective percentage wound healing $\pm$ SD in the groups treated with saline or Ca-P nanoparticles, relative to that in the B1 siRNA-treated group, on different days were as follows: i) day 7, $15.8 \pm 3.6\%$ and $15.7 \pm 2.4\%$ vs. $20.0 \pm 2.0\%$, both $P < 0.01$; ii) day 14, $56.6 \pm 1.2\%$ and $56.7 \pm 1.6\%$ vs. $60.4 \pm 1.4\%$, both $P < 0.001$; iii) day 21, $73.1 \pm 2.3\%$ and $73.4 \pm 2.6\%$ vs. $77.2 \pm 1.3\%$, both $P < 0.01$; and iv) day 28, $90.6 \pm 1.4\%$ and $90.8 \pm 0.9\%$ vs. $97.2 \pm 0.8\%$, both $P < 0.001$. There were no significant differences between the percent wound contracture in the NSS-treated control and Ca-P nanoparticle groups. Furthermore, significant differences were observed amongst the control and Ca-P nanoparticle compared with the B1 siRNA treatment group, particularly on days 14 and 28 post-injury (Fig. 41).
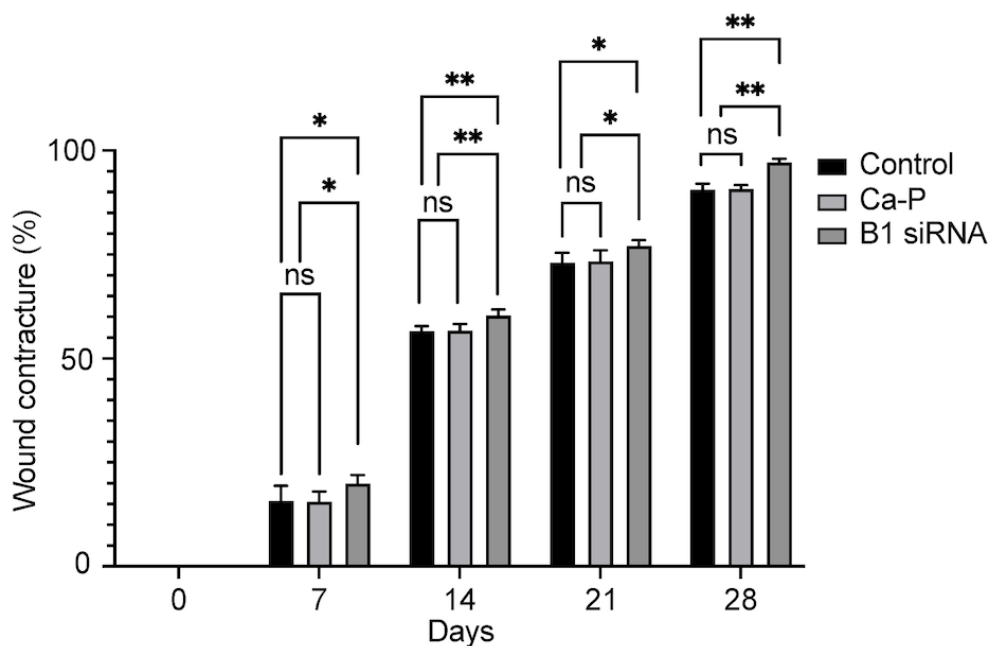
Figure 41. % Wound contracture in different treatment days; Kruskal–Wallis followed by a Dunn's post-hoc (*P 0.05, **P 0.01 and ***P 0.001; N = 6 per group)

B1 siRNA promotes methylation through siRNA directed DNA methylation (Mathieu & Bender, 2004; Marjori A. Matzke & Rebecca A. Mosher, 2014); it improves DNA stability and enhances proliferation of the cells. (Patchsung et al., 2018) The methylation levels of the B1 siRNA group were significantly higher than those of the saline-treated control and Ca-P nanoparticle groups, especially on days 14 and 28. The respective percentage methylation $\pm$ SD in the NSS control, Ca-P nanoparticle, and B1 siRNA-treated wounds on different days were as follows: i) day 3, $30.3 \pm 1.5\%$ and $29.0 \pm 1.0\%$ vs. $33.00 \pm 1.0\%$, both $P < 0.05$; ii) day 7, $30.0 \pm 2.0\%$ and 31.0 ± 2.0 vs. $35.0 \pm 1.0\%$, both $P < 0.001$; iii) day 14, $33.7 \pm 1.5\%$ and $33.0 \pm 1.7\%$ vs. $45.0 \pm 1.0\%$, both $P < 0.001$; iv) day 21, $33.7 \pm 2.0\%$ and $34.7 \pm 0.6\%$ vs. $41.0 \pm 1.0\%$, both $P < 0.001$; and v) day 28, $34.3 \pm 0.6\%$ and $34.3 \pm 0.6\%$ vs. $38.00 \pm 1.00\%$, both $P < 0.05$ (Fig. 42). The differences were shown in the B1 siRNA-treated group compared with the control groups three days post-injury.
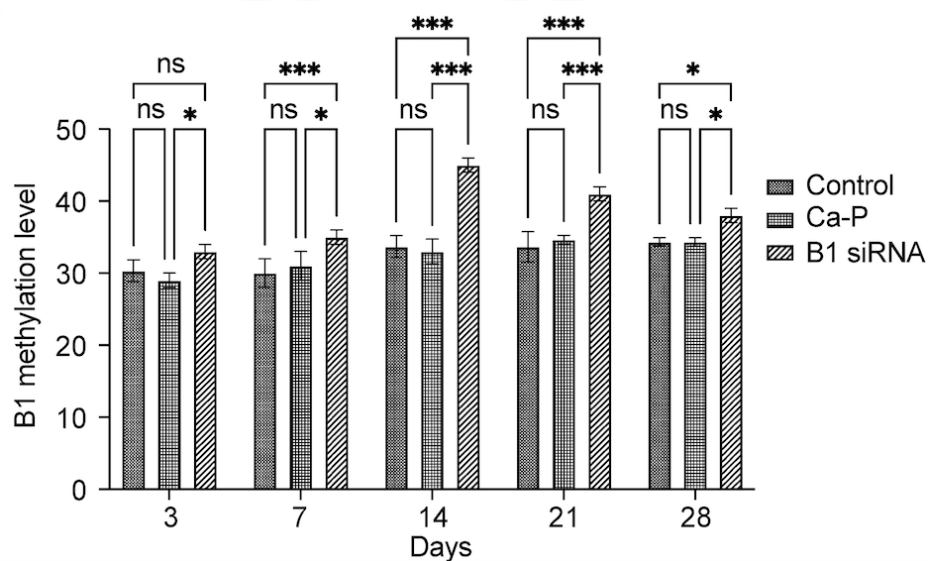
Figure 42. The B1 methylation levels in second-degree burn wounds; Kruskal–Wallis followed by a Dunn's post-hoc (*P 0.05, **P 0.01 and ***P 0.001; N = 6 per group)

Pathological and immunohistochemical changes in the rat model of burn wound

Individual histopathological scores were combined to provide an overall score for each wound. Blinded scoring of the wounds by the three dermatopathologists confirmed that the rats treated with B1 siRNA displayed much better pathological scores than those treated with NSS or Ca-P nanoparticles, with the greatest improvement observed on days 14, 21, and 28 post-injury. The pathological scores ± SD in the NSS and Ca-P nanoparticle-treated groups (respectively), relative to those in the B1 siRNA-treated group, on different days were as follows: i) day 3, $1.3 \pm 0.6\%$ and $1.7 \pm 0.6\%$ vs. $2.7 \pm 0.6\%$, both $P > 0.05$; ii) day 7, 7.7 ± 1.2 and $7.7 \pm 0.6\%$ vs. 7.0 ± 1.0, both $P > 0.05$; iii) day 14, $12.3 \pm 0.6\%$ and $11.3 \pm 1.2\%$ vs. $15.7 \pm 0.6\%$, both $P < 0.01$; iv) day 21, $13.3 \pm 0.6\%$ and $12.3 \pm 1.5\%$ vs. $16.0 \pm 0.0\%$, $P < 0.05$; and v) day 28, $15.0 \pm 1.0\%$ and $14.3 \pm 0.58\%$ vs. $16.6 \pm 1.53\%$, $P < 0.05$ (Fig. 43 A and B).
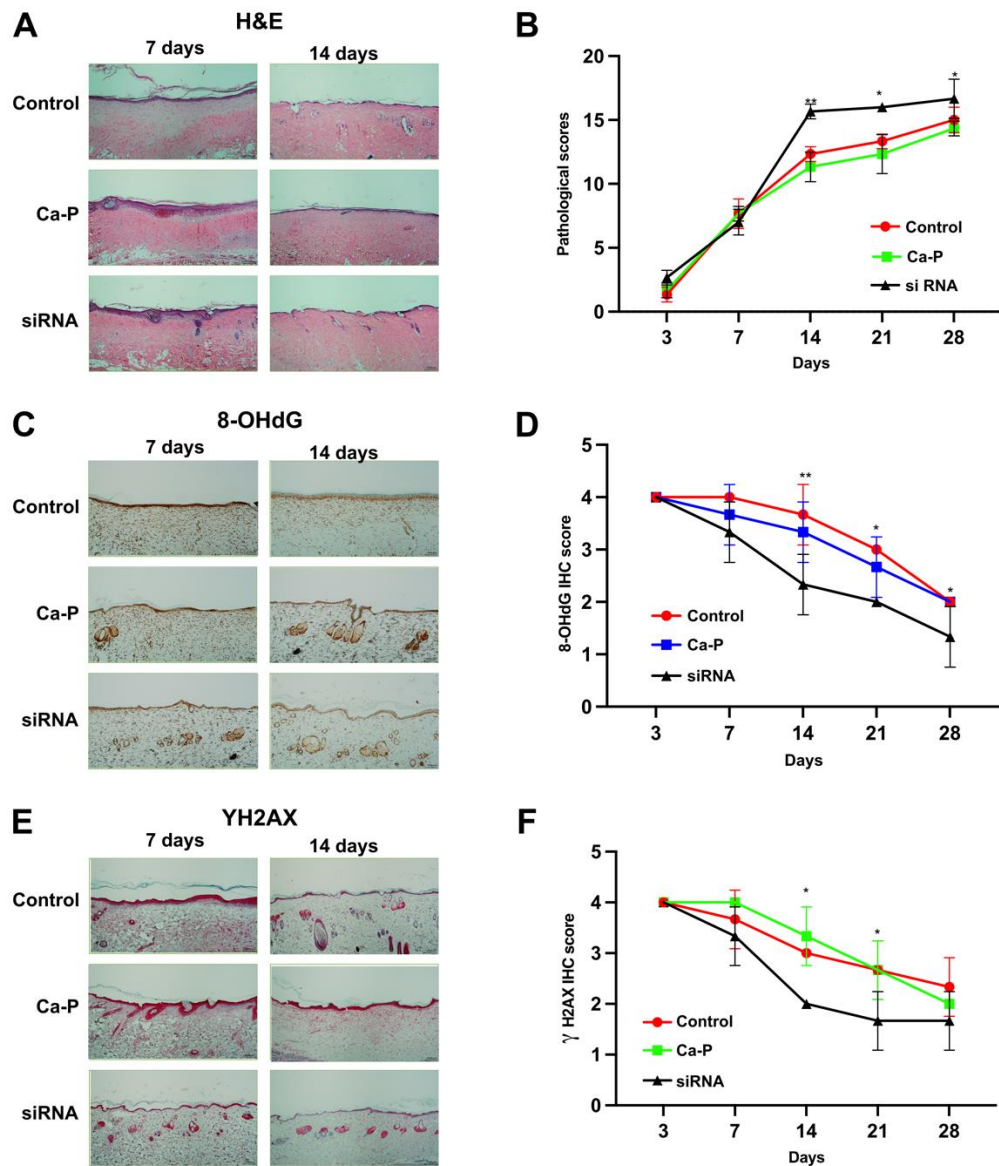
Figure 43. H&E staining and 8-OHdG and γH2AX immunohistochemical staining to assess burn wound healing in rats treated daily with 150 nM B1 siRNA. (A) Sections of tissue immunostained with H&E after 14 d of wounding and healing. (B) Pathological wound healing scores of six second-degree burn wounds/timepoint. (C) Sections of wounded tissues immunostained for 8-OHdG after 7 and 14 d. (D) Quantification of 8-OHdG staining. (E) Sections of wound tissue immunostained for γH2AX after 7 and 14 d. (F) Quantification of γH2AX (one-way ANOVA); Kruskal–Wallis followed by a Dunn's post-hoc (*P 0.05, **P 0.01 and ***P 0.001; N = 6 per group)

8-OHdG and γH2AX scores were determined to measure DNA damage response after introducing burn injuries. A low immunohistochemistry score for 8-OHdG and γH2AX reflected a low DNA damage response. The B1 siRNA-treated group exhibited lower levels of 8-OHdG than the NSS and Ca-P nanoparticle groups

on days 14 and 21. In addition, the wounds in the B1 siRNA-treated group showed significantly lower γH2AX levels from days 7 to 21 than did the NSS- and Ca-P nanoparticle-treated groups, with the highest level observed 14 days post-injury. The respective 8-OHdG immunohistochemistry score ± SD in the NSS and Ca-P nanoparticle-treated groups, respectively, relative to those in the B1 siRNA-treated group were as follows: i) day 3; $4.0 \pm 0.0\%$ and $4.0 \pm 0.0\%$ vs. $4.0 \pm 0.0\%$, both $P > 0.05$; ii) day 7; $4.0 \pm 0.0\%$ and $3.7 \pm 0.6\%$ vs. $3.33 \pm 0.6\%$, both $P > 0.05$; iii) day 14, $3.0 \pm 0.0\%$ and $3.3 \pm 0.6\%$ vs. $2.7 \pm 0.6\%$; both $P < 0.01$; iv) day 21, $3.0 \pm 0.0\%$ and $2.7 \pm 0.6\%$ vs. $2.0\% \pm 0.0\%$, both $P < 0.05$; and v) day 28, $2.0 \pm 0.0\%$ and $2.0 \pm 0.0\%$ vs. $1.7 \pm 0.6\%$, $P < 0.05$ (Fig. 43 C and D). Furthermore, the γH2AX immunohistochemistry scores ± SD in the NSS and Ca-P nanoparticle groups, relative to those in the B1 siRNA-treated group, were as follows: i) day 3, $4.0 \pm 0.0\%$ and $4.0 \pm 0.0\%$ vs. $4.0 \pm 0.0\%$, both $P > 0.05$, ii) day 7, $3.7 \pm 0.6\%$ and $4.0 \pm 0.0\%$ vs. $3.3 \pm 0.6\%$, both $P > 0.05$, iii) day 14, $3.0 \pm 0.0\%$ and $3.3 \pm 0.6\%$ vs. $2.7 \pm 0.6\%$, both $P < 0.05$, iv) day 21, $2.7 \pm 0.6\%$ and $2.7 \pm 0.6\%$ vs. $2.0 \pm 0.0\%$, both $P < 0.05$; and v) day 28, $2.0 \pm 0.0\%$ and $2.0 \pm 0.0\%$ vs. $1.7 \pm 0.6\%$; both $P > 0.05$ (Fig. 43 E and F).

Part B: Box A of HMGB1 protein

In vitro PHY-RIND-EDSB level

The PHY-RIND-EDSB fold change expression level of REK cells that induce burns by boiling in digital water bath at 37 degrees Celsius, 45 degrees Celsius, 60 degrees Celsius, 75 degrees Celsius, and 90 degrees Celsius : i) 45 degrees Celsius , 0.515 ± 0.036; ii) 60 degrees Celsius, 0.365 ± 0.022; iii) 75 degrees Celsius, $0.327 \pm$

0.016 and iv) 90 degrees Celsius, 0.288 ± 0.001. The normalised data uses an average

of 37 degrees Celsius' PHY-RIND-EDSB level (Fig. 44). *P < 0.05, **P < 0.01, and

***P < 0.001; N = 9/group
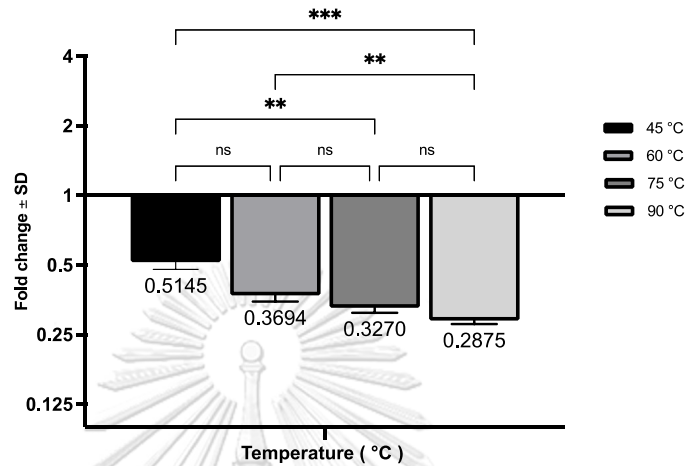
Figure 44. The PHY-RIND-EDSB fold change expression level of REK cells that induce burns. The Y axis of the graph is normalized to the levels digested ligated control DNA (*P 0.05, **P 0.01 and ***P 0.001; Kruskal–Wallis followed by a Dunn's post-hoc, N = 9 per group).

The PHY-RIND-EDSB levels of REKs were increased in the Box A plasmid-

treated group compared to the control, Ca-P, and scramble plasmid-treated groups in

both 45 and 90 degrees Celsius: i) 45 degrees Celsius, 0.515 ± 0.036 , 0.514 ± 0.031

and 0.516 ± 0.035 vs. 0.72 ± 0.03, P < 0.001; ii) 90 degrees Celsius, 0.288 ± 0.01, 0.284

± 0.008 and 0.289 ± 0.01 vs. 0.371 ± 0.03, P < 0.035 (Fig. 45).
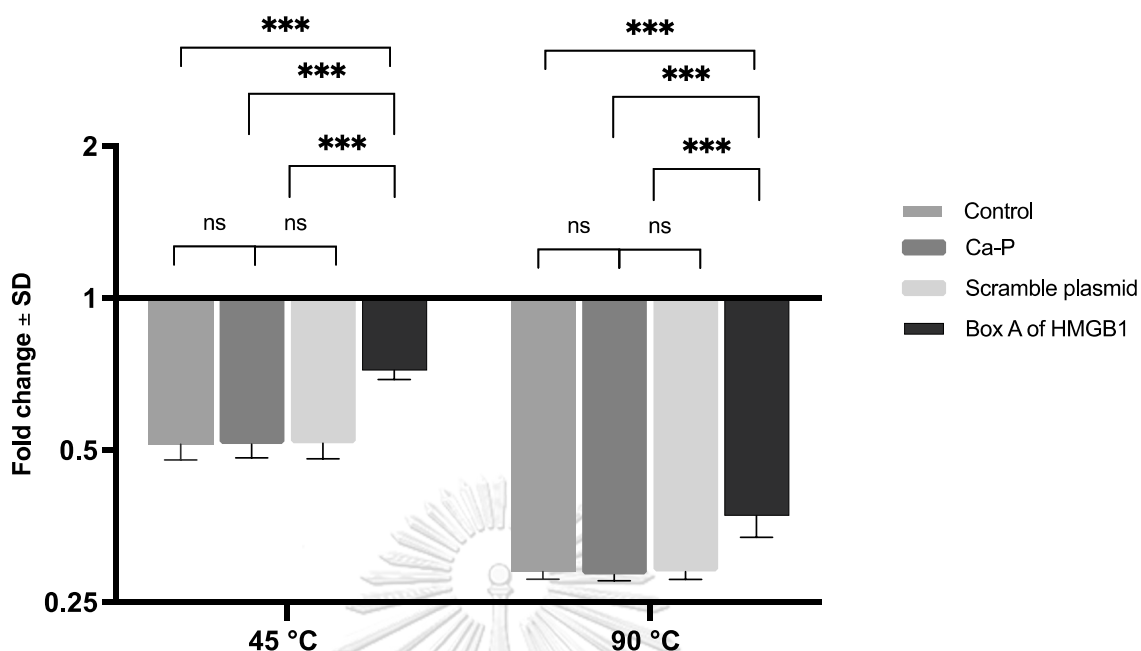
Figure 45. The PHY-RIND-EDSB fold change expression level of REK cells that induce burns at 45 and 90 Celsius. The Y axis of the graph is normalized to the levels digested ligated control DNA (*P 0.05, **P 0.01 and ***P 0.001; Kruskal–Wallis followed by a Dunn's post-hoc, N = 9 per group).

Treatment with Box A of HMGB1 protein increased the healing rate of second-degree burn wounds and PHY-RIND-EDSB level

I treated second-degree burn wounds each day with 5 μg of plasmid in 100 μL of CA-P nanoparticles and measured the wound areas, using photographs taken weekly (Fig. 46 A). Statistically significant improvements in wound healing were observed in the NSS and Ca-P nanoparticle groups compared with the wounds in the Box A of HMGB1-treated group. The respective % wound healing ± SD in the groups treated with saline or Ca-P nanoparticles, relative to that in the Box A of HMGB1-treated group, on different days was as follows: (i) day 7: 15.8% ± 3.6% and 15.7% ± 2.4% vs. 21.0% ± 2.1%; P < 0.05, (ii) day 14: 56.6% ± 1.2% and 56.7% ± 1.6% vs. 63.5% ± 1.6%; P < 0.001, (iii) day 21: 73.1% ± 2.3% and 73.4% ± 2.6% vs. 79.0% ± 1.3%; P <

0.01, and (iv) day 28: 90.6% ± 1.4% and 90.8% ± 0.9% vs. 100.0% ± 0.0%; P < 0.001.

The NSS-treated control and Ca-P nanoparticle groups showed no difference. Furthermore, significant differences were observed among the control, Ca-P nanoparticle, and Box A of HMGB1 treatment groups, especially at 14- and 28-d post-injury (Fig. 46 B).
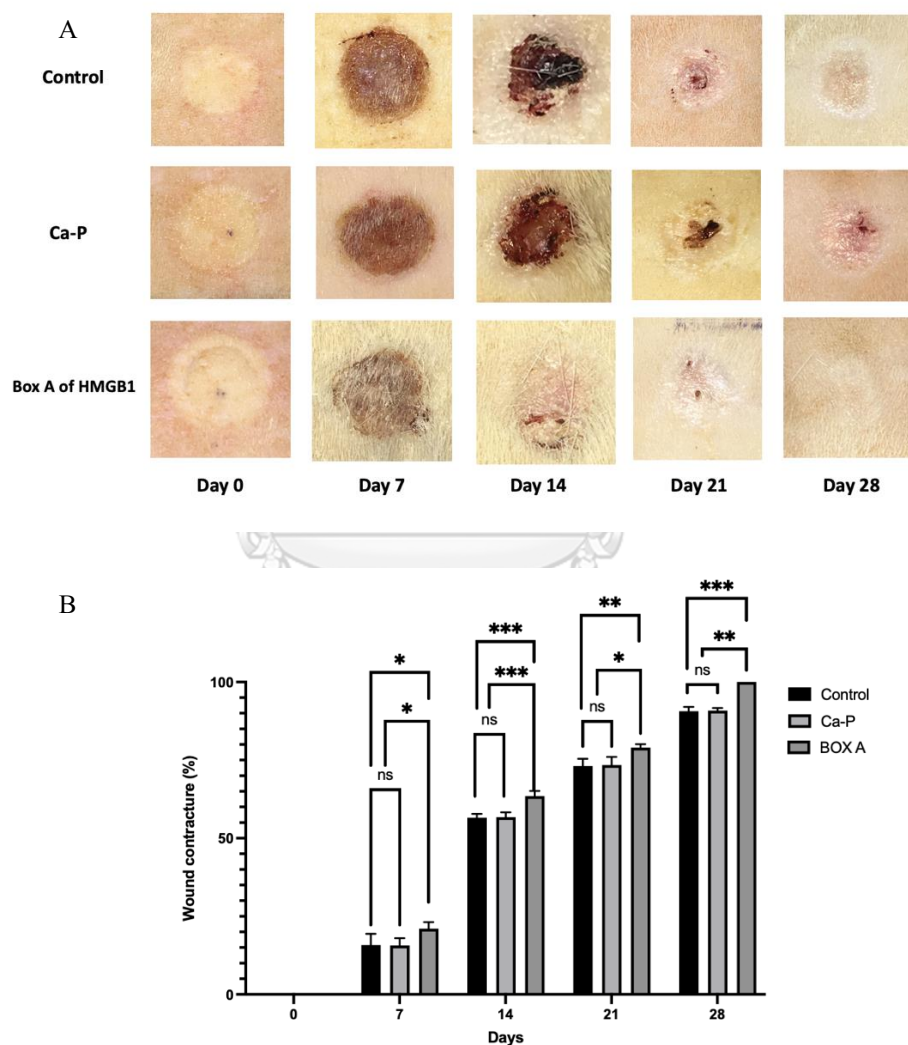
Figure 46. Effect of Box A of HMGB1 treatment on the contracture rate of second-degree burn wounds. (A) Images of wounds in rats whose wounds were treated daily. (B) Wound healing plotted as a % wound contracture/week; Kruskal–Wallis followed by a Dunn's post-hoc (*P 0.05, **P 0.01 and ***P 0.001; N = 6 per group)

The PHY-RIND-EDSB levels of the group of Box A of HMGB1 were higher than those in saline-treated and Ca-P nanoparticle groups, especially on days 7, 14, and 21. The respective fold change ± SD compared with saline or Ca-P nanoparticles and Box A of HMGB1-treated wounds on different days were as follows: i) day 3, 1.0 ± 0.0 and 1.1 ± 0.1 vs. 1.1 ± 0.1, both $P > 0.05$; ii) day 7, 1.1 ± 0.1 and 1.1 ± 0.1 vs. 1.7 ± 0.2, both $P < 0.05$; iii) day 14, 1.1 ± 0.1 and 1.1 ± 0.1 vs. 2.2 ± 0.1, both $P < 0.01$; and iv) day 21, 1.1 ± 0.1 and 1.1 ± 0.1 vs. 2.1 ± 0.0, both $P < 0.01$ and, (v) day 28: 1.1 ± 0.1 and 1.1 ± 0.1 vs. 1.6 ± 0.0, both $P < 0.01$. The contrasts were detected among the treatment groups at three days post-injury (Figure 47).
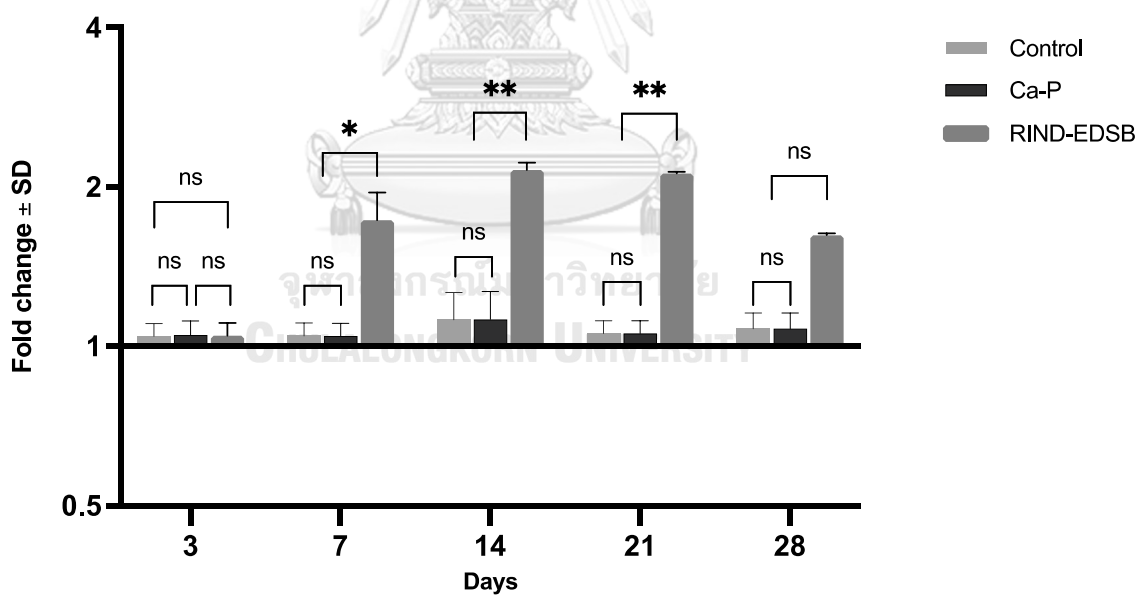
Figure 47. Effect of Box A of HMGB1 treatment on the PHY-RIND-EDSB level; SD: standard deviation The Y axis of the graph is normalized to the levels digested ligated control DNA (*P 0.05, **P 0.01 and ***P 0.001; Kruskal–Wallis followed by a Dunn's post-hoc, N = 6 per group).

Pathological and immunohistochemical skin changes in a rat model of burn wound

Individual histopathological scores were combined to provide an overall score for each wound. Blinded scoring of the wounds by the three pathologists confirmed that the rats treated with Box A of HMGB1 protein displayed considerably higher pathological scores than those treated with NSS or Ca-P nanoparticles, with the greatest improvement observed on days 14, 21, and 28 post-injury. The pathological score $\pm$ SD in the NSS- and Ca-P nanoparticle-treated groups, relative to those in the Box A of HMGB1-treated group, on different days were as follows: (i) day 3: 1.3% $\pm$ 0.6% and 1.7% $\pm$ 0.6% vs. 2.3% $\pm$ 0.5%; P > 0.05, (ii) day 7: 7.7% $\pm$ 1.1% and 7.7% $\pm$ 0.6% vs. 8.0% $\pm$ 0.9%; P < 0.05, (iii) day 14: 12.3% $\pm$ 0.6% and 11.3% $\pm$ 1.2% vs. 13.5% $\pm$ 0.9%; P < 0.01, (iv) day 21: 13.3% $\pm$ 0.6% and 12.3% $\pm$ 1.5% vs. 16.4% $\pm$ 0.5%; P < 0.001, and (v) day 28: 15.0% $\pm$ 1.0% and 14.3% $\pm$ 0.6% vs. 16.9% $\pm$ 1.3%; P < 0.01 (Fig. 48 A and B).

I determined 8-OHdG and γH2AX scores to measure DNA damage responses after introducing burn injuries. A low immunohistochemistry score for 8-OHdG and γH2AX reflected a low DNA damage response. The Box A of HMGB1-treated group exhibited lower levels of 8-OHdG than did the NSS and Ca-P nanoparticle groups on days 14 and 21. In addition, the wounds in the Box A of HMGB1-treated group showed significantly lower γH2AX levels from days 7 to 21 than did those in the NSS- and Ca-P nanoparticle-treated groups, with the highest level observed 14 days post-injury. The respective 8-OHdG immunohistochemistry score $\pm$ SD in the NSS- and Ca-P nanoparticle-treated groups, relative to those in the Box A of HMGB1-treated group, were as follows: (i) day 3: 4.0% $\pm$ 0.0% and 4.0% $\pm$ 0.0% vs. 4.0% $\pm$ 0.0%, (ii) day 7:

4.0% ± 0.0% and 3.7% ± 0.6% vs. 3.0% ± 0.8%; P < 0.05, (iii) day 14: 3.0% ± 0.0% and 3.3% ± 0.6% vs. 2.0% ± 0.0%; P < 0.001, (iv) day 21: 3.0% ± 0.0% and 2.7% ± 0.6% vs. 1.6% ± 0.5%; P < 0.001, and (v) day 28: 2.0% ± 0.0% and 2.0% ± 0.0% vs. 1.9% ± 0.4%; P < 0.05. Furthermore, the γH2AX immunohistochemistry score ± SD in the NSS and Ca-P nanoparticle groups, relative to that in the Box A of HMGB1-treated group, was as follows: (i) day 3: 4.0% ± 0.0% and 4.0% ± 0.0% vs. 4.0% ± 0.0%; P > 0.05, (ii) day 7: 3.7% ± 0.6% and 4.0% ± 0.00% vs. 2.9% ± 0.9%; P <0.05, (iii) day 14: 3.0% ± 0.0% and 3.3% ± 0.6% vs. 2.1% ± 0.4%; P < 0.001, (iv) day 21: 2.7% ± 0.6% and 2.7% ± 0.6% vs. 1.6% ± 0.5%; P < 0.01, and (v) day 28: 2.0% ± 0.0% and 2.0% ± 0.0% vs. 1.8% ± 0.5%; P > 0.05 (Fig. 48).
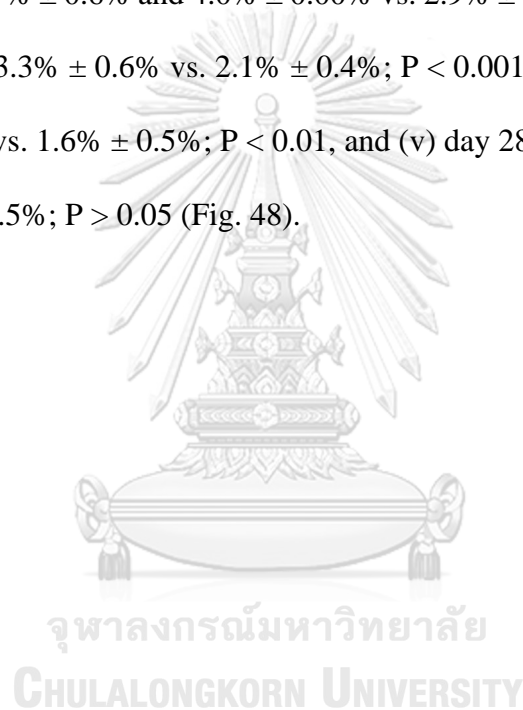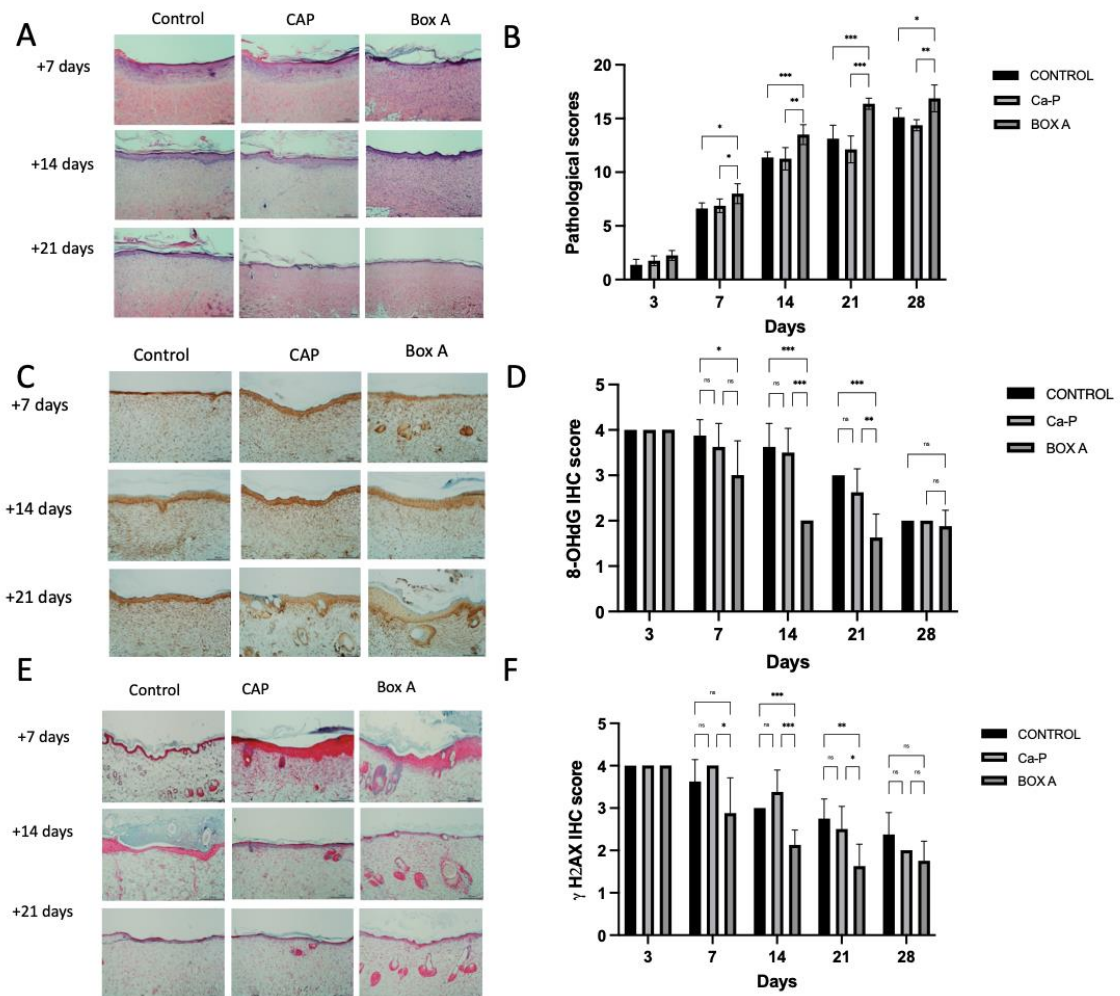
Figure 48. H&E, 8-OHdG and γH2AX staining to assess burn wound healing immunohistochemical staining to assess burn wound healing in rats treated daily with 5 μg of Box A of HMGB1 plasmid. (A) Sections of tissue immunostained with H&E at 7,14, and 21 d. (B) Pathological wound healing scores from three dermatopathologists for six second-degree burn wounds/timepoint. (C) Sections of wounded tissues immunostained for 8-OHdG at 7,14, and 21 d. (D) Quantitation of 8-OHdG. (E) Sections of wound tissue immunostained for γH2AX at 7,14, and 21 d. (F) Quantification of γH2AX; Kruskal–Wallis followed by a Dunn's post-hoc (*P 0.05, **P 0.01 and ***P 0.001; N = 6 per group)

Part C: Laminin 511 E8

LM511-E8 treatment increased dermal fibroblast scratch closure rate

The effect of LM511-E8 (0.5, 1, 2.5, and 5 □g/□L) concentration on the scratch

closure of RDF cells was compared with the control group (Fig. 49,50). Mean migration

velocity significantly increased with treatment of 1, 2.5, and 5 µg/µL compared to

control at 2.5 µg/µL (mean ± SD in mm/h of: control 0.76 ± 0.074; 0.5 µg/µL 0.75 ± 0.23; 1 µg/µL 0.89 ± 0.17; 2.5 µg/µL 0.99 ± 0.082; 5 µg/µL 0.79 ± 0.16, 2.5 µg/µL vs control; P = 0.025).
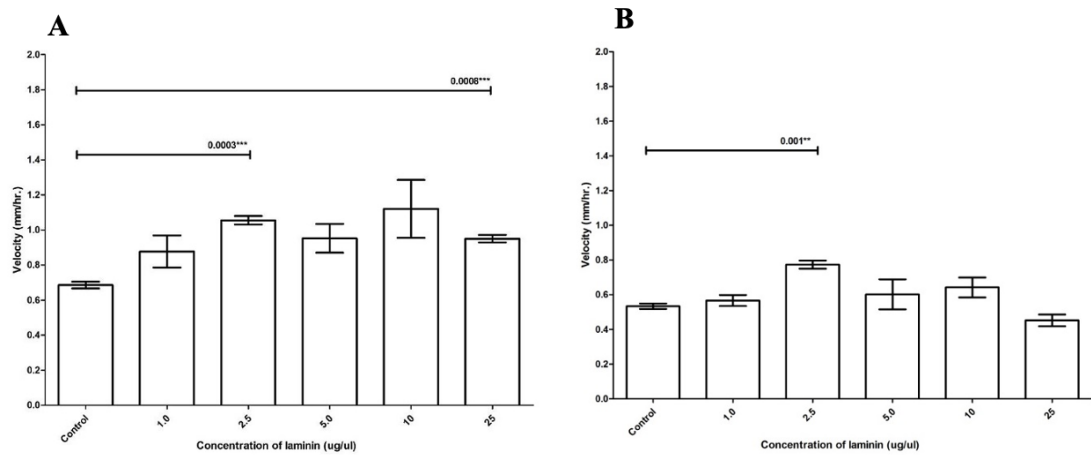
Figure 49. Bar graph of migratory velocity among all groups were expressed
as the mean ± SEM. (A) Comparison of migratory velocity in RDF cells between 2.5 µg/µL. (B) Comparison of migratory velocity in REK cells between 2.5 µg/µL of laminin; SD: standard deviation; Kruskal–Wallis followed by a Dunn's post-hoc (*P 0.05, **P 0.01 and ***P 0.001; N = 3 per group)
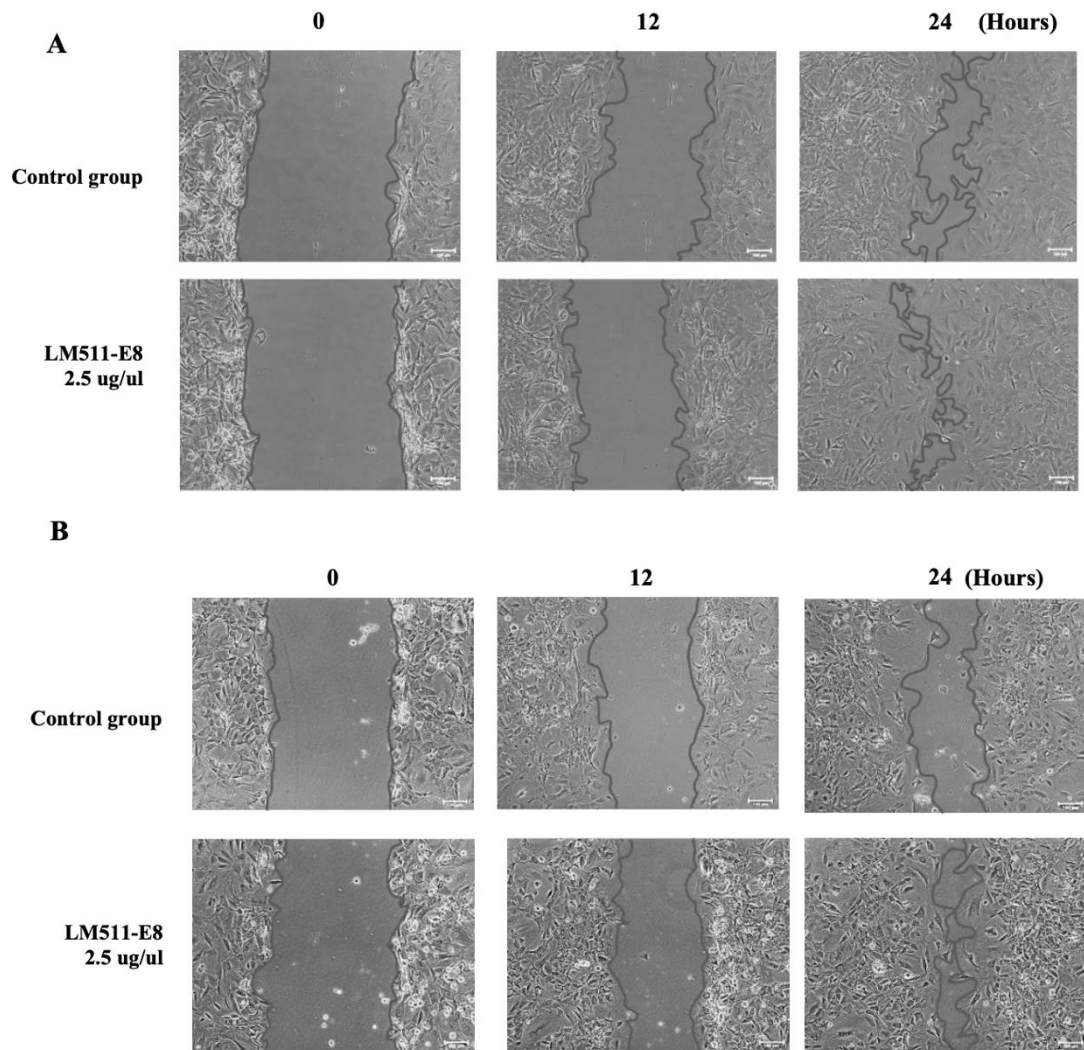
Figure 50. Effects of laminin from a scratch assay experiment at different time points in RDF cells and REK cells. (A) and (B) Representative microphotographs of the experiment at 0, 6, and 24 h compared to 2.5 µg/µL of laminin experimental group and control group (magnification, 200×) of RDF cells and REK cells, respectively

Effects of laminin in rat skin cells

The effects of each LM511-E8 concentration in RDF cells and REK cells include 1.0, 2.5, 5.0, 10, and 25 µg/µL were determined for the migratory velocity compared to the control group. The mean and SD of migratory velocity of each laminin concentrations from the 1.0, 2.5, 5.0, 10, and 25 µg/µL of laminin experimental groups and control group of RDF cells were 0.9 ± 0.1 (N = 3), 1.1 ± 0.0 (N = 3), 1.0 ± 0.1 (N

= 3), 1.1 ± 0.2 (N = 3), 1.0 ± 0.0 (N = 3), and 0.7 ± 0.0 (N = 3), respectively (P = 0.0018), as shown in Figure. 50 A. The mean and SD of migratory velocity of each laminin concentrations from the 1.0, 2.5, 5.0, 10, and 25 µg/µL of laminin experimental groups and control group of REK cells were 0.6 ± 0.0 (N = 3), 1.0 ± 0.0 (N = 3), 0.6 ± 0.1 (N = 3), 0.6 ± 0.1 (N = 3), 0.5 ± 0.0 (N = 3) and 0.5 ± 0.0 (N = 3), respectively (P = 0.0093), as shown in Figure. 50 B.

In vitro scratch wound healing assays in RDF and REK cell monolayers were photographed at 0, 6, and 24 h after scratching. The results of the images showed that cells moved into the scratched area significantly increased with laminin at 6 and 24 h after scratching in RDF cells and REK cells compared between the 2.5 µg/µL of laminin experimental group and the control group.

Treatment with LM511-E8 increased healing of second-degree burn wounds

Next, I treated second-degree burn wounds with 2.5 µg per wound per day and measured the contraction area from wound photographs (Fig 51 A). Significant improvements in wound contracture were observed with LM511-E8 treated wounds compared with saline-treated controls from 7 d post-wounding (% wound contractions control vs LM511-E8: day 7 15.8 ± 0 .9% vs 21.2 ± 0.7% P < 0.001; day 14 57.8 ± 0.4% vs 61.4 ± 0.8% P < 0.01; day 21 74.7 ± 1.0% vs 78.1 ± 0.4% P < 0.01; day 28 95.8 ± 0.5% vs 99.1 ± 0.5% P < 0.05, Figure 51 B-C).
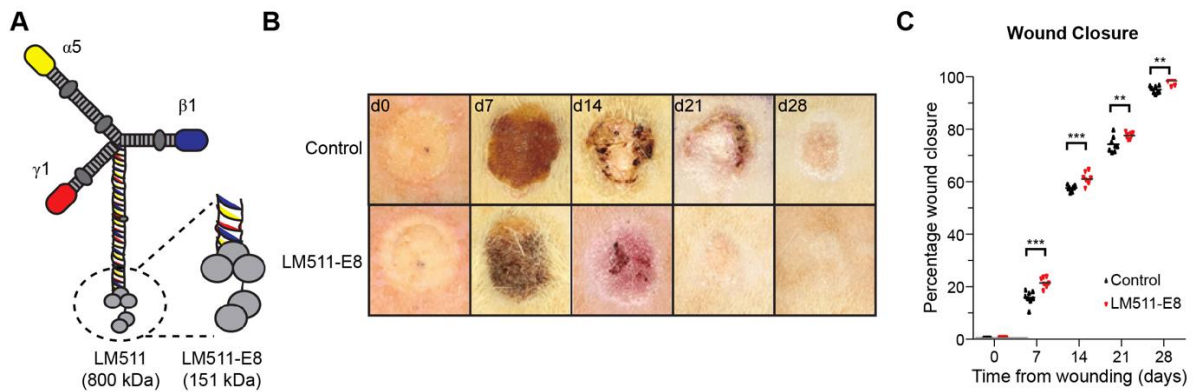
Figure 51. Effect of LM511-E8 treatment on second-degree burn wound contracture rate. (A) Images of second-degree burn wounds in rats treated daily with 2.5 □g of LM511-E8 and control rats treated with normal saline solution. (B) Wound contracture plotted as percentage of original wound area; Kruskal–Wallis followed by a Dunn's post-hoc (*P 0.05, **P 0.01 and ***P 0.001; N = 8 per group)
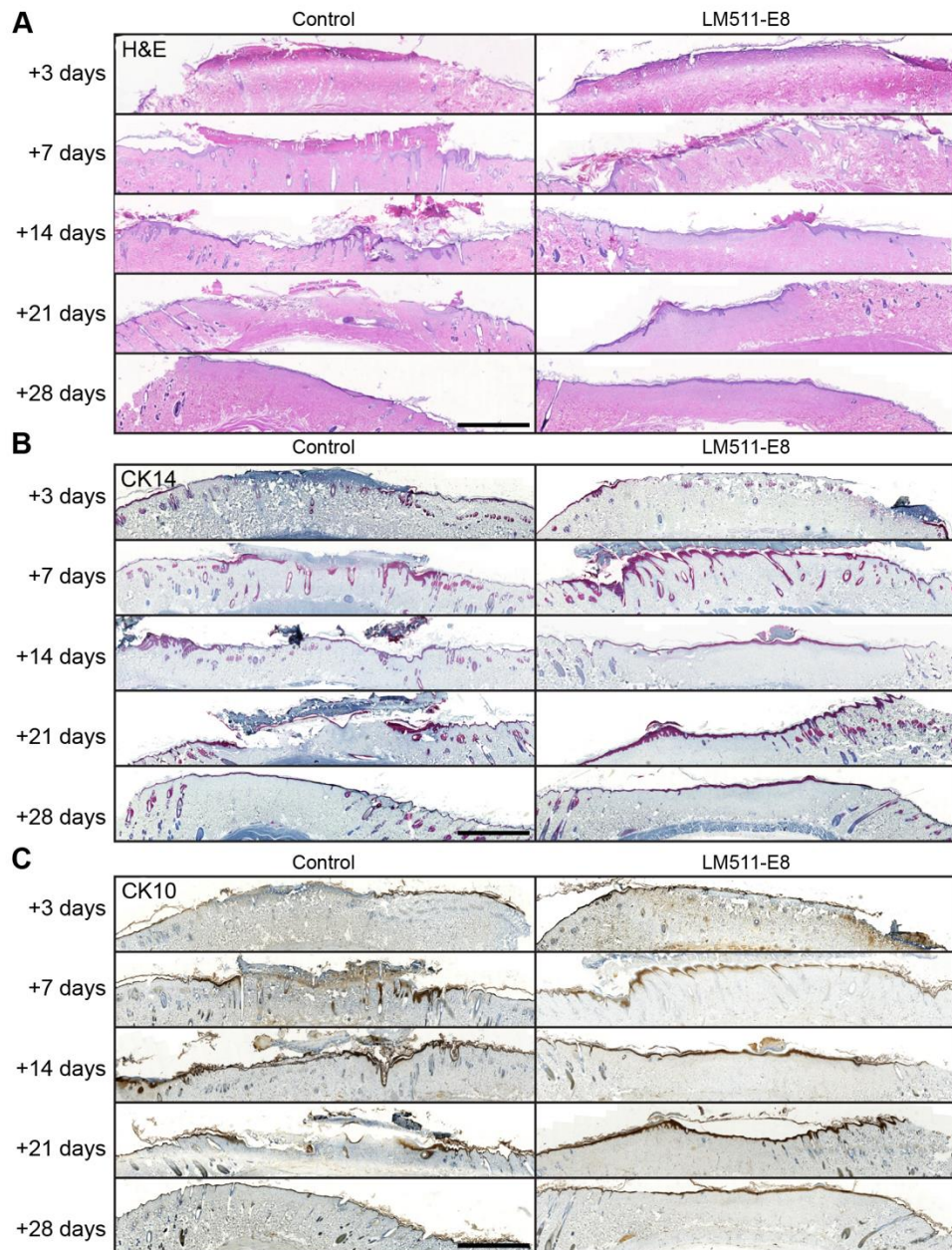
Figure 52. LM511-E8 treatment improves the histology and cytokeratin expression
of burn wounds. Rat back-skin burn wounds were treated daily with either normal saline solution
(control) or 2.5 μg of LM511-E8 and euthanised at 3, 7, 14, 21, or 28 d. Tissues were paraffin-fixed,
and formalin embedded for histology and immunohistochemistry. (A) Representative images from
hematoxylin and eosin-stained sections. (B and C) sections processed for immunohistochemistry with
antibodies against cytokeratin 14 (CK14, B) or cytokeratin 10 (CK10, C). Scale bar represents 2000
μm

Rat burn wounds treated with LM511-E8 treatment display histological improvements compared with control-treated wounds.

The results of histological assessment revealed well-formed, horizontally oriented collagen fibres in the LM511-E8-treated group and significantly improved pathological scores compared to controls on days 14, 21, and 28 post-wounding (pathological score control vs LM511-E8: day 3 1.3 ± 0.6 vs 1.3 ± 1.2; day 7 7.7 ± 1.2 vs 8.0 ± 1.0; day 14 12.3 ± 0.6 vs 15.0 ± 1.0 $P < 0.01$; day 21 13.3 ± 0.6 vs 15.7 ± 0.6 $P < 0.01$; day 28 15.0 ± 1.0 vs 17.3 ± 0.6 $P < 0.05$, Figure 52 A, 53)

The epithelialisation rate of the LM511-E8-treated group was considerably greater than that of the other groups between days 7 and 28, with the greatest improvement exhibited 7 and 14 days post-wounding (epithelialisation score control vs LM511-E8: day 1 0.7 ± 0.6 vs 1.3 ± 0.6; day 7 1.7 ± 0.6 vs 3.0 ± 0.0 $P < 0.01$; day 14 2.3 ± 0.6 vs 3.7 ± 0.6 $P < 0.01$, day 21 3.0 ± 0.0 vs 4.0 ± 0.0 $P < 0.05$; day 28 3.0 ± 0.0 vs 4.0 ± 0.0 $P < 0.05$, Figure 52 A, 53).
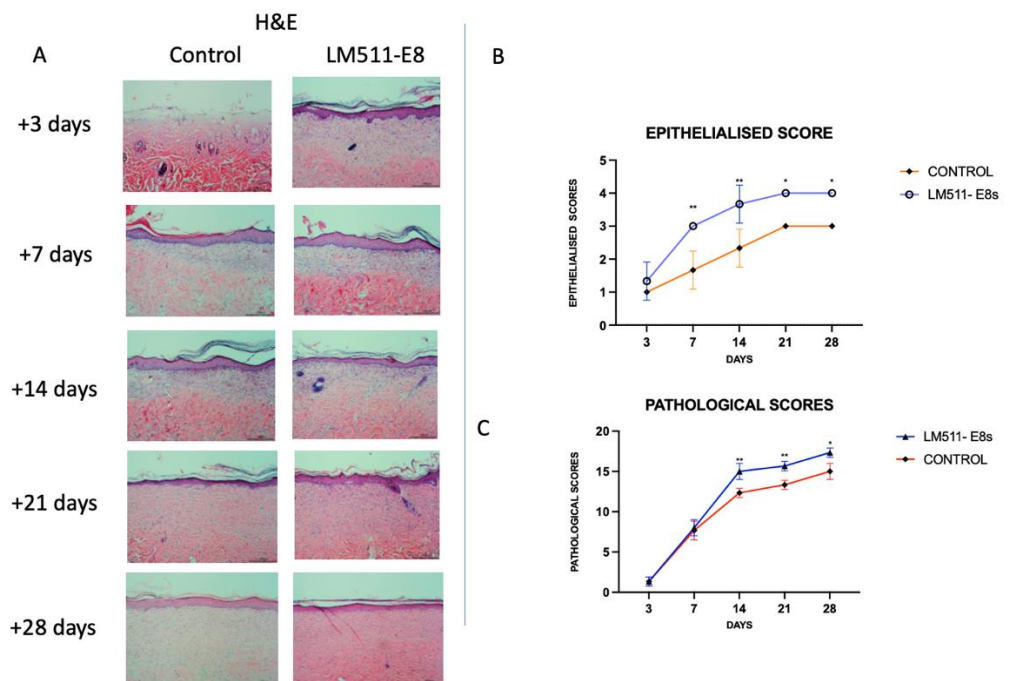
Figure 53. Histological parameters of second-degree burn wound. (A) pathological Scores and (B) epithelialised scores for second-degree burn wounds after daily treatment with normal saline solution (control) and 2.5 □g of LM511-E8; Kruskal–Wallis followed by a Dunn's post-hoc (*P 0.05, **P 0.01 and ***P 0.001; N = 8 per group)

Immunohistochemical changes in a skin of rat burn wound model

A higher score of cytokeratin 14 and 10 immunohistochemistry reflects better epithelialisation. (F. Wang et al., 2016) The LM511-E8-treated group exhibited higher levels of cytokeratin-10 than the control group on days 14 and 21. Moreover, the LM511-E8-treated group showed a significantly higher level of cytokeratin 14 from days 7–21 than the control group with the greatest highest level exhibited 14 d post-wounding, as shown in Table 6 and Figures 52 B, C and 54.

Table 6. Cytokeratin 14 and 10 immunohistochemistry score

Cytokeratin 14 immunohistochemistry score

Day after treatment	Control	Laminin 511 E 8
3	0.33 ± 0.57	0.66 ± 0.57
7	0.66 ± 0.57	2.00 ± 1.00*
14	2.00 ± 0.00	3.66 ± 0.57**
21	2.66 ± 0.57	4.00 ± 0.00*
28	3.33 ± 0.57	4.00 ± 0.00

Cytokeratin 10 immunohistochemistry score

Day after treatment	Control	Laminin 511 E 8
3	0.33 ± 0.57	0.66 ± 0.57
7	0.66 ± 0.57	2.00 ± 1.00
14	1.33 ± 0.57	3.00 ± 0.00*
21	1.66 ± 0.57	3.33 ± 0.57*
28	3.33 ± 0.57	4.00 ± 0.00
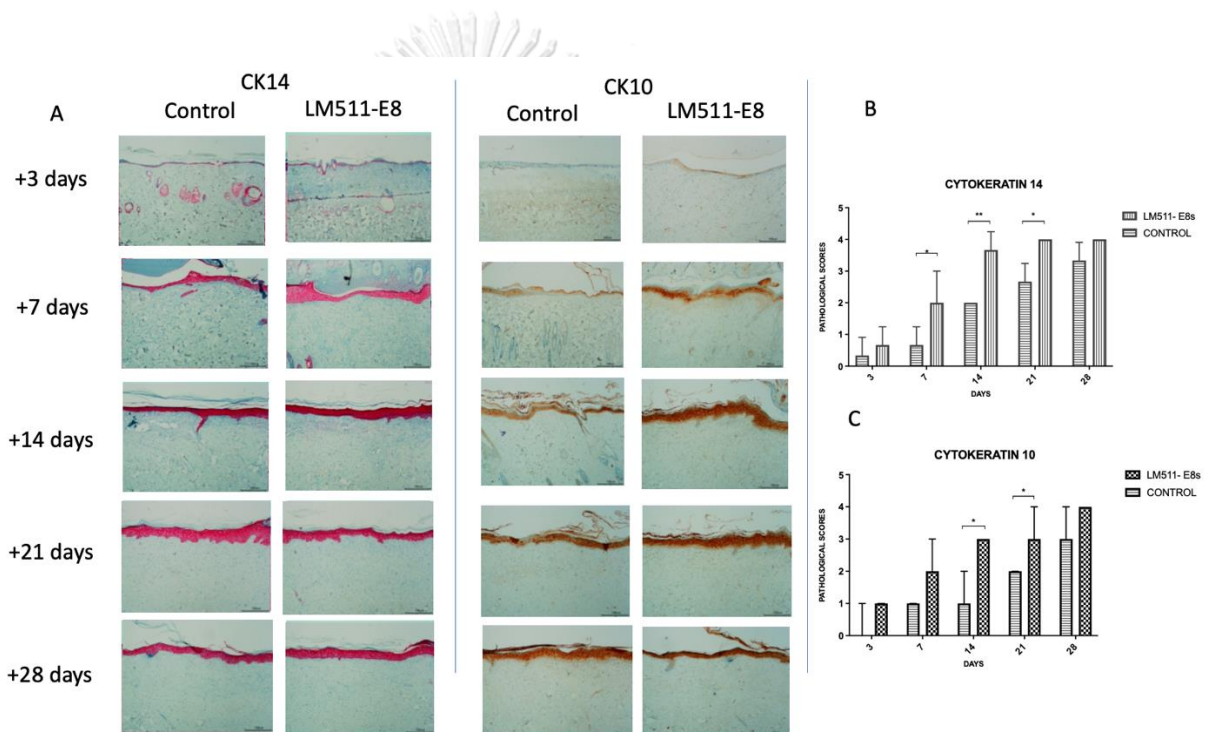
Figure 54. Cytokeratin 14 and 10 immunohistochemical features in rat burn wound treated daily with 2.5 □g of LM511-E8. (A) Sections of tissue immunostained with antibodies against cytokeratin 14 and 10 at 14 d, control and LM511 E8s. (B) Quantitation of cytokeratin 14. (C) Quantitation of cytokeratin 14; Kruskal–Wallis followed by a Dunn's post-hoc (*P 0.05, **P 0.01 and ***P 0.001; N = 8 per group)

Real-time PCR result
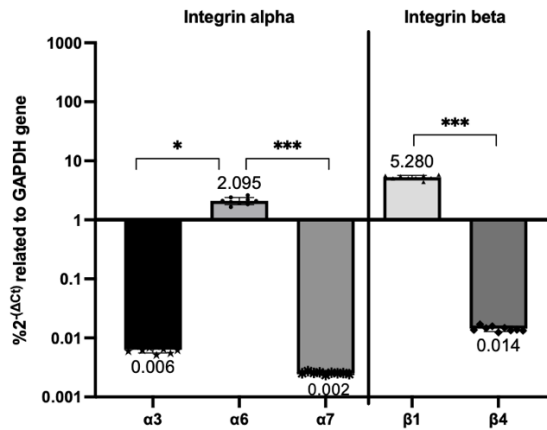
Figure 55. Integrins gene expression in REK cells normalised to total RNA;
and reference genes; the Y axis of the graph is normalized to the levels of GAPDH expression (*P
0.05, **P 0.01 and ***P 0.001; Kruskal–Wallis followed by a Dunn's post-hoc, N = 3 per group).
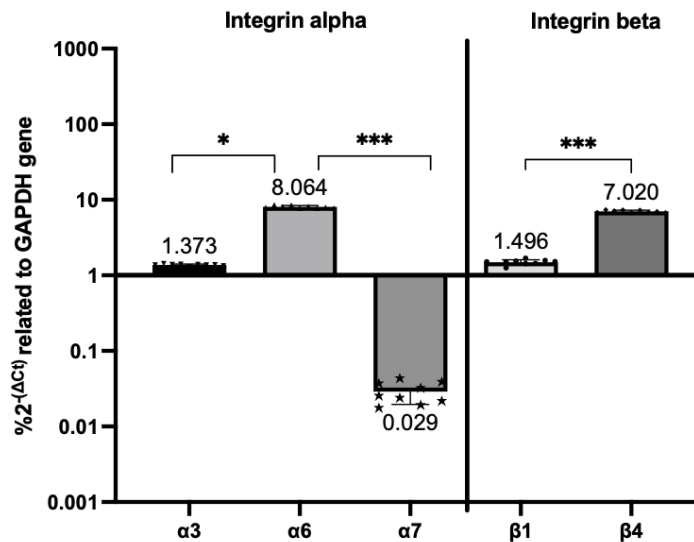
Figure 56. Integrins gene expression in HaCaT cells normalised to total RNA and reference genes; the
Y axis of the graph is normalized to the levels of GAPDH expression (*P 0.05, **P 0.01 and ***P
0.001; Kruskal–Wallis followed by a Dunn's post-hoc, N = 3 per group).

The RT-qPCR demonstrate the level of integrin alpha and beta in REK and
HaCaT cell (Fig. 55-56). In REK cell show the integrin level: i) alpha 3, 0.0063 ±
0.0007; ii) alpha 6, 2.10 ± 0.29; iii) alpha 7, 0.0025 ± 0.0001; iv) beta 1, 5.30 ± 0.43;

v) beta 4, 0.0140 ± 0.001% (Kruskal–Wallis test) (Fig. 55). In HaCaT cells the integrin levels were as follows: i) alpha 3, 1.373 ± 0.037; ii) alpha 6, 8.064 ± 0.328; iii) alpha 7, 0.029 ± 0.009; iv) beta 1, 1.496 ± 0.116; v) beta 4, 7.020 ± 0.265% (Kruskal–Wallis test) (Fig. 56).

Subsequently, REK and HaCaT were treated with fibronectin or LM511-E8 2.5 □g/□L. In general, integrin fold change expression in REK cells in the fibronectin compared with that in the LM511-E8 treated group expression (Fig. 57): i) alpha 3, 1.743 ± 0.089 vs 1.861 ± 0.094, P < 0.05; ii) alpha 6, 0.801 ± 0.096 vs 2.594 ± 0.197, P < 0.001; iii) alpha 7, 1.018 ± 0.057 vs 2.594 ± 0.197, P > 0.05; iv) beta 1, 0.990 ± 0.049 vs 1.196 ± 0.060, P < 0.01; v) beta 4, 1.522 ± 0.068 vs 1.578 ± 0.062, P > 0.05. The alpha 6 and beta 1 integrin gene expressions were highly upregulated in the REK cells-LM511-E8 treatment group, according to these fold change data.

In addition, integrin expression in HaCaT cells treated with fibronectin was compared to that in the LM511-E8 treated group (Fig.58) : i) alpha 3, 1.017 ± 0.045 vs 1.007 ± 0.037, P > 0.05; ii) alpha 6, 1.302 ± 0.056 vs 2.265 ± 0.339, P < 0.001; iii) alpha 7, 1.507 ± 0.067 vs 1.623 ± 0.067, P < 0.05; iv) beta 1, 0.894 ± 0.040 vs 1.854 ± 0.073, P < 0.01; v) beta 4, 1.007 ± 0.047 vs 1.013 ± 0.053, P > 0.05:(Unpaired t-test).
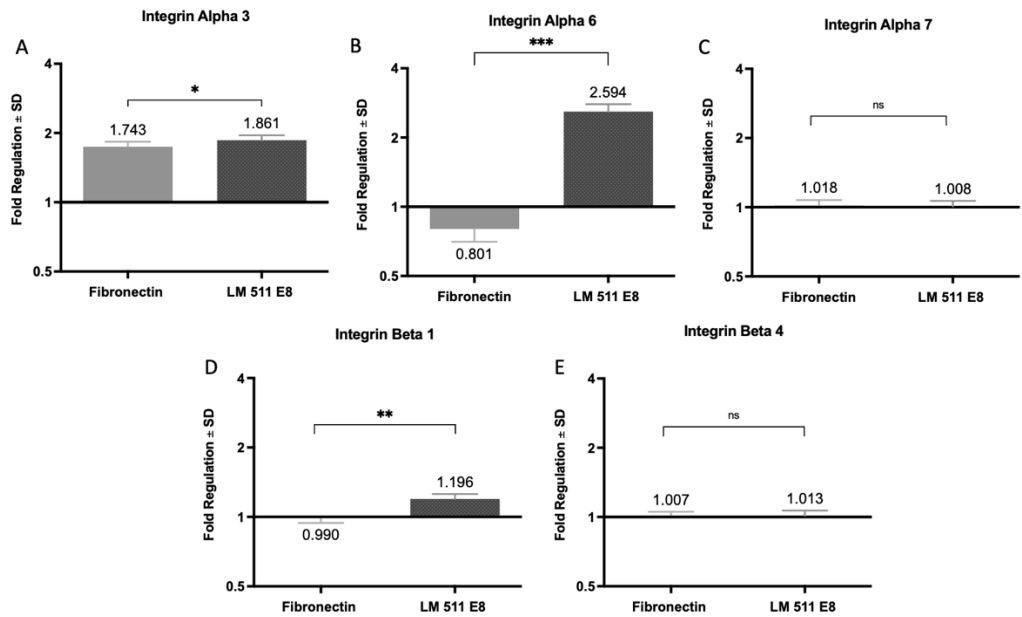
Figure 57. Gene expression for alpha integrin expression in REK cells (A–C) and beta integrin (D–E) following fibronectin 2.5 □g/□L and LM 511 E8 2.5 □g/□L treated; the Y axis of the graph is normalized to the levels of GAPDH expression (*P 0.05, **P 0.01 and ***P 0.001; Unpaired t-test, N = 3 per group).
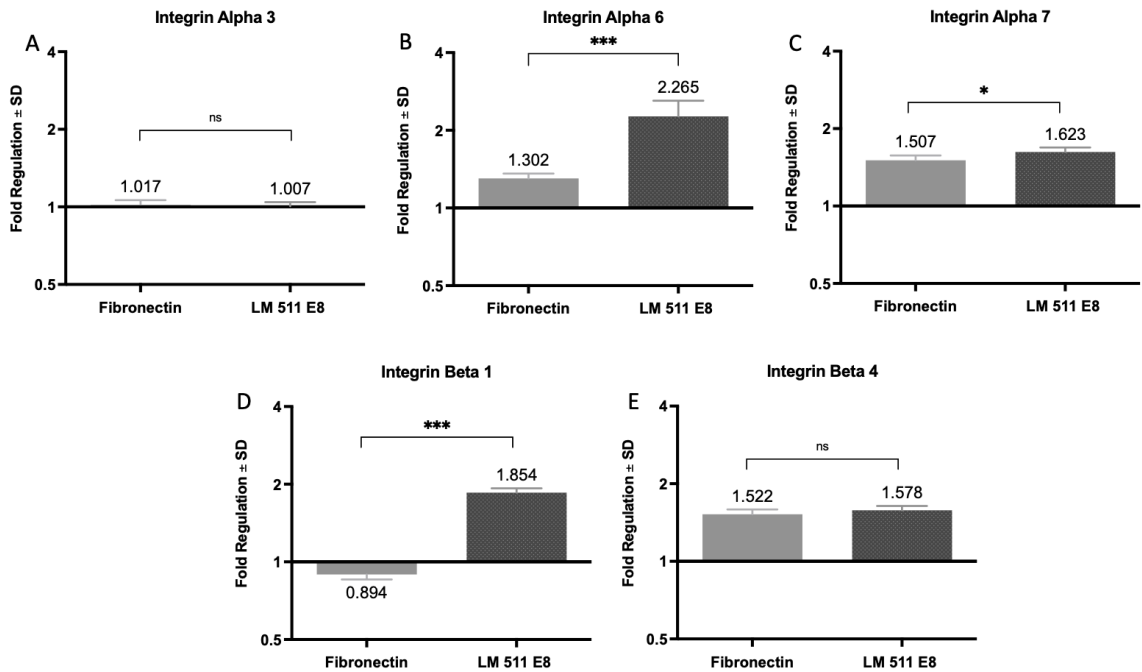
Figure 58. Gene expression for alpha integrin expression in HaCaT cells (A–C) and beta integrin (D–E) following fibronectin 2.5 □g/□L and LM 511 E8 2.5 □g/□L treatmented; the Y axis of the graph is normalized to the levels of GAPDH expression (*P 0.05, **P 0.01 and ***P 0.001; Unpaired t-test, N = 3 per group).

Flow Cytometry results

The integrins α6β4 and α6β1 on the cell surfaces of HaCaT and REK cells are the most abundant integrins in these cells, respectively. (Goodman, 1992; Koivisto et al., 2014; Longmate & Dipersio, 2014; Sonnenberg et al., 1990) Flow cytometry was conducted to characterised the integrin expression after cells were treated with LM511 E8. It was discovered that the expression of integrin α6β1 was greatly increased in both cells after treatment with LM511 E8 (Fig 59-60).
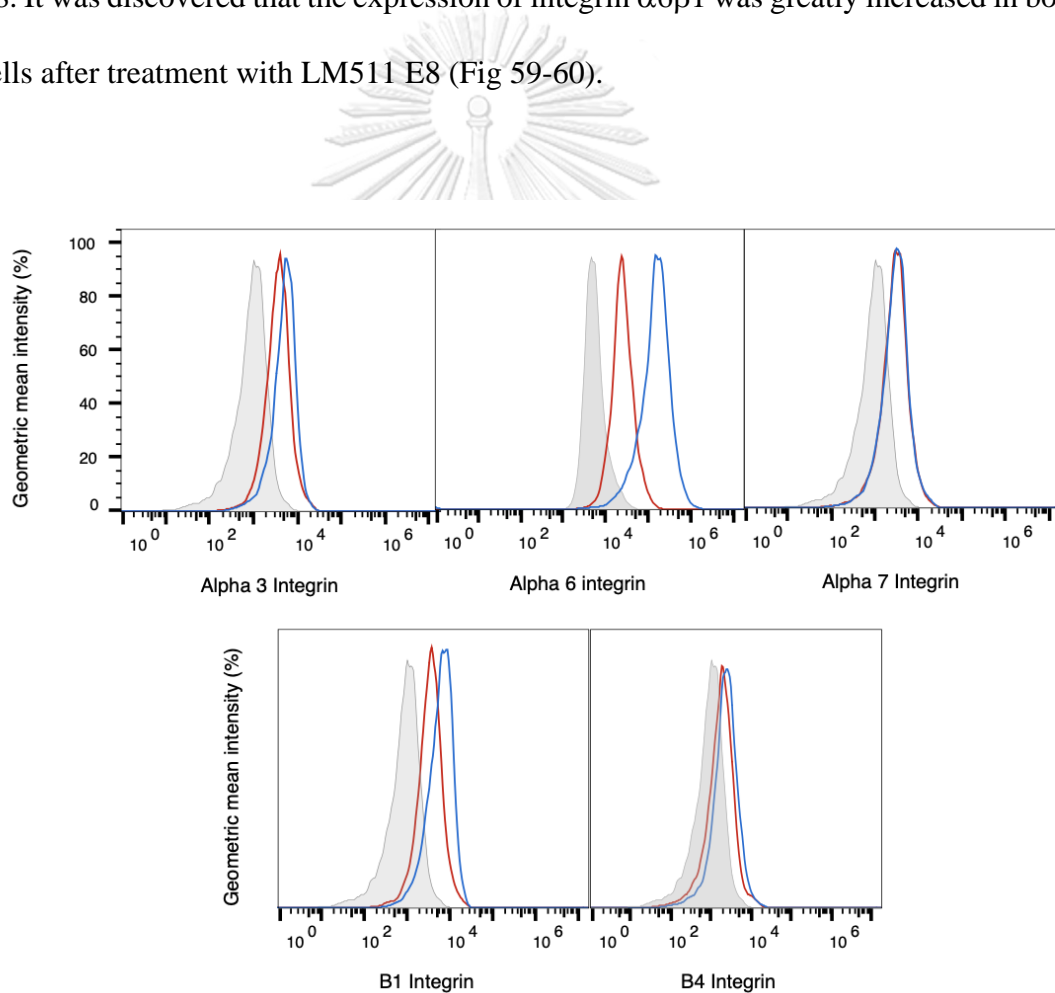
Figure 59. Flow cytometry results of integrin expression after REK cells being treated with LM 511 E8.
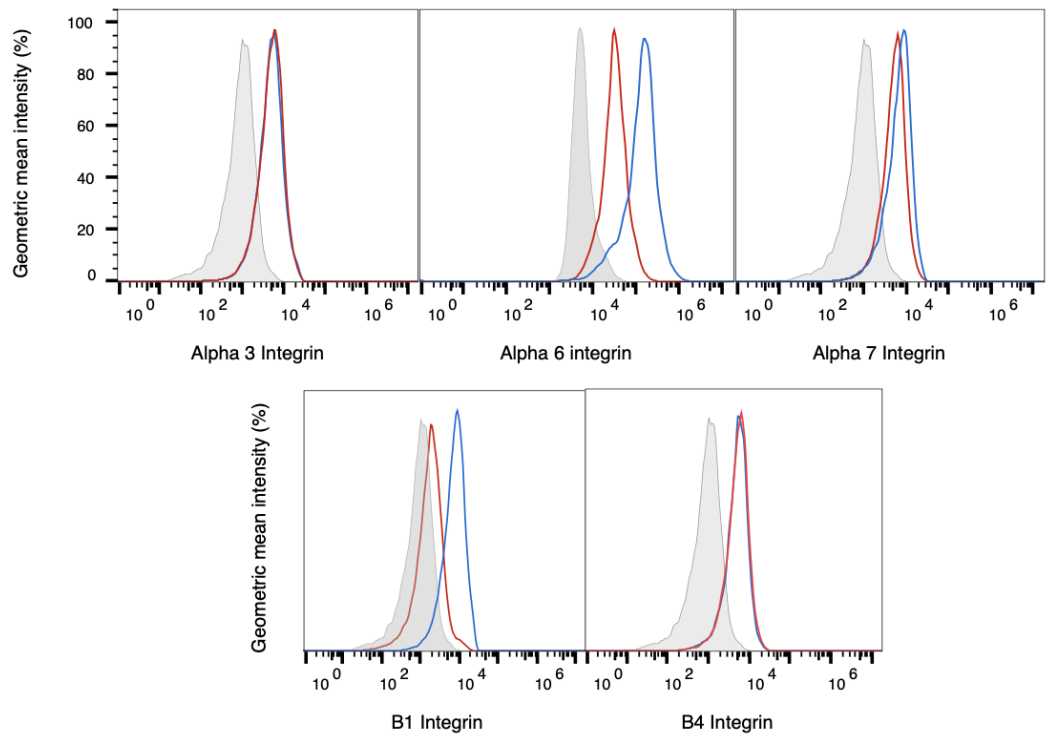
Figure 60. Flow cytometry results of integrin expression after HaCaT cells being treated with LM 511 E8.

The geometric means intensity levels of $\alpha6\beta1$ in the LM511 E8 group were higher than those of the saline-treated control significantly. The respective percentage geometric means intensity levels $\pm$ standard deviation in the control and LM511 E8-treated group of REK cells were: i) $\alpha3$, $4{,}750 \pm 50$ vs. $4{,}900 \pm 100$; ii) $\alpha6$, $30{,}200 \pm 120$ vs. $117{,}500 \pm 150$; iii) $\alpha7$, $5{,}200 \pm 50$ vs. $6{,}450 \pm 50$; iv) $\beta1$, $1{,}700 \pm 30$ vs. 7000 ± 30; and v) $\beta4$, $5{,}000 \pm 50$ vs. $4{,}850 \pm 30$ (Fig. 59) ; HaCaT cells were: i) $\alpha3$, $3{,}500 \pm 10$ vs. $4{,}800 \pm 20$; ii) $\alpha6$, $24{,}900 \pm 235$ vs. $138{,}200 \pm 515$; iii) $\alpha7$, $2{,}600 \pm 165$ vs. $2{,}770 \pm 120$; iv) $\beta1$, $3{,}450 \pm 30$ vs. $5{,}900 \pm 40$; and v) $\beta4$, $1{,}800 \pm 20$ vs. $2{,}300 \pm 70$; (Fig. 60).

Fluorescence microscopy

Immunofluorescence of REK demonstrated that α6β1 was found scattering on the cells' surfaces before and after treated with LM 511 E8, respectively (Fig. 61).
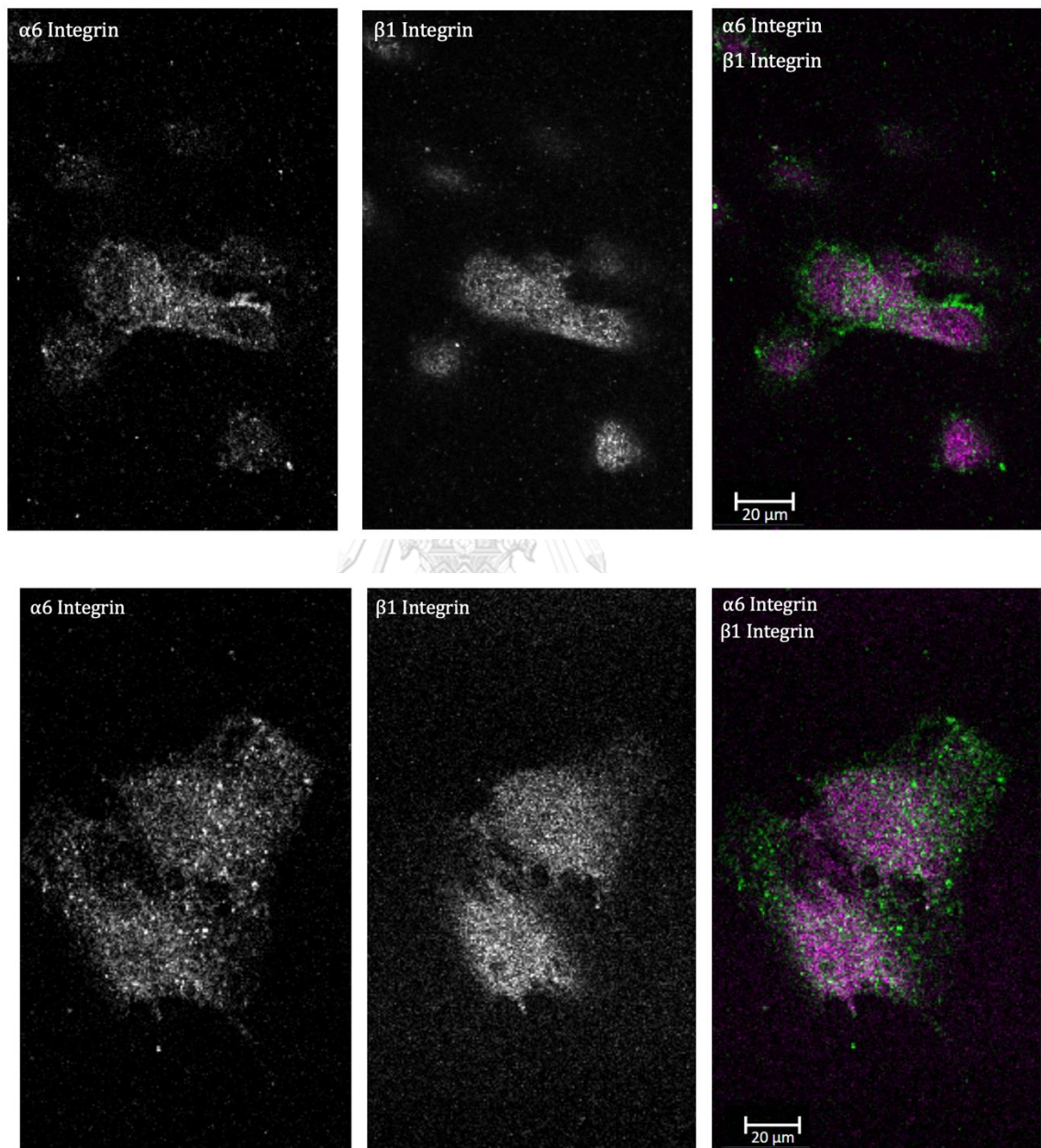
Figure 61. REK cells demonstrated α6β1 integrin on the cell surface.

A

Talin

B
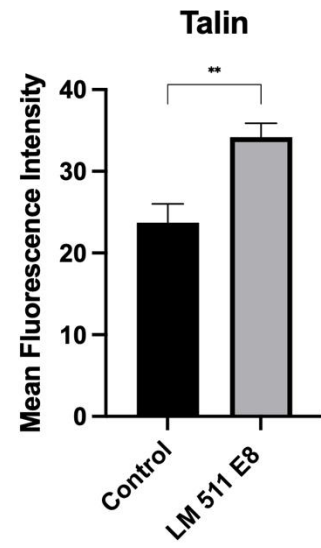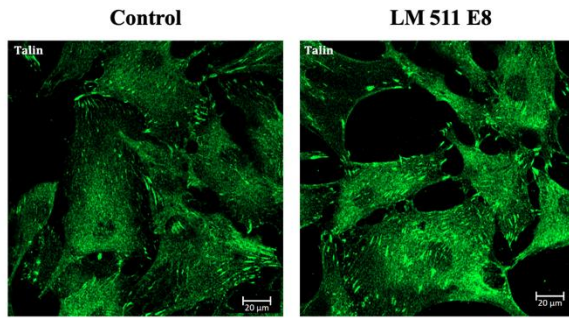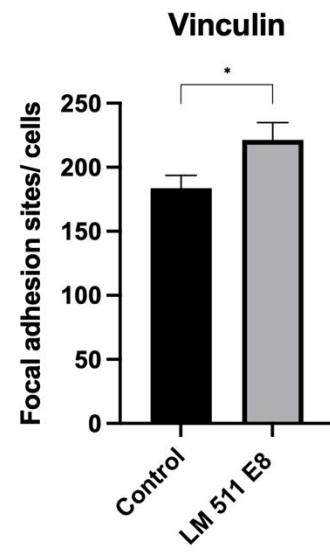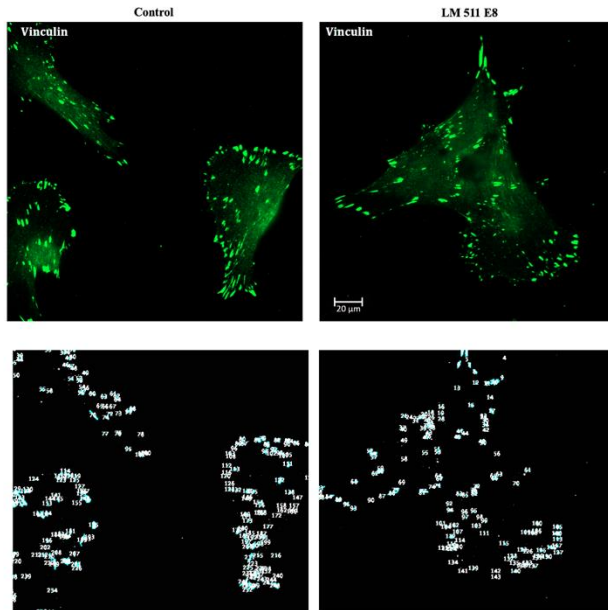
Vinculin

X
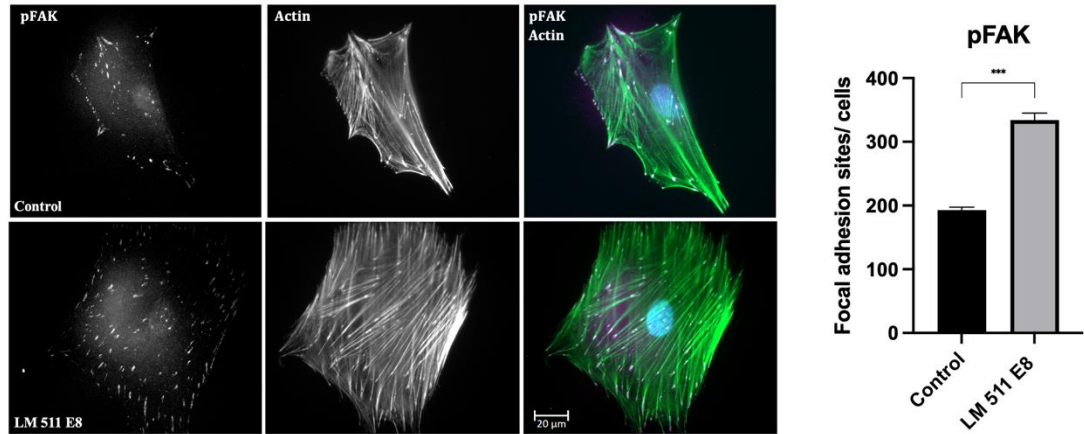
Figure 62. REK cells processed with antibodies against talin (A), vinculin (B), phosphorylated-FAK, and actin expression (C) before-after treated with LM 511 E8; t-test (*P 0.05, **P 0.01 and ***P 0.001; N = 3 per group)

The mean fluorescence intensity per cell in the control and LM 511 E8 groups showed that the levels were significantly higher in LM 511 E8 groups ($29.4 \pm 2.5\%$ and $35.6 \pm 3.2\%$, respectively; $p < 0.01$) (Fig. 62 A)

The number of focal adhesions per cell in the control and LM 511 E8 groups showed that the levels were significantly higher in LM 511 E8 groups, i) vinculin, 183 ± 9 vs. 220 ± 10; and ii) phosphorylated-FAK, 193 ± 5 vs. 334 ± 10; (Fig. 62 B, C).

Chapter 5. DISCUSSION

Burns may have local and systemic consequences. Inflammation after burn injuries could induce pain and various cytokines such as tumour necrosis factor (TNF) and interleukin (IL). (Aarabi, Longaker, & Gurtner, 2007; Baxter & Shires, 1968; Chua et al., 2016; da Silva et al., 2015) Furthermore, burn injuries cause increased oxidative stress as a result of the remarkable creation of ROS creation. This stress is the most important cause of local and systemic responses. Previous research has suggested that ROS causes lipid, membrane, nucleic acid, and protein damage, which can result in DNA breaks (SSB and DSB), and cell apoptosis. (da Silva et al., 2015; Karni et al., 2013). By slowing down this process, we can both accelerate burn wound healing and improve the quality of the wound healing process overall.

B1 siRNA

To date, however, there are no available studies on DNA methylation in burn wounds or burn scars. A hypertrophic scar is the most prevalent post-burn consequence. Hypertrophic scars are benign fibroproliferative disorders that do not extend beyond the areas of the original wound and are distinguished by the exaggerated production and deposition of collagen after burn injuries. (Aarabi et al., 2007; Zhu, Ding, & Tredget, 2016) The pathogenesis of hypertrophic scars remains unclear and poorly understood. Epigenetic alteration is an essential factor during the stimulation of fibroblasts in fibrotic diseases, such as pulmonary fibrosis, liver fibrosis, renal fibrosis, and systemic sclerosis. (Pal & Tyler, 2016; P. Sen et al., 2016) Moreover, recent studies have suggested that epigenetic alterations may be associated with keloid scar formation. (He et al., 2017; P. Sen et al., 2016) Here, I hypothesised that hypertrophic scar

formation may be associated with epigenetic changes and sought to examine this hypothesis by comparing Alu methylation levels and patterns between normal skin and hypertrophic scars.

I found the Alu methylation levels in tissue samples from the hypertrophic scar group were lower than those in normal skin samples (Fig. 36). The stratified statistical analysis between burn types, percent burn, depth of burn wound, time to injury, and scar complication in the level of methylation did not yield significant differences. To increase precision, I performed a dual assessment of methylation levels and patterns because of the inhomogeneous alteration of Alu methylation. I applied the COBRA-Alu technique instead of the standard DNA sequencing method (pyrosequencing). The COBRA technique can provide the same precision in measuring the percentage of methylation, although it consists of fewer CpGs than does pyrosequencing. (Jintaridth & Mutirangura, 2010; Pobsook, Subbalekha, Sannikorn, & Mutirangura, 2011; A. S. Yang et al., 2004) Moreover, the COBRA-Alu technique can provide essential information. The percentages of complete methylation, unmethylation, and two patterns of partial methylation were evaluated. Consequently, COBRA-Alu provides supplemental parameters for the evaluation of methylation status. These data are superior because pyrosequencing cannot differentiate among $^{m}C^{m}C$, $^{u}C^{m}C$, $^{m}C^{u}C$, and $^{u}C^{u}C$.

ROC analysis indicated that the $^{u}C^{m}C$ and $^{u}C^{u}C$ patterns have high sensitivity (Fig. 38) and specificity to monitor the hypertrophic scar progression and might be used for monitoring treatment with DNA methylation increasing agents such as Alu siRNA and targeted CRISPR-Cas9 DNA methylation soon. (Aigner, 2008; Patchsung et al., 2018; Vojta et al., 2016) ROC analysis indicated the potential use of the $^{u}C^{m}C$ and $^{u}C^{u}C$

patterns as DNA methylation markers to determine the progression and prognosis of hypertrophic scars and monitor treatment using DNA methylation-increasing agents with high sensitivity and specificity. Mutirangura et al. demonstrated that the hypomethylation process can cause genomic instability and DNA damage. DNA damage activates the intracellular DDR cascade, which is in responsible for DNA repair. Excess DDR and ROS may inhibit a kinase pathway, such as extracellular signal-regulated kinase/mitogen-activated protein kinase (ERK-MAPK), causing DNMT1 to function less efficiently. (Apiwat, 2019; Kongruttanachok et al., 2010; Mutirangura, 2019b; Patchsung et al., 2018) Excessive DDR, on the other hand, disrupts the cell cycle and alters cellular metabolism, potentially leading to senescence, inflammation, and apoptosis. (Lu et al., 2007; Sun et al., 2007) Based on our results, I hypothesised that burn trauma can promote Alu hypomethylation and DNA damage, which contribute to delayed wound healing in post-burn patients (Fig. 63). Given these phenomena, Marjolin's ulcer (Sadegh Fazeli, Lebaschi, Hajirostam, & Keramati, 2013), a rare skin cancer in burn scar patients, may be associated with epigenetic changes. (Zuo & Tredget, 2014) Therefore, $^{u}C^{m}C$ and $^{u}C^{u}C$ patterns of methylation may be used as markers for this kind of skin cancer; however, further studies are required to confirm our hypothesis.
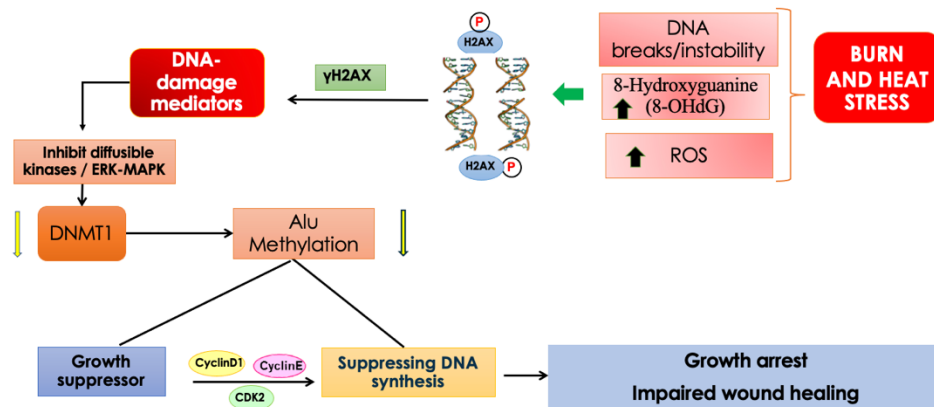
Figure 63. Hypomethylation as a result of burns and heat stress.

Previous studies have suggested that paracrine secretion from squamous cell tumours of the head and neck regions cause LINE-1 hypomethylation in circulating WBC. (Arayataweegool et al., 2019; Hsiung et al., 2007) Hence, hypertrophic scar tissue may release different secretory signals to regulate alterations in Alu methylation in the opposite direction, causing hypermethylation of WBCs. Further studies are needed to confirm this hypothesis.

Once I have determined that heat stress and burns may cause Alu hypomethylation, next I determined if B1siRNA can correct this hypomethylation and improve wound healing in a rat burn wound. B1 siRNA can be beneficial in recovering the genome and improving the wound healing process in rat second degree burn wounds. B1 methylation makes the genome more stable by counteracting the gathering of DNA damage.

The *in vitro* results demonstrated that B1 siRNA substantial increased B1 methylation, whereas the scrambled siRNA marginally increased B1 methylation. There were no off-target effects in the scrambled siRNA group (Fig. 39).

In the animal model experiments, 7–28 d post-injury, the B1 siRNA-treated group showed faster wound-contracture and higher re-epithelialisation rates than the

control group (Fig.40-41). An examination of wound tissue sections also revealed that treatment with B1 siRNA induced favourable pathological alterations in the repaired tissues. The ability of B1 siRNA to increase the B1 methylation levels and heal thermally induced injury corresponded with a decrease in DNA damage responses, based on 8-OHdG and γH2AX scores in the wound tissues (Fig. 43).

A molecular substance that can manage DNA methylation at a precise target, reduce DNA damage responses, stabilise the genome, and improve second-degree burn wound healing in a rat model was developed in the present study. A previous *in vitro* study showed that increased Alu methylation increases cell tolerance to toxic substances and increases the proliferation of these cells. (Patchsung et al., 2018) B1 siRNA specifically increased the methylation of B1 repetitive sequences by RdDM (Fig. 64). (Chalertpet et al., 2019; Marjori A. Matzke & Rebecca A. Mosher, 2014)
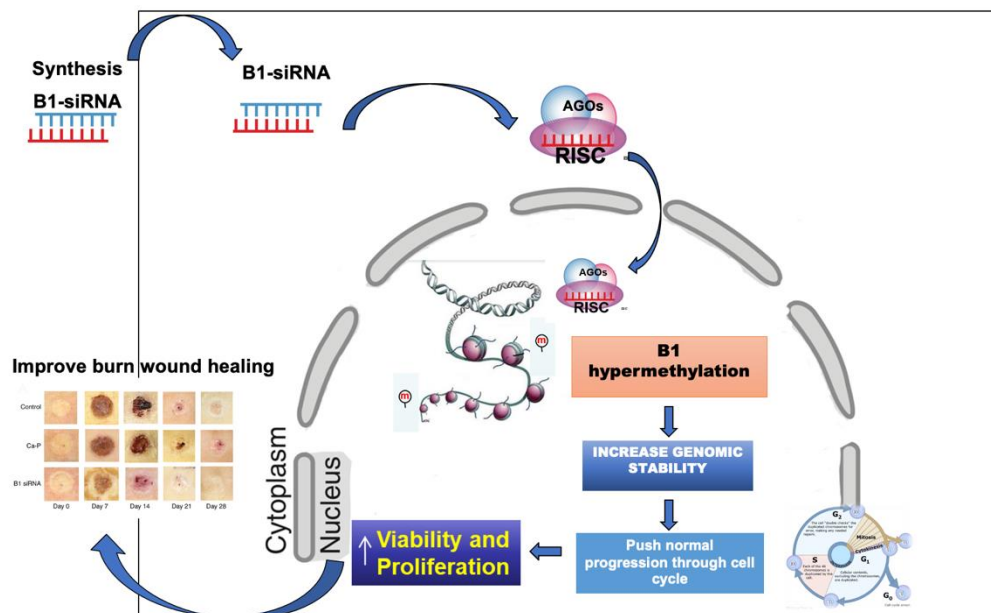
Figure 64. B1 repetitive sequence methylation enhances wound healing of second-degree burns in rats.

DNA damage responses can lead to mutations and delay (Velichko et al., 2015) cell cycle progression or cause cell cycle arrest. (Kantidze et al., 2016) Therefore, the reduction in DNA damage responses, as assessed using 8-OHdG and γH2AX scores, (Fig. 43), induced by increased B1 methylation using B1 siRNA, led to increased wound contraction rates and improved overall pathological scores in the wounded sections. Reduced inflammation, greater epithelialisation, new collagen deposition, fibroblast migration, and new blood vessel growth were also observed (Fig. 43).

However, the mechanism by which B1 methylation decreases DNA damage responses remains to be determined. (Koturbash et al., 2016) It is not clear how B1 siRNA can accelerate burn wound healing and reduce DNA damage responses; based on the results of the present study, it is hypothesised that IRS methylation is associated with other epigenetic phenomena, such as the formation of heterochromatin. (Baylin et al., 2001; J. H. Kim, 2019) Therefore, heterochromatin may protect DNA from damage and damage responses, and downregulate DNA replication and transcription processes. (Grewal & Jia, 2007) Another possibility is that a change in the chromatin form could ameliorate DNA repair activity. (Jakob et al., 2011; Y. Xu, Xu, & Price, 2012) This process might reduce DNA damage response in the heterochromatin region altered by B1 hypermethylation. Enhanced B1 methylation might lower oxidative stress and, consequently, DNA damage.

Box A of HMGB1

Box A of the HMGB1 protein may be a good potential nuclear protein that can effectively reduce genomic instability and increase the levels of PHY-RIND-EDSB in cellular damage after burn and heat stress, as well as potentially improve or reverse

117

damaging phenotypes by restoring impaired wound healing in burn wounds. PHY-RIND-EDSB protect cells from the DNA damage response as well as from H2AX and 8-OHdG. (Yasom et al., 2022b) Furthermore, 8-OHdG is one of the most prevalent lesions caused by ROS, which can result in mispairing with adenine, leading to $G > T$ alterations in the resultant strand of DNA. (Tubbs & Nussenzweig, 2017) The expression of the H2AX gene was investigated. H2AX is a highly specific and sensitive molecular marker for DNA damage that may be used to track the progression of the damage. After DNA double-strand breaks are produced, the enzyme H2AX responds rapidly. (Valdiglesias, Giunta, Fenech, Neri, & Bonassi, 2013)

At 7–28 days post-injury, the Box A of HMGB1-treated group demonstrated quicker wound contracture and greater re-epithelialisation rates than the control group in animal model studies (Fig.46-47).An analysis of injured tissue sections demonstrated that treatment with Box A of HMGB1 caused extensive pathological changes in the healed tissues. I also observed reduced inflammation, greater epithelialisation, new collagen deposition, fibroblast migration, and new blood vessel growth. The capacity of HMGB1 Box A to enhance PHY-RIND-EDSB levels and repair thermal injury correlated with a large decrease in DNA damage responses in wound tissues, as measured by 8-OHdG and H2AX scores (Fig. 48).

Box A improved DNA durability by producing PHY-RIND-EDSBs and did not promote DNA repair. (Yasom et al., 2022b) Here I showed that Box A improved burn wound healing. Therefore, this study suggests secondary DNA damage in burn wounds due to PHY-RIND-EDSBs reduction. In addition to DNA damage reduction, Box A produced PHY-RIND-EDSBs and gradually reduced all DNA damage consequences. So, Box A should limit burn complication sequelae such as fibrosis and cancer. While

performing rat rejuvenation studies, Box A could diminish liver fibrosis. (Yasom et al., 2022b) Intriguingly, Box A may possess the potential to remove burn fibrosis.

PHY-RIND-EDSB are associated with other epigenetic phenomena, such as the formation of heterochromatin and IRS methylation (J. H. Kim, 2019). Therefore, heterochromatin might protect DNA from damage and damage response and downregulate DNA replication and transcription processes. Another assumption is that a change in the chromatin form could ameliorate DNA repair activity. (Jakob et al., 2011) In this work, I revealed that HMGB1 is a crucial protein that can play a critical function in reducing DNA damage and preventing genomic instability in order to avoid genomic instability. First and foremost, HMGB1 is responsible for the generation and maintenance of PHY-RIND-EDSB in the genome. Second, HMGB1 produced PHY-RIND-EDSB and shielded DNA from the DNA damage response, both of which were important findings. First, I investigated the possibility that Box A of HMGB1 is responsible for the generation of PHY-RIND-EDSB. The amounts of PHY-RIND-EDSB in rat burn wounds following treatment with Box A of the HMGB1 protein were evaluated in this study (Fig. 65). As demonstrated in the study, the larger number of PHY-RIND-EDSB found in the HMGB1 treated group led to enhanced burn wound healing. These findings are in agreement with prior research, which established the importance of HMGB1 in the maintenance of PHY-RIND-EDSB. (Thongsroy et al., 2013; Yasom et al., 2022a)
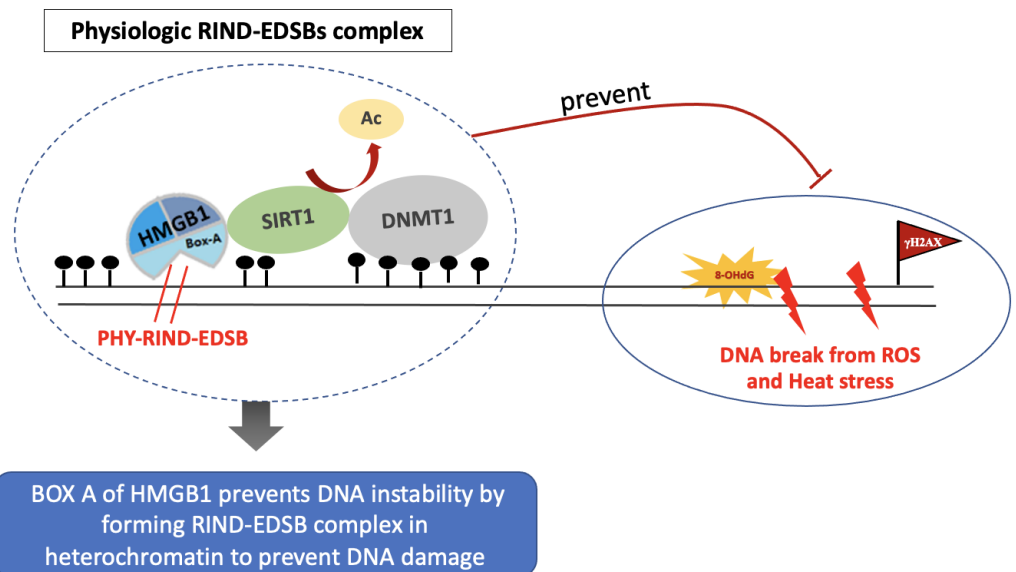
Figure 65. BOX A of HMGB1 prevents DNA instability by forming PHY-RIND-EDSB complex.

Laminin 511 E8

The data presented here demonstrate that the repair process of burn wounds can be improved using a short protein fragment derived from LM511. Specifically, increasing the epithelialisation rate, especially during the proliferation phase of wound healing, accelerating wound contracture rate, improving the total pathological score, increasing the rate of new collagen synthesis, and increasing cytokeratin expression. These studies have also demonstrated that LM511-E8 could increase the quantity of well-organised bands of collagen and the number of fibroblasts, while there were fewer inflammatory cells. Together these data support that LM511-E8 is a promising a new method to treat burn patients.

Optimum healing of a burn wound needs the coordinated interaction between many pathways, such as inflammation, proliferation, neovascularisation, and remodelling. After the blood clot formation immediately following an injury,

keratinocytes and fibroblasts migrate to the wound. Therefore, epithelialisation is also a crucial process for wound healing, with insufficient epithelialisation resulting in impaired wound healing. (Velnar, Bailey, & Smrkolj, 2009) The overall pathological score that comprises epithelialisation, polymorphonuclear leukocyte (PMNL) infiltration, collagen formation, the number of fibroblasts, and the presence of new blood vessels was higher in the proliferation phase of wound healing from day 14 to 28 compared with the control group (Fig. 51-54). LM511 has been widely studied, and the E8 portion, in particular, contains high-affinity cell surface receptor binding sites, including that for integrin α6β1 and enhances human pluripotent stem cell adhesion and accelerates the migration of human limbal melanocyte via FAK. (DiPersio et al., 2016; Januszyk et al., 2017; Takamichi Miyazaki et al., 2012; Y. Sugawara et al., 2019; Takizawa et al., 2017) The LM511-E8 might drive these behaviours, through the FAK pathway after stimulating integrin α6β1 expression. (Leu et al., 2003; M, 1992; Murayama, Nishida, & Sekiguchi, 1996; Vitillo, Baxter, Iskender, Whiting, & Kimber, 2016) To test this I use RT-qPCR measured the prevalence of integrin types on the cell. On the REK cells, integrin α6 was the most prevalent among other alpha-type integrins that were discovered to be capable of binding to laminin proteins, and integrin β1 was found to be among other beta-type integrins, followed by integrin β4, that were also capable of interacting with laminins (Fig. 55-58). When cells were treated with LM 511 E8, the expression of the integrin α6β1 increased in comparison to the other integrins. I confirmed this result by flow cytometry and immunofluorescence staining showed that integrin α6β1 was prominent among other integrin types on the REK and HaCaT cells (Fig. 59-60). Furthermore, after treating REK with LM511-E8, talin, vinculin, and pFAK protein expression increased (Fig. 61-62), which may be the cause of improved

121

epithelialisation (Choi, Yang, Kulkarni, Moh, & Kim, 2015; McLean et al., 2004), as well as increased fibroblast and collagen formation and angiogenesis. (Cabrita et al., 2011; X. Peng et al., 2004; Vitillo et al., 2016; X. Zhao & Guan, 2011)

As a result of these findings, I hypothesised that integrin $\alpha6\beta1$ is responsible for the attachment of LM 511 E8 to its host basement membrane and is capable of attaching to keratinocytes and stimulating their proliferation and epithelialisation via the focal adhesion that increases after treatment (Fig. 66). (Naresh Polisetti et al., 2020)
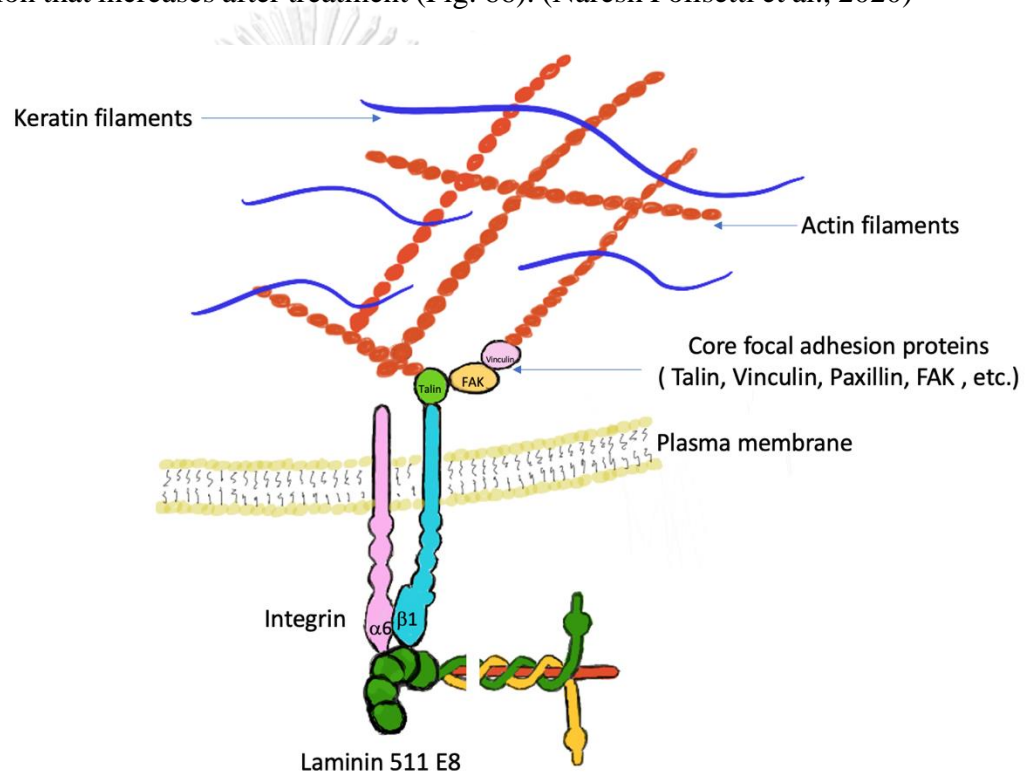
Figure 66. Cellular focal adhesion.

I believe that these findings will be of clinical relevance for large and slow-to-heal wounds, where the provision of an exogenous substrate to promote repair would be most beneficial for recovery. (Pouliot & Kusuma, 2013; Takizawa et al., 2017) Moreover, LM511 is usually found in the mature endothelial basement membrane, and therefore, LM511-E8 fragment could be involved in the maturation of endothelial cells. (Hallmann et al., 2005; Sorokin et al., 1997)

This study has shown that LM511-E8 treatment improves the second-degree burn wound repair in rats and suggests that the development of a therapeutic intervention employing LM511-E8 to improve burn wound outcomes represents an extremely promising avenue for future research.

Chapter 6. CONCLUSIONS AND OUTLOOK

I propose that the three substances studied could ameliorate and heal second-degree burn wounds. I believe that B1siRNA, Box A of HMGB1 and laminin 511 E8, have potential as novel therapeutic agents for burn wound therapy.
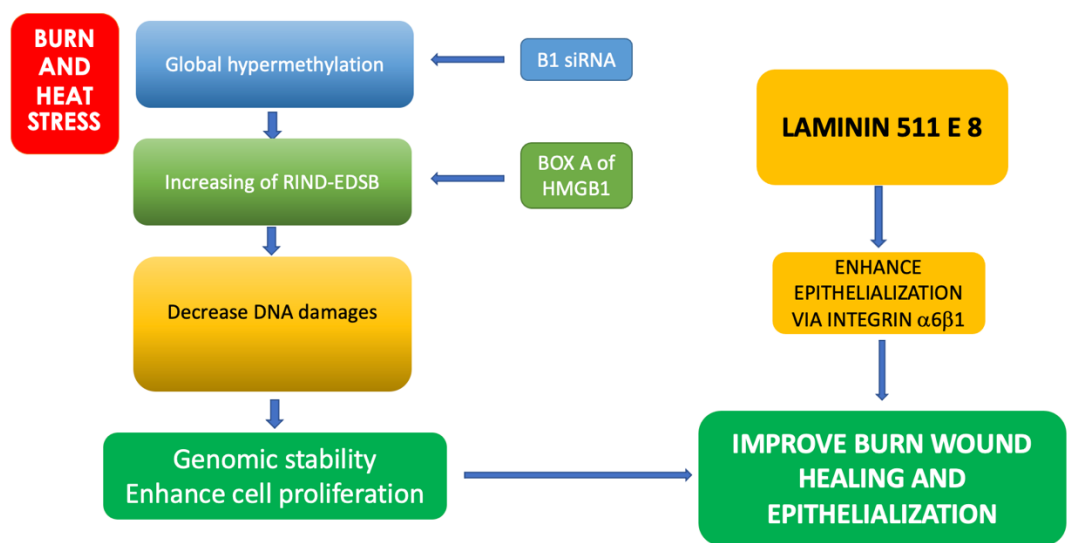
Figure 67. The three substances used throughout the study improved and treated second-degree burns.

In conclusion, epigenetic modifications may play a major role in hypertrophic scar pathogenesis. This study could be the starting point for developing a novel technique for scar treatment in post-burn patients.

Furthermore, B1 siRNA can promote the healing of second-degree burn wounds in rats by increasing the epithelialisation rate, improving pathological scores, and accelerating the wound healing rate. These results indicate that B1 siRNA promotes wound healing by reducing the DNA damage response and enhancing global DNA methylation. B1 siRNA assisted in genomic recovery and improved the healing pr

of second-degree burn wounds in rats; this suggests that B1 siRNA may serve as a novel treatment method for burn wounds in clinical practice, perhaps as a topical agent against repetitive sequences. Further studies to evaluate the efficacy of B1 siRNA against different types of burns with different severities will prove highly beneficial for determining the clinical potential of this treatment.

this research revealed that HMGB1 is involved in the conduction of PHY-RIND-EDSB. PHY-RIND-EDSB have a function in the prevention of genomic instability as well as the improvement of wound healing following burn injury. By enhancing the rate of epithelialisation, improving pathological scores, and speeding wound healing, Box A of HMGB1 could enhance the healing of second-degree burn wounds in rats. These findings suggest that Box A of HMGB1 enhances wound healing by inhibiting the DNA damage response and increasing PHY-RIND-EDSB (Fig. 67). Box A of HMGB1 facilitated in the recovery of the genome and the improvement of the healing process in second-degree burn wounds in rats; this implies that Box A of HMGB1 might represent a new therapy option for burn wounds in practical practice, potentially as a topical medication for the treatment of burns. Experiments studies of Box-A of HMGB1 against a variety of burns of varying severity would be remarkably valuable in assessing the clinical potential of this medication. Experiments studies of Box-A of HMGB1 against a variety of burns of varying severity would be remarkably valuable in assessing the clinical potential of this therapy.

For the last substance, the main research question unexplored yet is the optimal mode of delivery. Here, I applied LM511-E8 in a drop-wise manner to the wounds. While this was effective in these small studies, it would be prohibitively expensive to apply to large wounds in a clinical setting. Integration of LM511-E8 into an artificial

substrate should be explored as a treatment option in the future. Further studies to assess the efficacy of LM511-E8 in patients or preclinical models of severe burn wounds and comorbidities such as diabetes.

จุฬาลงกรณ์มหาวิทยาลัย
CHULALONGKORN UNIVERSITY

REFERENCES

AARABI, S., LONGAKER, M. T. & GURTNER, G. C. 2007. Hypertrophic Scar Formation Following Burns and Trauma: New Approaches to Treatment. *PLOS Medicine,* 4**,** e234.

ABDULLAHI, A., AMINI-NIK, S. & JESCHKE, M. G. 2014. Animal models in burn research. *Cell Mol Life Sci,* 71**,** 3241-55.

AGUILAR, C. & GARDINER, D. M. 2015. DNA Methylation Dynamics Regulate the Formation of a Regenerative Wound Epithelium during Axolotl Limb Regeneration. *PLOS ONE,* 10**,** e0134791.

AIGNER, A. 2008. Cellular delivery in vivo of siRNA-based therapeutics. *Curr Pharm Des,* 14**,** 3603-19.

ALGHAMDI, M. A., WALLACE, H. J., MELTON, P. E., MOSES, E. K., STEVENSON, A., AL-EITAN, L. N., REA, S., DUKE, J. M., DANIELSEN, P. L., PRÊLE, C. M., WOOD, F. M. & FEAR, M. W. 2020. Identification of Differentially Methylated CpG Sites in Fibroblasts from Keloid Scars. *Biomedicines,* 8.

AMIRSHEYBANI, H. R., CRECELIUS, G. M., TIMOTHY, N. H., PFEIFFER, M., SAGGERS, G. C. & MANDERS, E. K. 2001. The natural history of the growth of the hand: I. Hand area as a percentage of body surface area. *Plast Reconstr Surg,* 107**,** 726-33.

APIWAT, M. 2019. A Hypothesis to Explain How the DNA of Elderly People Is Prone to Damage: Genome-Wide Hypomethylation Drives Genomic Instability in the Elderly by Reducing Youth-Associated Gnome-Stabilizing DNA Gaps.

ARAKI, E., MOMOTA, Y., TOGO, T., TANIOKA, M., HOZUMI, K., NOMIZU, M., MIYACHI, Y. & UTANI, A. 2009. Clustering of syndecan-4 and integrin beta1 by laminin alpha 3 chain-derived peptide promotes keratinocyte migration. *Mol Biol Cell,* 20**,** 3012-24.

ARAYATAWEEGOOL, A., SRISUTTEE, R., MAHATTANASAKUL, P., TANGJATURONSASME, N., KEREKHANJANARONG, V., KITKUMTHORN, N. & MUTIRANGURA, A. 2019. Head and neck squamous cell carcinoma drives long interspersed element-1 hypomethylation in the peripheral blood mononuclear cells. *Oral Dis,* 25**,** 64-72.

AUMAILLEY, M., NURCOMBE, V., EDGAR, D., PAULSSON, M. & TIMPL, R. 1987. The cellular interactions of laminin fragments. Cell adhesion correlates with two fragment-specific high affinity binding sites. *J Biol Chem,* 262**,** 11532-8.

BARBOT, W., DUPRESSOIR, A., LAZAR, V. & HEIDMANN, T. 2002. Epigenetic regulation of an IAP retrotransposon in the aging mouse: progressive demethylation and de-silencing of the element by its repetitive induction. *Nucleic Acids Res,* 30**,** 2365-73.

BATZER, M. A. & DEININGER, P. L. 2002. Alu repeats and human genomic diversity. *Nat Rev Genet,* 3**,** 370-9.

BAXTER, C. R. & SHIRES, T. 1968. Physiological response to crystalloid resuscitation of severe burns. *Ann N Y Acad Sci,* 150**,** 874-94.

BAYLIN, S. B., ESTELLER, M., ROUNTREE, M. R., BACHMAN, K. E., SCHUEBEL, K. & HERMAN, J. G. 2001. Aberrant patterns of DNA methylation, chromatin formation and gene expression in cancer. *Hum Mol Genet,* 10**,** 687-92.

BEDELBAEVA, K., SNYDER, A., GOUREVITCH, D., CLARK, L., ZHANG, X.-M., LEFEROVICH, J., CHEVERUD, J. M., LIEBERMAN, P. & HEBER-KATZ, E. 2010. Lack of p21 expression links cell cycle control and appendage regeneration in mice. *Proceedings of the National Academy of Sciences,* 107**,** 5845.

BELANCIO, V. P., DEININGER, P. L. & ROY-ENGEL, A. M. 2009. LINE dancing in the human genome: transposable elements and disease. *Genome Med,* 1**,** 97.

BIND, M.-A., ZANOBETTI, A., GASPARRINI, A., PETERS, A., COULL, B., BACCARELLI, A., TARANTINI, L., KOUTRAKIS, P., VOKONAS, P. & SCHWARTZ, J. 2014. Effects of temperature and relative humidity on DNA methylation. *Epidemiology (Cambridge, Mass.),* 25**,** 561-569.

BIND, M. C., COULL, B. A., BACCARELLI, A., TARANTINI, L., CANTONE, L., VOKONAS, P. & SCHWARTZ, J. 2016. Distributional changes in gene-specific methylation associated with temperature. *Environ Res,* 150**,** 38-46.

BOLLATI, V., SCHWARTZ, J., WRIGHT, R., LITONJUA, A., TARANTINI, L., SUH, H., SPARROW, D., VOKONAS, P. & BACCARELLI, A. 2009. Decline in genomic DNA methylation through aging in a cohort of elderly subjects. *Mech Ageing Dev,* 130**,** 234-9.

BOMBARO, K. M., ENGRAV, L. H., CARROUGHER, G. J., WIECHMAN, S. A., FAUCHER, L., COSTA, B. A., HEIMBACH, D. M., RIVARA, F. P. & HONARI, S. 2003. What is the prevalence of hypertrophic scarring following burns? *Burns,* 29**,** 299-302.

BRUSKOV, V. I., MALAKHOVA, L. V., MASALIMOV, Z. K. & CHERNIKOV, A. V. 2002. Heat-induced formation of reactive oxygen species and 8-oxoguanine, a biomarker of damage to DNA. *Nucleic Acids Res,* 30**,** 1354-63.

CABRITA, M. A., JONES, L. M., QUIZI, J. L., SABOURIN, L. A., MCKAY, B. C. & ADDISON, C. L. 2011. Focal adhesion kinase inhibitors are potent anti-angiogenic agents. *Molecular Oncology,* 5**,** 517-526.

CAI, E. Z., ANG, C. H., RAJU, A., TAN, K. B., HING, E. C., LOO, Y., WONG, Y. C., LEE, H., LIM, J., MOOCHHALA, S. M., HAUSER, C. A. & LIM, T. C. 2014. Creation of consistent burn wounds: a rat model. *Arch Plast Surg,* 41**,** 317-24.

CANCIO, L. C. 2020. Topical Antimicrobial Agents for Burn Wound Care: History and Current Status. *Surgical Infections,* 22**,** 3-11.

CAO, X., DENG, W., WEI, Y., SU, W., YANG, Y., WEI, Y., YU, J. & XU, X. 2011. Encapsulation of plasmid DNA in calcium phosphate nanoparticles: stem cell uptake and gene transfer efficiency. *Int J Nanomedicine,* 6**,** 3335-49.

CASTANOTTO, D., TOMMASI, S., LI, M., LI, H., YANOW, S., PFEIFER, G. P. & ROSSI, J. J. 2005. Short hairpin RNA-directed cytosine (CpG) methylation of the RASSF1A gene promoter in HeLa cells. *Mol Ther,* 12**,** 179-83.

CHALERTPET, K., PIN-ON, P., APORNTEWAN, C., PATCHSUNG, M., INGRUNGRUANGLERT, P., ISRASENA, N. & MUTIRANGURA, A. 2019.

Argonaute 4 as an Effector Protein in RNA-Directed DNA Methylation in Human Cells. *Front Genet,* 10**,** 645.

CHAN, T., GHAHARY, A., DEMARE, J., YANG, L., IWASHINA, T., SCOTT, P. G. & TREDGET, E. E. 2002. Development, characterization, and wound healing of the keratin 14 promoted transforming growth factor-beta1 transgenic mouse. *Wound Repair Regen,* 10**,** 177-87.

CHAN, Y., ANTON-LAMPRECHT, I., YU, Q. C., JÄCKEL, A., ZABEL, B., ERNST, J. P. & FUCHS, E. 1994. A human keratin 14 "knockout": the absence of K14 leads to severe epidermolysis bullosa simplex and a function for an intermediate filament protein. *Genes Dev,* 8**,** 2574-87.

CHEN, L., HE, X., XIAN, J., LIAO, J., CHEN, X., LUO, Y., WANG, Z. & LI, N. 2021. Development of a framework for managing severe burns through a 17-year retrospective analysis of burn epidemiology and outcomes. *Scientific Reports,* 11**,** 9374.

CHENAIS, B. 2015. Transposable elements in cancer and other human diseases. *Curr Cancer Drug Targets,* 15**,** 227-42.

CHIANG, R. S., BOROVIKOVA, A. A., KING, K., BANYARD, D. A., LALEZARI, S., TORANTO, J. D., PAYDAR, K. Z., WIRTH, G. A., EVANS, G. R. D. & WIDGEROW, A. D. 2016. Current concepts related to hypertrophic scarring in burn injuries. *Wound repair and regeneration : official publication of the Wound Healing Society [and] the European Tissue Repair Society,* 24**,** 466-477.

CHISHOLM, K. M., AUBERT, S. D., FREESE, K. P., ZAKIAN, V. A., KING, M. C. & WELCSH, P. L. 2012. A genomewide screen for suppressors of Alu-mediated rearrangements reveals a role for PIF1. *PLoS One,* 7**,** e30748.

CHOI, Y.-H., YANG, D. J., KULKARNI, A., MOH, S. H. & KIM, K. W. 2015. Mycosporine-Like Amino Acids Promote Wound Healing through Focal Adhesion Kinase (FAK) and Mitogen-Activated Protein Kinases (MAP Kinases) Signaling Pathway in Keratinocytes. *Marine Drugs,* 13.

CHUA, A. W., KHOO, Y. C., TAN, B. K., TAN, K. C., FOO, C. L. & CHONG, S. J. 2016. Skin tissue engineering advances in severe burns: review and therapeutic applications. *Burns Trauma,* 4**,** 3.

CORDAUX, R. & BATZER, M. A. 2009. The impact of retrotransposons on human genome evolution. *Nat Rev Genet,* 10**,** 691-703.

COULOMBE, P. A., HUTTON, M. E., LETAI, A., HEBERT, A., PALLER, A. S. & FUCHS, E. 1991. Point mutations in human keratin 14 genes of epidermolysis bullosa simplex patients: genetic and functional analyses. *Cell,* 66**,** 1301-11.

COULOMBE, P. A. & LEE, C. H. 2012. Defining keratin protein function in skin epithelia: epidermolysis bullosa simplex and its aftermath. *J Invest Dermatol,* 132**,** 763-75.

DA SILVA, N. T., QUINTANA, H. T., BORTOLIN, J. A., RIBEIRO, D. A. & DE OLIVEIRA, F. 2015. Burn injury induces skeletal muscle degeneration, inflammatory host response, and oxidative stress in wistar rats. *J Burn Care Res,* 36**,** 428-33.

DEFLORIN, C., HOHENAUER, E., STOOP, R., VAN DAELE, U., CLIJSEN, R. & TAEYMANS, J. 2020. Physical Management of Scar Tissue: A Systematic Review and Meta-Analysis. *The Journal of Alternative and Complementary Medicine,* 26**,** 854-865.

DESPA, F., ORGILL, D. P., NEUWALDER, J. & LEE, R. C. 2005. The relative thermal stability of tissue macromolecules and cellular structure in burn injury. *Burns,* 31**,** 568-77.

DEUTZMANN, R., AUMAILLEY, M., WIEDEMANN, H., PYSNY, W., TIMPL, R. & EDGAR, D. 1990. Cell adhesion, spreading and neurite stimulation by laminin fragment E8 depends on maintenance of secondary and tertiary structure in its rod and globular domain. *Eur J Biochem,* 191**,** 513-22.

DEWHIRST, M. W., LORA-MICHIELS, M., VIGLIANTI, B. L., DEWEY, W. C. & REPACHOLI, M. 2003. Carcinogenic effects of hyperthermia. *Int J Hyperthermia,* 19**,** 236-51.

DINGEMANS, A. M., VAN DEN BOOGAART, V., VOSSE, B. A., VAN SUYLEN, R. J., GRIFFIOEN, A. W. & THIJSSEN, V. L. 2010. Integrin expression profiling identifies integrin alpha5 and beta1 as prognostic factors in early stage non-small cell lung cancer. *Mol Cancer,* 9**,** 152.

DIPERSIO, C. M., ZHENG, R., KENNEY, J. & VAN DE WATER, L. 2016. Integrin-mediated regulation of epidermal wound functions. *Cell and Tissue Research,* 365**,** 467-482.

DOI, M., THYBOLL, J., KORTESMAA, J., JANSSON, K., IIVANAINEN, A., PARVARDEH, M., TIMPL, R., HEDIN, U., SWEDENBORG, J. & TRYGGVASON, K. 2002. Recombinant human laminin-10 (alpha5beta1gamma1). Production, purification, and migration-promoting activity on vascular endothelial cells. *J Biol Chem,* 277**,** 12741-8.

DOMOGATSKAYA, A., RODIN, S. & TRYGGVASON, K. 2012. Functional diversity of laminins. *Annu Rev Cell Dev Biol,* 28**,** 523-53.

DOS SANTOS-SILVA, M. A., TRAJANO, E. T., SCHANUEL, F. S. & MONTE-ALTO-COSTA, A. 2017. Heat delays skin wound healing in mice. *Exp Biol Med (Maywood),* 242**,** 258-266.

DRIDI, S. 2012. <i>Alu</i> Mobile Elements: From Junk DNA to Genomic Gems. *Scientifica,* 2012**,** 545328.

DURBEEJ, M. 2010. Laminins. *Cell Tissue Res,* 339**,** 259-68.

EDRAKI, M., AKBARZADEH, A., HOSSEINZADEH, M., TANIDEH, N., SALEHI, A. & KOOHI-HOSSEINABADI, O. 2014. Healing effect of sea buckthorn, olive oil, and their mixture on full-thickness burn wounds. *Adv Skin Wound Care,* 27**,** 317-23.

ERICHSEN, L., BEERMANN, A., ARAUZO-BRAVO, M. J., HASSAN, M., DKHIL, M. A., AL-QURAISHY, S., HAFIZ, T. A., FISCHER, J. C. & SANTOURLIDIS, S. 2018. Genome-wide hypomethylation of LINE-1 and Alu retroelements in cell-free DNA of blood is an epigenetic biomarker of human aging. *Saudi journal of biological sciences,* 25**,** 1220-1226.

ERMOLAEVA, M. A. & SCHUMACHER, B. 2014. Systemic DNA damage responses: organismal adaptations to genome instability. *Trends Genet,* 30**,** 95-102.

ESSAYEM, S., KOVACIC-MILIVOJEVIC, B., BAUMBUSCH, C., MCDONAGH, S., DOLGANOV, G., HOWERTON, K., LAROCQUE, N., MAURO, T., RAMIREZ, A., RAMOS, D. M., FISHER, S. J., JORCANO, J. L., BEGGS, H. E., REICHARDT, L. F. & ILIC, D. 2006. Hair cycle and wound healing in mice with a keratinocyte-restricted deletion of FAK. *Oncogene,* 25**,** 1081-1089.

FARGHALI, H. A., ABDELKADER, N. A., KHATTAB, M. S. & ABUBAKR, H. O. 2017. Evaluation of subcutaneous infiltration of autologous platelet-rich plasma on skin-wound healing in dogs. *Biosci Rep,* 37.

FAUL, F., ERDFELDER, E., BUCHNER, A. & LANG, A.-G. 2009. Statistical power analyses using G*Power 3.1: Tests for correlation and regression analyses. *Behavior Research Methods,* 41**,** 1149-1160.

FAUL, F., ERDFELDER, E., LANG, A. G. & BUCHNER, A. 2007. G*Power 3: a flexible statistical power analysis program for the social, behavioral, and biomedical sciences. *Behav Res Methods,* 39**,** 175-91.

FERNANDES, A. C., FRANÇA, J. P., GAIBA, S., ALOISE, A. C., OLIVEIRA, A. F., MORAES, A. A., FRANÇA, L. P. & FERREIRA, L. M. 2014. Development of experimental in vitro burn model. *Acta Cir Bras,* 29 Suppl 2**,** 15-20.

FINLAY, V., BURROWS, S., BURMAZ, M., YAWARY, H., LEE, J., EDGAR, D. W. & WOOD, F. M. 2017. Increased burn healing time is associated with higher Vancouver Scar Scale score. *Scars, Burns & Healing,* 3**,** 2059513117696324.

FINNERTY, C. C., JESCHKE, M. G., BRANSKI, L. K., BARRET, J. P., DZIEWULSKI, P. & HERNDON, D. N. 2016. Hypertrophic scarring: the greatest unmet challenge after burn injury. *Lancet (London, England),* 388**,** 1427-1436.

FIRSANOV, D. V., SOLOVJEVA, L. V. & SVETLOVA, M. P. 2011. H2AX phosphorylation at the sites of DNA double-strand breaks in cultivated mammalian cells and tissues. *Clinical Epigenetics,* 2**,** 283-297.

FUCHS, E., ESTEVES, R. A. & COULOMBE, P. A. 1992. Transgenic mice expressing a mutant keratin 10 gene reveal the likely genetic basis for epidermolytic hyperkeratosis. *Proc Natl Acad Sci U S A,* 89**,** 6906-10.

GATES, R. E., KING, L. E., JR., HANKS, S. K. & NANNEY, L. B. 1994. Potential role for focal adhesion kinase in migrating and proliferating keratinocytes near epidermal wounds and in culture. *Cell Growth Differ,* 5**,** 891-9.

GAUDET, F., HODGSON, J. G., EDEN, A., JACKSON-GRUSBY, L., DAUSMAN, J., GRAY, J. W., LEONHARDT, H. & JAENISCH, R. 2003. Induction of Tumors in Mice by Genomic Hypomethylation. *Science,* 300**,** 489.

GEBHARD, W., MEITINGER, T., HOCHTL, J. & ZACHAU, H. G. 1982. A new family of interspersed repetitive DNA sequences in the mouse genome. *J Mol Biol,* 157**,** 453-71.

GIAVARA, S., KOSMIDOU, E., HANDE, M. P., BIANCHI, M. E., MORGAN, A., D'ADDA DI FAGAGNA, F. & JACKSON, S. P. 2005. Yeast Nhp6A/B and mammalian Hmgb1 facilitate the maintenance of genome stability. *Curr Biol,* 15**,** 68-72.

GOGOLEVSKAYA, I. K., VENIAMINOVA, N. A. & KRAMEROV, D. A. 2010. Nucleotide sequences of B1 SINE and 4.5S(I) RNA support a close relationship of zokors to blind mole rats (Spalacinae) and bamboo rats (Rhizomyinae). *Gene,* 460**,** 30-8.

GOLSHAN, A., PATEL, C. & HYDER, A. A. 2013. A systematic review of the epidemiology of unintentional burn injuries in South Asia. *J Public Health (Oxf),* 35**,** 384-96.

GOMES, M. V., MANFREDO, M. H., TOFFOLI, L. V., CASTRO-ALVES, D. C., DO NASCIMENTO, L. M., DA SILVA, W. R., KASHIMOTO, R. K.,

RODRIGUES, G. M., JR., ESTRADA, V. B., ANDRAUS, R. A. & PELOSI, G. G. 2016. Effects of the led therapy on the global DNA methylation and the expression of Dnmt1 and Dnmt3a genes in a rat model of skin wound healing. *Lasers Med Sci,* 31**,** 1521-6.

GOODMAN, S. L. 1992. Alpha 6 beta 1 integrin and laminin E8: an increasingly complex simple story. *Kidney Int,* 41**,** 650-6.

GREWAL, S. I. & JIA, S. 2007. Heterochromatin revisited. *Nat Rev Genet,* 8**,** 35-46.

GUILLAUMET-ADKINS, A., YANEZ, Y., PERIS-DIAZ, M. D., CALABRIA, I., PALANCA-BALLESTER, C. & SANDOVAL, J. 2017. Epigenetics and Oxidative Stress in Aging. *Oxid Med Cell Longev,* 2017**,** 9175806.

HAGHDOOST, F., BARADARAN MAHDAVI, M. M., ZANDIFAR, A., SANEI, M. H., ZOLFAGHARI, B. & JAVANMARD, S. H. 2013. Pistacia atlantica Resin Has a Dose-Dependent Effect on Angiogenesis and Skin Burn Wound Healing in Rat. *Evid Based Complement Alternat Med,* 2013**,** 893425.

HALLMANN, R., HORN, N., SELG, M., WENDLER, O., PAUSCH, F. & SOROKIN, L. M. 2005. Expression and function of laminins in the embryonic and mature vasculature. *Physiol Rev,* 85**,** 979-1000.

HAMILL, K. J., KLIGYS, K., HOPKINSON, S. B. & JONES, J. C. 2009. Laminin deposition in the extracellular matrix: a complex picture emerges. *J Cell Sci,* 122**,** 4409-17.

HAN, J. S., SZAK, S. T. & BOEKE, J. D. 2004. Transcriptional disruption by the L1 retrotransposon and implications for mammalian transcriptomes. *Nature,* 429**,** 268-74.

HAO, Y., CUI, Y. & GU, X. 2016. Genome-wide DNA methylation profiles changes associated with constant heat stress in pigs as measured by bisulfite sequencing. *Scientific reports,* 6**,** 27507-27507.

HE, Y., DENG, Z., ALGHAMDI, M., LU, L., FEAR, M. W. & HE, L. 2017. From genetics to epigenetics: new insights into keloid scarring. *Cell Prolif,* 50.

HINTZSCHE, H., RIESE, T. & STOPPER, H. 2012. Hyperthermia-induced micronucleus formation in a human keratinocyte cell line. *Mutation Research/Fundamental and Molecular Mechanisms of Mutagenesis,* 738-739**,** 71-74.

HOHENESTER, E. & YURCHENCO, P. D. 2013. Laminins in basement membrane assembly. *Cell Adh Migr,* 7**,** 56-63.

HOLZER, J. C. J., TIFFNER, K., KAINZ, S., REISENEGGER, P., BERNARDELLI DE MATTOS, I., FUNK, M., LEMARCHAND, T., LAAFF, H., BAL, A., BIRNGRUBER, T., KOTZBECK, P. & KAMOLZ, L. P. 2020. A novel human ex-vivo burn model and the local cooling effect of a bacterial nanocellulose-based wound dressing. *Burns,* 46**,** 1924-1932.

HOPKINSON, S. B., HAMILL, K. J., WU, Y., EISENBERG, J. L., HIROYASU, S. & JONES, J. C. 2014. Focal Contact and Hemidesmosomal Proteins in Keratinocyte Migration and Wound Repair. *Adv Wound Care (New Rochelle),* 3**,** 247-263.

HORZUM, U., OZDIL, B. & PESEN-OKVUR, D. 2014. Step-by-step quantitative analysis of focal adhesions. *MethodsX,* 1**,** 56-59.

HOUSTON, B. J., NIXON, B., MARTIN, J. H., DE IULIIS, G. N., TRIGG, N. A., BROMFIELD, E. G., MCEWAN, K. E. & AITKEN, R. J. 2018. Heat exposure induces oxidative stress and DNA damage in the male germ line. *Biol Reprod,* 98**,** 593-606.

HSIUNG, D. T., MARSIT, C. J., HOUSEMAN, E. A., EDDY, K., FURNISS, C. S., MCCLEAN, M. D. & KELSEY, K. T. 2007. Global DNA methylation level in whole blood as a biomarker in head and neck squamous cell carcinoma. *Cancer Epidemiol Biomarkers Prev,* 16**,** 108-14.

HWANG, J. S., CHOI, H. S., HAM, S. A., YOO, T., LEE, W. J., PAEK, K. S. & SEO, H. G. 2015. Deacetylation-mediated interaction of SIRT1-HMGB1 improves survival in a mouse model of endotoxemia. *Sci Rep,* 5**,** 15971.

IORIO, V., TROUGHTON, L. D. & HAMILL, K. J. 2015a. Laminins: Roles and Utility in Wound Repair. *Adv Wound Care (New Rochelle),* 4**,** 250-263.

IORIO, V., TROUGHTON, L. D. & HAMILL, K. J. 2015b. Laminins: Roles and Utility in Wound Repair. *Adv Wound Care (New Rochelle).* United States.

IRIYAMA, S., YASUDA, M., NISHIKAWA, S., TAKAI, E., HOSOI, J. & AMANO, S. 2020. Decrease of laminin-511 in the basement membrane due to photoaging reduces epidermal stem/progenitor cells. *Scientific Reports,* 10**,** 12592.

JAKOB, B., SPLINTER, J., CONRAD, S., VOSS, K. O., ZINK, D., DURANTE, M., LÖBRICH, M. & TAUCHER-SCHOLZ, G. 2011. DNA double-strand breaks in heterochromatin elicit fast repair protein recruitment, histone H2AX phosphorylation and relocation to euchromatin. *Nucleic Acids Res,* 39**,** 6489-99.

JANUSZYK, M., KWON, S. H., WONG, V. W., PADMANABHAN, J., MAAN, Z. N., WHITTAM, A. J., MAJOR, M. R. & GURTNER, G. C. 2017. The Role of Focal Adhesion Kinase in Keratinocyte Fibrogenic Gene Expression. *International journal of molecular sciences,* 18**,** 1915.

JESCHKE, M. G., VAN BAAR, M. E., CHOUDHRY, M. A., CHUNG, K. K., GIBRAN, N. S. & LOGSETTY, S. 2020. Burn injury. *Nature Reviews Disease Primers,* 6**,** 11.

JIANG, D., DE VRIES, J. C., MUSCHHAMMER, J., SCHATZ, S., YE, H., HEIN, T., FIDAN, M., ROMANOV, V. S., RINKEVICH, Y. & SCHARFFETTER-KOCHANEK, K. 2020. Local and transient inhibition of p21 expression ameliorates age-related delayed wound healing. *Wound Repair Regen,* 28**,** 49-60.

JINTARIDTH, P. & MUTIRANGURA, A. 2010. Distinctive patterns of age-dependent hypomethylation in interspersed repetitive sequences. *Physiol Genomics,* 41**,** 194-200.

JINTARIDTH, P., TUNGTRONGCHITR, R., PREUTTHIPAN, S. & MUTIRANGURA, A. 2013. Hypomethylation of Alu elements in post-menopausal women with osteoporosis. *PLoS One,* 8**,** e70386.

JONES, L. R., GREENE, J., CHEN, K. M., DIVINE, G., CHITALE, D., SHAH, V., DATTA, I. & WORSHAM, M. J. 2017. Biological significance of genome-wide DNA methylation profiles in keloids. *Laryngoscope,* 127**,** 70-78.

JORDÀ, M., DÍEZ-VILLANUEVA, A., MALLONA, I., MARTÍN, B., LOIS, S., BARRERA, V., ESTELLER, M., VAVOURI, T. & PEINADO, M. A. 2017.

The epigenetic landscape of Alu repeats delineates the structural and functional genomic architecture of colon cancer cells. *Genome Res,* 27**,** 118-132.

KANEKO, H., IGARASHI, K., KATAOKA, K. & MIURA, M. 2005. Heat shock induces phosphorylation of histone H2AX in mammalian cells. *Biochem Biophys Res Commun,* 328**,** 1101-6.

KANG, R., ZHANG, Q., ZEH, H. J., 3RD, LOTZE, M. T. & TANG, D. 2013. HMGB1 in cancer: good, bad, or both? *Clin Cancer Res,* 19**,** 4046-57.

KANG, S., CHOVATIYA, G. & TUMBAR, T. 2019. Epigenetic control in skin development, homeostasis and injury repair. *Exp Dermatol*.

KANTIDZE, O. L., VELICHKO, A. K., LUZHIN, A. V. & RAZIN, S. V. 2016. Heat Stress-Induced DNA Damage. *Acta Naturae,* 8**,** 75-8.

KARNI, M., ZIDON, D., POLAK, P., ZALEVSKY, Z. & SHEFI, O. 2013. Thermal degradation of DNA. *DNA Cell Biol,* 32**,** 298-301.

KATIYAR-AGARWAL, S., MORGAN, R., DAHLBECK, D., BORSANI, O., VILLEGAS, A., ZHU, J.-K., STASKAWICZ, B. J. & JIN, H. 2006. A pathogen-inducible endogenous siRNA in plant immunity. *Proceedings of the National Academy of Sciences,* 103**,** 18002-18007.

KERSCHBAUM, S., WEGROSTEK, C., RIEGEL, E. & CZERNY, T. 2021. Senescence in a cell culture model for burn wounds. *Experimental and Molecular Pathology,* 122**,** 104674.

KIM, H., SHIN, S. & HAN, D. 2022. Review of History of Basic Principles of Burn Wound Management. *Medicina (Kaunas),* 58.

KIM, J. H. 2019. Chromatin Remodeling and Epigenetic Regulation in Plant DNA Damage Repair. *Int J Mol Sci,* 20.

KINNER, A., WU, W., STAUDT, C. & ILIAKIS, G. 2008. γ-H2AX in recognition and signaling of DNA double-strand breaks in the context of chromatin. *Nucleic Acids Research,* 36**,** 5678-5694.

KLIFTO, K. M., ASIF, M. & HULTMAN, C. S. 2020. Laser management of hypertrophic burn scars: a comprehensive review. *Burns Trauma,* 8**,** tkz002.

KOIVISTO, L., HEINO, J., HÄKKINEN, L. & LARJAVA, H. 2014. Integrins in Wound Healing. *Advances in wound care,* 3**,** 762-783.

KONGRUTTANACHOK, N., PHUANGPHAIROJ, C., THONGNAK, A., PONYEAM, W., RATTANATANYONG, P., PORNTHANAKASEM, W. & MUTIRANGURA, A. 2010. Replication independent DNA double-strand break retention may prevent genomic instability. *Mol Cancer,* 9**,** 70.

KORKMAZ, K. S., BUTUNER, B. D. & ROGGENBUCK, D. 2018. Detection of 8-OHdG as a diagnostic biomarker. *Journal of Laboratory and Precision Medicine,* 3.

KOTURBASH, I., MIOUSSE, I. R., SRIDHARAN, V., NZABARUSHIMANA, E., SKINNER, C. M., MELNYK, S. B., PAVLIV, O., HAUER-JENSEN, M., NELSON, G. A. & BOERMA, M. 2016. Radiation-induced changes in DNA methylation of repetitive elements in the mouse heart. *Mutat Res,* 787**,** 43-53.

KULABEROGLU, Y., GUNDOGDU, R. & HERGOVICH, A. 2016. Chapter 15 - The Role of p53/p21/p16 in DNA-Damage Signaling and DNA Repair. *In:* KOVALCHUK, I. & KOVALCHUK, O. (eds.) *Genome Stability.* Boston: Academic Press.

KUMAI, J., YAMADA, Y., HAMADA, K., KATAGIRI, F., HOZUMI, K., KIKKAWA, Y. & NOMIZU, M. 2019. Identification of active sequences in human laminin α5 G domain. *J Pept Sci,* 25**,** e3218.

KUSU-ORKAR, T.-E., ISLAM, U., HALL, B., ARAIA, E. & ALLORTO, N. 2019. The use of a non-medicated dressing for superficial-partial thickness burns in children: a case series and review. *Scars, Burns & Healing,* 5**,** 2059513119896954.

LADHANI, H. A., YOUNG, B. T., POSILLICO, S. E., YOWLER, C. J., BRANDT, C. P., CLARIDGE, J. A. & KHANDELWAL, A. K. 2020. Risk Factors for Wound Infection in Outpatients With Lower Extremity Burns. *The American Surgeon,* 87**,** 1118-1125.

LAKIN, N. D. & JACKSON, S. P. 1999. Regulation of p53 in response to DNA damage. *Oncogene,* 18**,** 7644-55.

LANG, T. C., ZHAO, R., KIM, A., WIJEWARDENA, A., VANDERVORD, J., XUE, M. & JACKSON, C. J. 2019. A Critical Update of the Assessment and Acute Management of Patients with Severe Burns. *Advances in wound care,* 8**,** 607-633.

LANTOS, J., FÖLDI, V., ROTH, E., WÉBER, G., BOGÁR, L. & CSONTOS, C. 2010. Burn trauma induces early HMGB1 release in patients: its correlation with cytokines. *Shock,* 33**,** 562-7.

LASKIN, J. D., WAHLER, G., CROUTCH, C. R., SINKO, P. J., LASKIN, D. L., HECK, D. E. & JOSEPH, L. B. 2020. Skin remodeling and wound healing in the Gottingen minipig following exposure to sulfur mustard. *Exp Mol Pathol,* 115**,** 104470.

LAWRENCE, J. W., MASON, S. T., SCHOMER, K. & KLEIN, M. B. 2012. Epidemiology and Impact of Scarring After Burn Injury: A Systematic Review of the Literature. *Journal of Burn Care & Research,* 33**,** 136-146.

LEU, S. J., LIU, Y., CHEN, N., CHEN, C. C., LAM, S. C. & LAU, L. F. 2003. Identification of a novel integrin alpha 6 beta 1 binding site in the angiogenic inducer CCN1 (CYR61). *J Biol Chem,* 278**,** 33801-8.

LI, Y., SAWALHA, A. H. & LU, Q. 2009. Aberrant DNA methylation in skin diseases. *Journal of dermatological science,* 54**,** 143-149.

LINDLEY, L. E., STOJADINOVIC, O., PASTAR, I. & TOMIC-CANIC, M. 2016. Biology and Biomarkers for Wound Healing. *Plastic and reconstructive surgery,* 138**,** 18S-28S.

LIOVIC, M., D'ALESSANDRO, M., TOMIC-CANIC, M., BOLSHAKOV, V. N., COATS, S. E. & LANE, E. B. 2009. Severe keratin 5 and 14 mutations induce down-regulation of junction proteins in keratinocytes. *Exp Cell Res,* 315**,** 2995-3003.

LIU, B., LIU, Y., WANG, L., HOU, C. & AN, M. 2018. RNA-seq-based analysis of the hypertrophic scarring with and without pressure therapy in a Bama minipig model. *Sci Rep,* 8**,** 11831.

LIVAK, K. J. & SCHMITTGEN, T. D. 2001. Analysis of relative gene expression data using real-time quantitative PCR and the 2(-Delta Delta C(T)) Method. *Methods,* 25**,** 402-8.

LONGMATE, W. M. & DIPERSIO, C. M. 2014. Integrin Regulation of Epidermal Functions in Wounds. *Advances in wound care,* 3**,** 229-246.

LOOTENS, L., BRUSSELAERS, N., BEELE, H. & MONSTREY, S. 2013. Keratinocytes in the treatment of severe burn injury: an update. *Int Wound J,* 10**,** 6-12.

LU, R., WANG, X., CHEN, Z. F., SUN, D. F., TIAN, X. Q. & FANG, J. Y. 2007. Inhibition of the extracellular signal-regulated kinase/mitogen-activated protein kinase pathway decreases DNA methylation in colon cancer cells. *J Biol Chem,* 282**,** 12249-59.

LUO, G., JING, X., YANG, S., PENG, D., DONG, J., LI, L., REINACH, P. S. & YAN, D. 2019. DNA Methylation Regulates Corneal Epithelial Wound Healing by Targeting miR-200a and CDKN2B. *Invest Ophthalmol Vis Sci,* 60**,** 650-660.

LUO, Y., LU, X. & XIE, H. 2014a. Dynamic Alu Methylation during Normal Development, Aging, and Tumorigenesis. *BioMed Research International,* 2014**,** 784706.

LUO, Y., LU, X. & XIE, H. 2014b. Dynamic Alu methylation during normal development, aging, and tumorigenesis. *Biomed Res Int,* 2014**,** 784706.

M, M. P. 1992. Basement Membrane Proteins: Structure, Assembly, and Cellular Interactions. *Critical Reviews in Biochemistry and Molecular Biology,* 27**,** 93-127.

MAGNA, M. & PISETSKY, D. S. 2014. The role of HMGB1 in the pathogenesis of inflammatory and autoimmune diseases. *Mol Med,* 20**,** 138-46.

MAH, L. J., EL-OSTA, A. & KARAGIANNIS, T. C. 2010. γH2AX: a sensitive molecular marker of DNA damage and repair. *Leukemia,* 24**,** 679-686.

MAHMOOD 2016. Pre-Differentiated Skin-Like Cells can Alleviate In Vitro Burn Injury. *Tissue Science & Engineering*.

MALINDA, K. M., WYSOCKI, A. B., KOBLINSKI, J. E., KLEINMAN, H. K. & PONCE, M. L. 2008. Angiogenic laminin-derived peptides stimulate wound healing. *Int J Biochem Cell Biol,* 40**,** 2771-80.

MANOHAR, A., SHOME, S. G., LAMAR, J., STIRLING, L., IYER, V., PUMIGLIA, K. & DIPERSIO, C. M. 2004. Alpha 3 beta 1 integrin promotes keratinocyte cell survival through activation of a MEK/ERK signaling pathway. *J Cell Sci,* 117**,** 4043-54.

MAO, Z., WU, J. H., DONG, T. & WU, M. X. 2016. Additive enhancement of wound healing in diabetic mice by low level light and topical CoQ10. *Sci Rep,* 6**,** 20084.

MARQUARDT, N., FEJA, M., HÜNIGEN, H., PLENDL, J., MENKEN, L., FINK, H. & BERT, B. 2018. Euthanasia of laboratory mice: Are isoflurane and sevoflurane real alternatives to carbon dioxide? *PloS one,* 13**,** e0203793-e0203793.

MATAIX, M., RODRÍGUEZ-LUNA, A., GUTIÉRREZ-PÉREZ, M., MILANI, M., GANDARILLAS, A., ESPADA, J. & PÉREZ-DAVÓ, A. 2020. Deschampsia antarctica extract (Edafence®) as a powerful skin protection tool against the aging exposome. *Plastic and Aesthetic Research,* 7**,** 69.

MATHIEU, O. & BENDER, J. 2004. RNA-directed DNA methylation. *J Cell Sci,* 117**,** 4881-8.

MATZKE, M. A. & MOSHER, R. A. 2014a. RNA-directed DNA methylation: an epigenetic pathway of increasing complexity. *Nature Reviews Genetics,* 15**,** 394-408.

MATZKE, M. A. & MOSHER, R. A. 2014b. RNA-directed DNA methylation: an epigenetic pathway of increasing complexity. *Nat Rev Genet,* 15**,** 394-408.

MAYS-HOOPES, L. L., BROWN, A. & HUANG, R. C. 1983. Methylation and rearrangement of mouse intracisternal a particle genes in development, aging, and myeloma. *Mol Cell Biol,* 3**,** 1371-80.

MCLEAN, G. W., KOMIYAMA, N. H., SERRELS, B., ASANO, H., REYNOLDS, L., CONTI, F., HODIVALA-DILKE, K., METZGER, D., CHAMBON, P., GRANT, S. G. & FRAME, M. C. 2004. Specific deletion of focal adhesion kinase suppresses tumor formation and blocks malignant progression. *Genes Dev,* 18**,** 2998-3003.

MEEVASSANA, J., SERIRODOM, S., PRABSATTRU, P., BOONSONGSERM, P., KAMOLRATANAKUL, S., SIRITIENTONG, T., MUTIRANGURA, A. & ANGSPATT, A. 2021. Alu repetitive sequence CpG methylation changes in burn scars. *Burns*.

MEEVASSANA, J., SUMONSRIWARANKUN, P., SUWAJO, P., NILPRAPHA, K., PROMNIYOM, P., IAMPHONGSAI, S., PUNGRASMI, P., JINDARAK, S., KANGKORN, T. & ANGSPATT, A. 2022. 3D PED BURN app: A precise and easy-to-use pediatric 3D burn surface area calculation tool. *Health Science Reports,* 5**,** e694.

MIYAZAKI, T., FUTAKI, S., SUEMORI, H., TANIGUCHI, Y., YAMADA, M., KAWASAKI, M., HAYASHI, M., KUMAGAI, H., NAKATSUJI, N., SEKIGUCHI, K. & KAWASE, E. 2012a. Laminin E8 fragments support efficient adhesion and expansion of dissociated human pluripotent stem cells. *Nat Commun,* 3**,** 1236.

MIYAZAKI, T., FUTAKI, S., SUEMORI, H., TANIGUCHI, Y., YAMADA, M., KAWASAKI, M., HAYASHI, M., KUMAGAI, H., NAKATSUJI, N., SEKIGUCHI, K. & KAWASE, E. 2012b. Laminin E8 fragments support efficient adhesion and expansion of dissociated human pluripotent stem cells. *Nature Communications,* 3**,** 1236.

MOSTAGHACI, B., LORETZ, B. & LEHR, C. M. 2016. Calcium Phosphate System for Gene Delivery: Historical Background and Emerging Opportunities. *Curr Pharm Des,* 22**,** 1529-33.

MURARI, A. 2017. A modified Lund and Browder chart. *Indian J Plast Surg,* 50**,** 220-221.

MURAYAMA, O., NISHIDA, H. & SEKIGUCHI, K. 1996. Novel peptide ligands for integrin alpha 6 beta 1 selected from a phage display library. *J Biochem,* 120**,** 445-51.

MUTIRANGURA, A. 2019a. A Hypothesis to Explain How the DNA of Elderly People Is Prone to Damage: Genome-Wide Hypomethylation Drives Genomic Instability in the Elderly by Reducing Youth-Associated Gnome-Stabilizing DNA Gaps.

MUTIRANGURA, A. 2019b. Is global hypomethylation a nidus for molecular pathogenesis of age-related noncommunicable diseases? *Epigenomics,* 11**,** 577-579.

NASCIMENTO-FILHO, C. H. V., SILVEIRA, E. J. D., GOLONI-BERTOLLO, E. M., DE SOUZA, L. B., SQUARIZE, C. H. & CASTILHO, R. M. 2020. Skin wound healing triggers epigenetic modifications of histone H4. *J Transl Med,* 18**,** 138.

NICOLAI, S., ROSSI, A., DI DANIELE, N., MELINO, G., ANNICCHIARICO-PETRUZZELLI, M. & RASCHELLA, G. 2015. DNA repair and aging: the impact of the p53 family. *Aging (Albany NY),* 7**,** 1050-65.

NITTA, M., OKAMURA, H., AIZAWA, S. & YAMAIZUMI, M. 1997. Heat shock induces transient p53-dependent cell cycle arrest at G1/S. *Oncogene,* 15**,** 561-8.

OKUMURA, N., KAKUTANI, K., NUMATA, R., NAKAHARA, M., SCHLOTZER-SCHREHARDT, U., KRUSE, F., KINOSHITA, S. & KOIZUMI, N. 2015. Laminin-511 and -521 enable efficient in vitro expansion of human corneal endothelial cells. *Invest Ophthalmol Vis Sci,* 56**,** 2933-42.

PADDOCK, H. N., SCHULTZ, G. S., BAKER, H. V., VARELA, J. C., BEIERLE, E. A., MOLDAWER, L. L. & MOZINGO, D. W. 2003. Analysis of gene expression patterns in human postburn hypertrophic scars. *J Burn Care Rehabil,* 24**,** 371-7.

PAL, S. & TYLER, J. K. 2016. Epigenetics and aging. *Sci Adv,* 2**,** e1600584.

PARK, S. Y., SEO, A. N., JUNG, H. Y., GWAK, J. M., JUNG, N., CHO, N.-Y. & KANG, G. H. 2014. Alu and LINE-1 Hypomethylation Is Associated with HER2 Enriched Subtype of Breast Cancer. *PLOS ONE,* 9**,** e100429.

PASTAR, I., STOJADINOVIC, O., YIN, N. C., RAMIREZ, H., NUSBAUM, A. G., SAWAYA, A., PATEL, S. B., KHALID, L., ISSEROFF, R. R. & TOMIC-CANIC, M. 2014. Epithelialization in Wound Healing: A Comprehensive Review. *Adv Wound Care (New Rochelle),* 3**,** 445-464.

PATCHSUNG, M., SETTAYANON, S., PONGPANICH, M., MUTIRANGURA, D., JINTARITH, P. & MUTIRANGURA, A. 2018. Alu siRNA to increase Alu element methylation and prevent DNA damage. *Epigenomics,* 10**,** 175-185.

PENG, L., YUAN, Z., LING, H., FUKASAWA, K., ROBERTSON, K., OLASHAW, N., KOOMEN, J., CHEN, J., LANE, W. S. & SETO, E. 2011. SIRT1 deacetylates the DNA methyltransferase 1 (DNMT1) protein and alters its activities. *Mol Cell Biol,* 31**,** 4720-34.

PENG, X., UEDA, H., ZHOU, H., STOKOL, T., SHEN, T.-L., ALCARAZ, A., NAGY, T., VASSALLI, J.-D. & GUAN, J.-L. 2004. Overexpression of focal adhesion kinase in vascular endothelial cells promotes angiogenesis in transgenic mice. *Cardiovascular Research,* 64**,** 421-430.

PEREZ, R. F., TEJEDOR, J. R., BAYON, G. F., FERNANDEZ, A. F. & FRAGA, M. F. 2018. Distinct chromatin signatures of DNA hypomethylation in aging and cancer. *Aging Cell,* 17**,** e12744.

PETROVA, N. V., VELICHKO, A. K., RAZIN, S. V. & KANTIDZE, O. L. 2016. Early S-phase cell hypersensitivity to heat stress. *Cell Cycle,* 15**,** 337-44.

PLIKUS, M. V., GUERRERO-JUAREZ, C. F., TREFFEISEN, E. & GAY, D. L. 2015. Epigenetic control of skin and hair regeneration after wounding. *Experimental dermatology,* 24**,** 167-170.

POBSOOK, T., SUBBALEKHA, K., SANNIKORN, P. & MUTIRANGURA, A. 2011. Improved measurement of LINE-1 sequence methylation for cancer detection. *Clin Chim Acta,* 412**,** 314-21.

POLANSKÁ, E., DOBŠÁKOVÁ, Z., DVOŘÁČKOVÁ, M., FAJKUS, J. & ŠTROS, M. 2012. HMGB1 gene knockout in mouse embryonic fibroblasts results in reduced telomerase activity and telomere dysfunction. *Chromosoma,* 121**,** 419-31.

POLISETTI, N., GIESS, A., LI, S., SOROKIN, L., KRUSE, F. E. & SCHLÖTZER-SCHREHARDT, U. 2020. Laminin-511-E8 promotes efficient in vitro expansion of human limbal melanocytes. *Scientific Reports,* 10**,** 11074.

POLISETTI, N., SOROKIN, L., OKUMURA, N., KOIZUMI, N., KINOSHITA, S., KRUSE, F. E. & SCHLÖTZER-SCHREHARDT, U. 2017. Laminin-511 and -521-based matrices for efficient ex vivo-expansion of human limbal epithelial progenitor cells. *Sci Rep,* 7**,** 5152.

PONGPANICH, M., PATCHSUNG, M., THONGSROY, J. & MUTIRANGURA, A. 2014. Characteristics of replication-independent endogenous double-strand breaks in Saccharomyces cerevisiae. *BMC Genomics,* 15**,** 750.

PORNTHANAKASEM, W., KONGRUTTANACHOK, N., PHUANGPHAIROJ, C., SUYARNSESTAKORN, C., SANGHANGTHUM, T., OONSIRI, S., PONYEAM, W., THANASUPAWAT, T., MATANGKASOMBUT, O. & MUTIRANGURA, A. 2008. LINE-1 methylation status of endogenous DNA double-strand breaks. *Nucleic Acids Res,* 36**,** 3667-75.

POULIOT, N. & KUSUMA, N. 2013. Laminin-511: a multi-functional adhesion protein regulating cell migration, tumor invasion and metastasis. *Cell Adh Migr,* 7**,** 142-9.

POULIOT, N., SAUNDERS, N. A. & KAUR, P. 2002. Laminin 10/11: an alternative adhesive ligand for epidermal keratinocytes with a functional role in promoting proliferation and migration. *Exp Dermatol,* 11**,** 387-97.

PRASAD, R., LIU, Y., DETERDING, L. J., POLTORATSKY, V. P., KEDAR, P. S., HORTON, J. K., KANNO, S., ASAGOSHI, K., HOU, E. W., KHODYREVA, S. N., LAVRIK, O. I., TOMER, K. B., YASUI, A. & WILSON, S. H. 2007. HMGB1 is a cofactor in mammalian base excision repair. *Mol Cell,* 27**,** 829-41.

PURSCHKE, M., LAUBACH, H. J., ANDERSON, R. R. & MANSTEIN, D. 2010. Thermal injury causes DNA damage and lethality in unheated surrounding cells: active thermal bystander effect. *J Invest Dermatol,* 130**,** 86-92.

REIS, A. H., VARGAS, F. R. & LEMOS, B. 2016. Biomarkers of genome instability and cancer epigenetics. *Tumour Biol,* 37**,** 13029-13038.

RENNEKAMPFF, H. O. & ALHARBI, Z. 2021. Burn Injury: Mechanisms of Keratinocyte Cell Death. *Med Sci (Basel),* 9.

RENSHAW, M. W., PRICE, L. S. & SCHWARTZ, M. A. 1999. Focal adhesion kinase mediates the integrin signaling requirement for growth factor activation of MAP kinase. *The Journal of cell biology,* 147**,** 611-618.

ROMAN, A. C., BENITEZ, D. A., CARVAJAL-GONZALEZ, J. M. & FERNANDEZ-SALGUERO, P. M. 2008. Genome-wide B1 retrotransposon binds the transcription factors dioxin receptor and Slug and regulates gene expression in vivo. *Proc Natl Acad Sci U S A,* 105**,** 1632-7.

ROMÁN, A. C., GONZÁLEZ-RICO, F. J. & FERNÁNDEZ-SALGUERO, P. M. 2011. B1-SINE retrotransposons: Establishing genomic insulatory networks. *Mobile genetic elements,* 1**,** 66-70.

ROUABHIA, M., PARK, H. J., ABEDIN-DO, A., DOUVILLE, Y., MÉTHOT, M. & ZHANG, Z. 2020. Electrical stimulation promotes the proliferation of human keratinocytes, increases the production of keratin 5 and 14, and increases the phosphorylation of ERK1/2 and p38 MAP kinases. *J Tissue Eng Regen Med,* 14**,** 909-919.

ROWAN, M. P., CANCIO, L. C., ELSTER, E. A., BURMEISTER, D. M., ROSE, L. F., NATESAN, S., CHAN, R. K., CHRISTY, R. J. & CHUNG, K. K. 2015. Burn wound healing and treatment: review and advancements. *Critical care (London, England),* 19**,** 243-243.

SADEGH FAZELI, M., LEBASCHI, A. H., HAJIROSTAM, M. & KERAMATI, M. R. 2013. Marjolin's ulcer: clinical and pathologic features of 83 cases and review of literature. *Medical journal of the Islamic Republic of Iran,* 27**,** 215-224.

SALAMEH, Y., BEJAOUI, Y. & EL HAJJ, N. 2020. DNA Methylation Biomarkers in Aging and Age-Related Diseases. *Frontiers in Genetics,* 11.

SCHLISSEL, M. S. 1998. Structure of nonhairpin coding-end DNA breaks in cells undergoing V(D)J recombination. *Mol Cell Biol,* 18**,** 2029-37.

SCHNEIDER, V., KRUSE, D., DE MATTOS, I. B., ZÖPHEL, S., TILTMANN, K. K., REIGL, A., KHAN, S., FUNK, M., BODENSCHATZ, K. & GROEBER-BECKER, F. 2021. A 3D In Vitro Model for Burn Wounds: Monitoring of Regeneration on the Epidermal Level. *Biomedicines,* 9.

SEN, G. L., REUTER, J. A., WEBSTER, D. E., ZHU, L. & KHAVARI, P. A. 2010. DNMT1 maintains progenitor function in self-renewing somatic tissue. *Nature,* 463**,** 563-7.

SEN, P., SHAH, P. P., NATIVIO, R. & BERGER, S. L. 2016. Epigenetic Mechanisms of Longevity and Aging. *Cell,* 166**,** 822-839.

SHIN, M. H., MOON, Y. J., SEO, J. E., LEE, Y., KIM, K. H. & CHUNG, J. H. 2008. Reactive oxygen species produced by NADPH oxidase, xanthine oxidase, and mitochondrial electron transport system mediate heat shock-induced MMP-1 and MMP-9 expression. *Free Radic Biol Med,* 44**,** 635-45.

SHORE, D. 2000. The Sir2 protein family: A novel deacetylase for gene silencing and more. *Proc Natl Acad Sci U S A,* 97**,** 14030-2.

SIMON-ASSMANN, P., OREND, G., MAMMADOVA-BACH, E., SPENLE, C. & LEFEBVRE, O. 2011. Role of laminins in physiological and pathological angiogenesis. *Int J Dev Biol,* 55**,** 455-65.

SITIA, G., IANNACONE, M., MÜLLER, S., BIANCHI, M. E. & GUIDOTTI, L. G. 2007. Treatment with HMGB1 inhibitors diminishes CTL-induced liver disease in HBV transgenic mice. *J Leukoc Biol,* 81**,** 100-7.

SLIMEN, I. B., NAJAR, T., GHRAM, A., DABBEBI, H., BEN MRAD, M. & ABDRABBAH, M. 2014. Reactive oxygen species, heat stress and oxidative-induced mitochondrial damage. A review. *International journal of hyperthermia : the official journal of European Society for Hyperthermic Oncology, North American Hyperthermia Group,* 30**,** 513-523.

SLOTKIN, R. K. & MARTIENSSEN, R. 2007. Transposable elements and the epigenetic regulation of the genome. *Nat Rev Genet,* 8**,** 272-85.

SON, B., LEE, S., KIM, H., KANG, H., KIM, J., YOUN, H., NAM, S. Y. & YOUN, B. 2019a. Low dose radiation attenuates inflammation and promotes wound healing in a mouse burn model. *J Dermatol Sci,* 96**,** 81-89.

SON, B., LEE, S., KIM, H., KANG, H., KIM, J., YOUN, H., NAM, S. Y. & YOUN, B. 2019b. Low dose radiation attenuates inflammation and promotes wound healing in a mouse burn model. *Journal of Dermatological Science,* 96**,** 81-89.

SONNENBERG, A., LINDERS, C. J., MODDERMAN, P. W., DAMSKY, C. H., AUMAILLEY, M. & TIMPL, R. 1990. Integrin recognition of different cell-

binding fragments of laminin (P1, E3, E8) and evidence that alpha 6 beta 1 but not alpha 6 beta 4 functions as a major receptor for fragment E8. *J Cell Biol,* 110**,** 2145-55.

SOROKIN, L. M., PAUSCH, F., FRIESER, M., KROGER, S., OHAGE, E. & DEUTZMANN, R. 1997. Developmental regulation of the laminin alpha5 chain suggests a role in epithelial and endothelial cell maturation. *Dev Biol,* 189**,** 285-300.

STEEN, S. B., GOMELSKY, L., SPEIDEL, S. L. & ROTH, D. B. 1997. Initiation of V(D)J recombination in vivo: role of recombination signal sequences in formation of single and paired double-strand breaks. *EMBO J,* 16**,** 2656-64.

STEINSTRAESSER, L., FOHN, M., KLEIN, R. D., AMINLARI, A., REMICK, D. G., SU, G. L. & WANG, S. C. 2001. Feasibility of biolistic gene therapy in burns. *Shock,* 15**,** 272-7.

SUGAWARA, K., TSURUTA, D., ISHII, M., JONES, J. C. & KOBAYASHI, H. 2008. Laminin-332 and -511 in skin. *Exp Dermatol,* 17**,** 473-80.

SUGAWARA, Y., HAMADA, K., YAMADA, Y., KUMAI, J., KANAGAWA, M., KOBAYASHI, K., TODA, T., NEGISHI, Y., KATAGIRI, F., HOZUMI, K., NOMIZU, M. & KIKKAWA, Y. 2019. Characterization of dystroglycan binding in adhesion of human induced pluripotent stem cells to laminin-511 E8 fragment. *Sci Rep,* 9**,** 13037.

SUN, L., ZHAO, H., XU, Z., LIU, Q., LIANG, Y., WANG, L., CAI, X., ZHANG, L., HU, L., WANG, G. & ZHA, X. 2007. Phosphatidylinositol 3-kinase/protein kinase B pathway stabilizes DNA methyltransferase I protein and maintains DNA methylation. *Cell Signal,* 19**,** 2255-63.

TAKAHASHI, A., MATSUMOTO, H., NAGAYAMA, K., KITANO, M., HIROSE, S., TANAKA, H., MORI, E., YAMAKAWA, N., YASUMOTO, J.-I., YUKI, K., OHNISHI, K. & OHNISHI, T. 2004. Evidence for the Involvement of Double-Strand Breaks in Heat-Induced Cell Killing. *Cancer Research,* 64**,** 8839.

TAKIZAWA, M., ARIMORI, T., TANIGUCHI, Y., KITAGO, Y., YAMASHITA, E., TAKAGI, J. & SEKIGUCHI, K. 2017. Mechanistic basis for the recognition of laminin-511 by α6β1 integrin. *Science advances,* 3**,** e1701497-e1701497.

TANIDEH, N., ROKHSARI, P., MEHRABANI, D., MOHAMMADI SAMANI, S., SABET SARVESTANI, F., ASHRAF, M. J., KOOHI HOSSEINABADI, O., SHAMSIAN, S. & AHMADI, N. 2014. The Healing Effect of Licorice on Pseudomonas aeruginosa Infected Burn Wounds in Experimental Rat Model. *World J Plast Surg,* 3**,** 99-106.

TANIGUCHI, Y., IDO, H., SANZEN, N., HAYASHI, M., SATO-NISHIUCHI, R., FUTAKI, S. & SEKIGUCHI, K. 2009. The C-terminal region of laminin beta chains modulates the integrin binding affinities of laminins. *J Biol Chem,* 284**,** 7820-31.

TAVARES PEREIRA DDOS, S., LIMA-RIBEIRO, M. H., DE PONTES-FILHO, N. T., CARNEIRO-LEAO, A. M. & CORREIA, M. T. 2012. Development of animal model for studying deep second-degree thermal burns. *J Biomed Biotechnol,* 2012**,** 460841.

THONGSROY, J., MATANGKASOMBUT, O., THONGNAK, A., RATTANATANYONG, P., JIRAWATNOTAI, S. & MUTIRANGURA, A.

2013. Replication-Independent Endogenous DNA Double-Strand Breaks in Saccharomyces cerevisiae Model. *PLOS ONE,* 8**,** e72706.

THONGSROY, J. & MUTIRANGURA, A. 2022. The association between Alu hypomethylation and the severity of hypertension. *PLOS ONE,* 17**,** e0270004.

THONGSROY, J., PATCHSUNG, M. & MUTIRANGURA, A. 2017. The association between Alu hypomethylation and severity of type 2 diabetes mellitus. *Clin Epigenetics,* 9**,** 93.

THONGSROY, J., PATCHSUNG, M., PONGPANICH, M., SETTAYANON, S. & MUTIRANGURA, A. 2018. Reduction in replication-independent endogenous DNA double-strand breaks promotes genomic instability during chronological aging in yeast. *Faseb j***,** fj201800218RR.

TI, D., LI, M., FU, X. & HAN, W. 2014. Causes and consequences of epigenetic regulation in wound healing. *Wound Repair Regen,* 22**,** 305-12.

TJIN, M. S., CHUA, A. W. C., MORENO-MORAL, A., CHONG, L. Y., TANG, P. Y., HARMSTON, N. P., CAI, Z., PETRETTO, E., TAN, B. K. & TRYGGVASON, K. 2018. Biologically relevant laminin as chemically defined and fully human platform for human epidermal keratinocyte culture. *Nat Commun,* 9**,** 4432.

TOUSSAINT, J. & SINGER, A. J. 2014. The evaluation and management of thermal injuries: 2014 update. *Clinical and experimental emergency medicine,* 1**,** 8-18.

TREDGET, E. E., LEVI, B. & DONELAN, M. B. 2014. Biology and principles of scar management and burn reconstruction. *Surg Clin North Am,* 94**,** 793-815.

TSIRIGOS, A. & RIGOUTSOS, I. 2009. Alu and b1 repeats have been selectively retained in the upstream and intronic regions of genes of specific functional classes. *PLoS computational biology,* 5**,** e1000610-e1000610.

TSOU, R., COLE, J. K., NATHENS, A. B., ISIK, F. F., HEIMBACH, D. M., ENGRAV, L. H. & GIBRAN, N. S. 2000. Analysis of hypertrophic and normal scar gene expression with cDNA microarrays. *J Burn Care Rehabil,* 21**,** 541-50.

TSURUTA, D., HASHIMOTO, T., HAMILL, K. J. & JONES, J. C. R. 2011. Hemidesmosomes and focal contact proteins: functions and cross-talk in keratinocytes, bullous diseases and wound healing. *Journal of dermatological science,* 62**,** 1-7.

TUBBS, A. & NUSSENZWEIG, A. 2017. Endogenous DNA Damage as a Source of Genomic Instability in Cancer. *Cell,* 168**,** 644-656.

UGRINOVA, I. & PASHEVA, E. 2017. HMGB1 Protein: A Therapeutic Target Inside and Outside the Cell. *Adv Protein Chem Struct Biol,* 107**,** 37-76.

UNTERGASSER, A., CUTCUTACHE, I., KORESSAAR, T., YE, J., FAIRCLOTH, B. C., REMM, M. & ROZEN, S. G. 2012. Primer3--new capabilities and interfaces. *Nucleic acids research,* 40**,** e115-e115.

VALDIGLESIAS, V., GIUNTA, S., FENECH, M., NERI, M. & BONASSI, S. 2013. γH2AX as a marker of DNA double strand breaks and genomic instability in human population studies. *Mutat Res,* 753**,** 24-40.

VAN DER VEER, W. M., BLOEMEN, M. C., ULRICH, M. M., MOLEMA, G., VAN ZUIJLEN, P. P., MIDDELKOOP, E. & NIESSEN, F. B. 2009. Potential cellular and molecular causes of hypertrophic scar formation. *Burns,* 35**,** 15-29.

VAN LIESHOUT, E. M., VAN YPEREN, D. T., VAN BAAR, M. E., POLINDER, S., BOERSMA, D., CARDON, A. Y., DE RIJCKE, P. A., GUIJT, M., KLEM, T. M., LANSINK, K. W., RINGBURG, A. N., STAARINK, M., VAN DE SCHOOT, L., VAN DER VEEN, A. H., VAN EIJCK, F. C., VAN EERTEN, P. V., VEGT, P. A., VOS, D. I., WALEBOER, M., VERHOFSTAD, M. H. & VAN DER VLIES, C. H. 2018. Epidemiology of injuries, treatment (costs) and outcome in burn patients admitted to a hospital with or without dedicated burn centre (Burn-Pro): protocol for a multicentre prospective observational study. *BMJ Open,* 8**,** e023709.

VARRIALE, A. & BERNARDI, G. 2006. DNA methylation and body temperature in fishes. *Gene,* 385**,** 111-21.

VELEZ-DELVALLE, C., MARSCH-MORENO, M., CASTRO-MUÑOZLEDO, F., GALVÁN-MENDOZA, I. J. & KURI-HARCUCH, W. 2016. Epithelial cell migration requires the interaction between the vimentin and keratin intermediate filaments. *Sci Rep,* 6**,** 24389.

VELICHKO, A. K., PETROVA, N. V., RAZIN, S. V. & KANTIDZE, O. L. 2015. Mechanism of heat stress-induced cellular senescence elucidates the exclusive vulnerability of early S-phase cells to mild genotoxic stress. *Nucleic Acids Res,* 43**,** 6309-20.

VELNAR, T., BAILEY, T. & SMRKOLJ, V. 2009. The wound healing process: an overview of the cellular and molecular mechanisms. *J Int Med Res,* 37**,** 1528-42.

VENIAMINOVA, N. A., VASSETZKY, N. S. & KRAMEROV, D. A. 2007a. B1 SINEs in different rodent families. *Genomics,* 89**,** 678-686.

VENIAMINOVA, N. A., VASSETZKY, N. S. & KRAMEROV, D. A. 2007b. B1 SINEs in different rodent families. *Genomics,* 89**,** 678-86.

VINOTH, A., THIRUNALASUNDARI, T., SHANMUGAM, M., UTHRAKUMAR, A., SUJI, S. & RAJKUMAR, U. 2018. Evaluation of DNA methylation and mRNA expression of heat shock proteins in thermal manipulated chicken. *Cell stress & chaperones,* 23**,** 235-252.

VITILLO, L., BAXTER, M., ISKENDER, B., WHITING, P. & KIMBER, SUSAN J. 2016. Integrin-Associated Focal Adhesion Kinase Protects Human Embryonic Stem Cells from Apoptosis, Detachment, and Differentiation. *Stem Cell Reports,* 7**,** 167-176.

VOJTA, A., DOBRINIĆ, P., TADIĆ, V., BOČKOR, L., KORAĆ, P., JULG, B., KLASIĆ, M. & ZOLDOŠ, V. 2016. Repurposing the CRISPR-Cas9 system for targeted DNA methylation. *Nucleic Acids Res,* 44**,** 5615-28.

WACHTEL, T. L., BERRY, C. C., WACHTEL, E. E. & FRANK, H. A. 2000. The inter-rater reliability of estimating the size of burns from various burn area chart drawings. *Burns,* 26**,** 156-70.

WANG, F., ZIEMAN, A. & COULOMBE, P. A. 2016. Skin Keratins. *Methods Enzymol,* 568**,** 303-50.

WANG, Y., BEEKMAN, J., HEW, J., JACKSON, S., ISSLER-FISHER, A. C., PARUNGAO, R., LAJEVARDI, S. S., LI, Z. & MAITZ, P. K. M. 2018. Burn injury: Challenges and advances in burn wound healing, infection, pain and scarring. *Adv Drug Deliv Rev,* 123**,** 3-17.

WATCHARANURAK, P. & MUTIRANGURA, A. 2022. Human RNA-directed DNA methylation methylates high-mobility group box 1 protein-produced DNA gaps. *Epigenomics,* 14**,** 741-756.

WATT, F. M. 2002. Role of integrins in regulating epidermal adhesion, growth and differentiation. *The EMBO Journal,* 21**,** 3919-3926.

WU, X., YAMAMOTO, H., NAKANISHI, H., YAMAMOTO, Y., INOUE, A., TEI, M., HIROSE, H., UEMURA, M., NISHIMURA, J., HATA, T., TAKEMASA, I., MIZUSHIMA, T., HOSSAIN, S., AKAIKE, T., MATSUURA, N., DOKI, Y. & MORI, M. 2015. Innovative Delivery of siRNA to Solid Tumors by Super Carbonate Apatite. *PLOS ONE,* 10**,** e0116022.

XIAO, Y., SUN, Y., ZHU, B., WANG, K., LIANG, P., LIU, W., FU, J., ZHENG, S., XIAO, S. & XIA, Z. 2018. Risk factors for hypertrophic burn scar pain, pruritus, and paresthesia development. *Wound Repair Regen,* 26**,** 172-181.

XIE, Y., CHEN, Y., SUN, M. & PING, Q. 2013. A mini review of biodegradable calcium phosphate nanoparticles for gene delivery. *Curr Pharm Biotechnol,* 14**,** 918-25.

XU, P., WU, Y., ZHOU, L., YANG, Z., ZHANG, X., HU, X., YANG, J., WANG, M., WANG, B., LUO, G., HE, W. & CHENG, B. 2020a. Platelet-rich plasma accelerates skin wound healing by promoting re-epithelialization. *Burns Trauma,* 8**,** tkaa028.

XU, R., LI, S., GUO, S., ZHAO, Q., ABRAMSON, M. J., LI, S. & GUO, Y. 2020b. Environmental temperature and human epigenetic modifications: A systematic review. *Environmental Pollution,* 259**,** 113840.

XU, X., LI, Z., ZHAO, X., KEEN, L. & KONG, X. 2016. Calcium phosphate nanoparticles-based systems for siRNA delivery. *Regen Biomater,* 3**,** 187-95.

XU, Y., XU, C. & PRICE, B. D. 2012. Mechanistic links between ATM and histone methylation codes during DNA repair. *Prog Mol Biol Transl Sci,* 110**,** 263-88.

YANG, A. S., ESTÉCIO, M. R. H., DOSHI, K., KONDO, Y., TAJARA, E. H. & ISSA, J.-P. J. 2004a. A simple method for estimating global DNA methylation using bisulfite PCR of repetitive DNA elements. *Nucleic acids research,* 32**,** e38-e38.

YANG, H., OCHANI, M., LI, J., QIANG, X., TANOVIC, M., HARRIS, H. E., SUSARLA, S. M., ULLOA, L., WANG, H., DIRAIMO, R., CZURA, C. J., WANG, H., ROTH, J., WARREN, H. S., FINK, M. P., FENTON, M. J., ANDERSSON, U. & TRACEY, K. J. 2004b. Reversing established sepsis with antagonists of endogenous high-mobility group box 1. *Proc Natl Acad Sci U S A,* 101**,** 296-301.

YANG, H., WANG, H., CHAVAN, S. S. & ANDERSSON, U. 2015. High Mobility Group Box Protein 1 (HMGB1): The Prototypical Endogenous Danger Molecule. *Mol Med,* 21 Suppl 1**,** S6-s12.

YAP, L., TAY, H. G., NGUYEN, M. T. X., TJIN, M. S. & TRYGGVASON, K. 2019. Laminins in Cellular Differentiation. *Trends in Cell Biology,* 29**,** 987-1000.

YASOM, S., WATCHARANURAK, P., BHUMMAPHAN, N., THONGSROY, J., PUTTIPANYALEARS, C., SETTAYANON, S., CHALERTPET, K., KHUMSRI, W., KONGKAEW, A., PATCHSUNG, M., SIRIWATTANAKANKUL, C., PONGPANICH, M., PIN-ON, P., JINDATIP, D., WANOTAYAN, R., ODTON, M., SUPASAI, S., OO, T. T., ARUNSAK, B., PRATCHAYASAKUL, W., CHATTIPAKORN, N., CHATTIPAKORN, S.

& MUTIRANGURA, A. 2022a. The roles of HMGB1-produced DNA gaps in DNA protection and aging biomarker reversal. *FASEB BioAdvances,* 4**,** 408-434.

YASOM, S., WATCHARANURAK, P., BHUMMAPHAN, N., THONGSROY, J., PUTTIPANYALEARS, C., SETTAYANON, S., CHALERTPET, K., KHUMSRI, W., KONGKAEW, A., PATCHSUNG, M., SIRIWATTANAKANKUL, C., PONGPANICH, M., PIN-ON, P., JINDATIP, D., WANOTAYAN, R., ODTON, M., SUPASAI, S., OO, T. T., ARUNSAK, B., PRATCHAYASAKUL, W., CHATTIPAKORN, N., CHATTIPAKORN, S. & MUTIRANGURA, A. 2022b. The roles of HMGB1-produced DNA gaps in DNA protection and aging biomarker reversal. *FASEB BioAdvances,* n/a.

YAZLOVITSKAYA, E. M., VIQUEZ, O. M., TU, T., DE ARCANGELIS, A., GEORGES-LABOUESSE, E., SONNENBERG, A., POZZI, A. & ZENT, R. 2019. The laminin binding α3 and α6 integrins cooperate to promote epithelial cell adhesion and growth. *Matrix Biol,* 77**,** 101-116.

YOON, S. & LEUBE, RUDOLF E. 2019. Keratin intermediate filaments: intermediaries of epithelial cell migration. *Essays in Biochemistry,* 63**,** 521-533.

YOOYONGSATIT, S., RUCHUSATSAWAT, K., SUPIYAPHUN, P., NOPPAKUN, N., MUTIRANGURA, A. & WONGPIYABOVORN, J. 2013. Alterations in the LINE-1 methylation pattern in patients with lichen simplex chronicus. *Asian Pac J Allergy Immunol,* 31**,** 51-7.

YÜKSEL, Ş., KUCUKAZMAN, S. O., KARATAŞ, G. S., OZTURK, M. A., PROMBHUL, S. & HIRANKARN, N. 2016. Methylation Status of Alu and LINE-1 Interspersed Repetitive Sequences in Behcet's Disease Patients. *Biomed Res Int,* 2016**,** 1393089.

ZHANG, H., ZHANG, S. B., SUN, W., YANG, S., ZHANG, M., WANG, W., LIU, C., ZHANG, K., SWARTS, S., FENTON, B. M., KENG, P., MAGUIRE, D., OKUNIEFF, P. & ZHANG, L. 2009. B1 sequence-based real-time quantitative PCR: a sensitive method for direct measurement of mouse plasma DNA levels after gamma irradiation. *Int J Radiat Oncol Biol Phys,* 74**,** 1592-9.

ZHAO, D., WANG, C. Q., ZHUO, R. X. & CHENG, S. X. 2014. Modification of nanostructured calcium carbonate for efficient gene delivery. *Colloids Surf B Biointerfaces,* 118**,** 111-6.

ZHAO, X. & GUAN, J.-L. 2011. Focal adhesion kinase and its signaling pathways in cell migration and angiogenesis. *Advanced Drug Delivery Reviews,* 63**,** 610-615.

ZHU, Z., DING, J. & TREDGET, E. E. 2016. The molecular basis of hypertrophic scars. *Burns Trauma,* 4**,** 2.

ZUO, K. J. & TREDGET, E. E. 2014. Multiple Marjolin's ulcers arising from irradiated post-burn hypertrophic scars: a case report. *Burns,* 40**,** e21-5.

Appendix A: Published Papers

Alu repetitive sequence CpG methylation changes in burn scars

Jiraroch Meevassana [a,b,c,*], Siwat Serirodom [b], Piyawan Prabsattru [c], Papatson Boonsongserm [c], Supitcha Kamolratanakul [d], Tippawan Siritientong [c,e], Apiwat Mutirangura [a], Apichai Angspatt [b,c]

[a] Department of Anatomy, Faculty of Medicine, Chulalongkorn University, Bangkok, Thailand
[b] Division of Plastic and Reconstructive Surgery, Department of Surgery, Faculty of Medicine, Chulalongkorn University, Bangkok, Thailand
[c] Center of Excellence in Burn and Wound Care, Chulalongkorn University, Bangkok, Thailand
[d] Department of Clinical Tropical Medicine, Faculty of Tropical Medicine, Mahidol University, Bangkok, Thailand
[e] Department of Food and Pharmaceutical Chemistry, Faculty of Pharmaceutical Sciences, Chulalongkorn University, Bangkok, Thailand

ARTICLE INFO

ABSTRACT

Alu elements are retrotransposons related to epigenetic modifications. To date, the role of epigenetics in hypertrophic scars from burn remains unknown. Here, our aim was to examine the pathophysiology of hypertrophic scars from an epigenetic perspective. For that, we performed a cross-sectional analytical study using tissue and blood samples from burned and healthy patients (n = 23 each) to detect Alu methylation levels and patterns. The results of the combined bisulfite restriction analysis technique were categorized into four groups based on the methylation status at the CpG dinucleotides from the 5′ to the 3′ ends of the Alu sequence: hypermethylated ($^mC^mC$), hypomethylated ($^uC^uC$), and partially methylated ($^uC^mC$ and $^mC^uC$). Alu methylation levels were significantly lower in hypertrophic scar tissues than in normal skin (29.37 ± 2.49% vs. 35.56 ± 3.18%, p = 0.0002). In contrast, the levels were significantly higher in white blood cells from blood samples of burned patients than in those of control blood samples (26.92 ± 4.04% vs. 24.58 ± 3.34%, p = 0.0278). Alu total methylation (^mC) and the $^uC^mC$ pattern were significantly lower, whereas $^uC^uC$ was significantly higher, in hypertrophic scar tissues than in normal skin (p < 0.0001). Receiver operating characteristic analysis indicated that the $^uC^mC$ and $^uC^uC$ patterns are useful as hypertrophic scar DNA methylation markers after burn, with 91.30% sensitivity and 96.23% specificity and 100% sensitivity and 94.23% specificity, respectively. Our findings suggest that epigenetic modifications play a major role in hypertrophic scar pathogenesis, and may be the starting point for developing a novel technique for burn scar treatment.

© 2021 Elsevier Ltd and ISBI. All rights reserved.

B1 repetitive sequence methylation enhances wound healing of second-degree burns in rats

JIRAROCH MEEVASSANA[1-3], PANUPONG NACHAROENKUL[2], JADE WITITSUWANNAKUL[4],
NAKARIN KITKUMTHORN[5], KEVIN J. HAMILL[6], APICHAI ANGSPATT[2,3] and APIWAT MUTIRANGURA[1]

[1]Department of Anatomy, Center of Excellence in Molecular Genetics of Cancer and Human Disease, Faculty of Medicine;
[2]Department of Surgery, Division of Plastic and Reconstructive Surgery, Faculty of Medicine;
[3]Center of Excellence in Burn and Wound Care, Faculty of Medicine; [4]Department of Medicine, Division of Dermatology,
Faculty of Medicine, Chulalongkorn University, Bangkok 10330;
[5]Department of Oral Biology, Faculty of Dentistry, Mahidol University, Bangkok 10400, Thailand;
[6]Institute of Life Course and Medical Sciences, Faculty of Health and Life Sciences,
University of Liverpool, Liverpool L69 7ZX, United Kingdom

Abstract. The accumulation of DNA damage in burn wounds delays wound healing. DNA methylation by short interspersed nuclear element (SINE) small interfering (si) RNA prevents DNA damage and promotes cell proliferation. Therefore, SINE siRNA may be able to promote burn wound healing. Here, a SINE B1 siRNA was used to treat burn wounds in rats. Second-degree burn wounds were introduced on the backs of rats. The rats were then divided into three groups: a B1 siRNA-treated, saline-treated control, and saline + calcium phosphate-nanoparticle-treated control group (n=15/group). The wounds were imaged on days 0, 7, 14, 21 and 28 post-injury. The tissue sections were processed for methylation, histological and immunohistochemical examination, and scored based on the overall expression of histone H2AX phosphorylated on serine 139 (γH2AX) and 8-hydroxy-2'-deoxyguanosine (8-OHdG). Burn wound closure improved in the B1 siRNA-treated group compared with that in the control group, especially from days 14-28 post-injury (P<0.001). The overall pathological score and degree of B1 methylation in the B1 siRNA-treated group improved significantly at days 14-28 post-injury, with the maximum improvement observed on day 14 (P<0.01) compared with the NSS and Ca-P nanoparticle groups. Immunohistochemical staining revealed lower expression of γH2AX and 8-OHdG in the B1 siRNA-treated group than in the control groups at days 14-28 post-injury; the maximum improvement was observed on days 14 and 21. These data imply that administering SINE siRNA is a promising therapeutic option for managing second-degree burns.

Introduction

Burn wounds can cause severe clinical injuries, and delayed wound healing leads to infection, prolonged hospital stays, increased morbidity and >250,000 deaths annually in the United States of America alone (1). Researchers and clinicians are actively studying the application of new substances to improve burn-treatment outcomes.

Interspersed repetitive sequences (IRSs) are the primary contributor to the genome (~45%), and their methylation levels are crucial for preserving the stability of the genome (2). Mutation rates are increased in cells with IRS hypomethylation (3,4). A short interspersed nuclear element (SINE) retrotransposon is a repetitive element of 85-500 bp in length. Two SINE families exist, namely the B1 (in mice, rats and hamsters) and Alu (in humans) families (5,6). Similar to the Alu element, the B1 element in rodents stems from 7SL RNA, which is cytoplasmic RNA; it facilitates protein excretion as a part of the signal recognition particle (7). The B1 element assists in transcriptional regulation and DNA stability by binding to the Aryl hydrocarbon (dioxin) receptor, which is a ligand-activated transcription factor (8,9); however, to the

Correspondence to: Dr Jiraroch Meevassana, Center of Excellence in Burn and Wound Care, Faculty of Medicine, Chulalongkorn University, 254 Phayathai Road, Pathum Wan, Bangkok 10330, Thailand
E-mail: jiraroch.m@chula.ac.th

Laminin 511-E8 Fragment Improves Second-Degree Burn Wound Healing in a Rat Model

Jiraroch Meevassana[1,2,3*], Manita Attasuriyanan[4], Apasee Sooksamran[4], Jade Wititsuwannakul[4], Papatson Boonsongserm[3], Supitcha Kamolratanakul[5], Nichakarn Ekprachayakoon[2], Kevin J Hamill[6], Apiwat Mutirangura[1], Apichai Angspatt[2,3]

[1]Department of Anatomy, Faculty of Medicine, Chulalongkorn University, Bangkok 10330, Thailand

[2]Division of Plastic and Reconstructive Surgery, Department of Surgery, Faculty of Medicine, Chulalongkorn University, Bangkok 10330, Thailand

[3]Center for Excellence in Burn and Wound Care, Chulalongkorn University, Bangkok 10330, Thailand

[4]Division of Dermatology, Department of Medicine, Faculty of Medicine, Chulalongkorn University, Bangkok 10330, Thailand

[5]Department of Clinical Tropical Medicine, Faculty of Tropical Medicine, Mahidol University, Bangkok 10400, Thailand

[6]Institute of Life Course and Medical Sciences, Faculty of Health and Life Sciences, University of Liverpool, Liverpool L69 7ZX, United Kingdom

*__Corresponding Author:__ Jiraroch Meevassana, Center for Excellence in Burn and Wound Care, Faculty of Medicine, Chulalongkorn University, Bangkok, Thailand; Email: jiraroch.m@chula.ac.th

Abstract

Background: The rate of re-epithelialization is the primary determinant of the morbidity and mortality in patients with severe burn injuries. Laminin $\alpha5\beta1\gamma1$ (LM511) is an extracellular structural protein that can support epithelial cell adhesion and migration. LM511-E8 is a functionally minimal form of LM511 with an efficacy similar to that of the full-length protein. To investigate whether treatment of burn wounds with the LM511-E8 fragment improves wound closure in a rat second-degree burn wound model.

Methods: Second-degree burn wounds were produced in vivo on the backs of rats. The rats were separated into saline-treated control and LM511-E8-treated groups (n=9 per group),

SUPPLEMENTARY

Primer table (human)

Gene symbol	Accession Number	Sequence 5′-3′
GAPDH	NM_001256799	GAAGGTGAAGGTCGGAGTC GAAGATGGTGATGGGATTTC
FAK	L13616.1	CCTTCAGCAGGAGTACAAGAAG GGAATTCTGGCAGGAAGGATAG
Itga3	NM_002204	AAGGGACCTTCAGGTGCA TGTAGCCGGTGATTTACCAT
Itga6	NM_001394928	TTGAATATACTGCTAACCCCG TCGAAACTGAACTCTTGAGGATAG
Itga7	AY358882	CTGTTTCAGCTACATTGCAGTC GCCTGGTGCTTGGGTTCT
Itgb1	NM_133376	GAAGGGTTGCCCTCCAGA GCTTGAGCTTCTCTGCTGTT
Itgb4	NM_001321123	AGACGAGATGTTCAGGGACC GGTCTCCTCTGTGATTTGGAA

Table 7. PCR primer (human)

Primer table (rat)

Gene symbol	Accession Number	Sequence 5′-3′
GAPDH	NM_017008.4	GAAGGTGAAGGTCGGAGTC GAAGATGGTGATGGGATTTC
FAK	AF020777.1	CCTTCAGCAGGAGTACAAGAAG GGAATTCTGGCAGGAAGGATAG
Itga3	NM_001108292.2	CCTCGCTTTGTACGGTTACTT GTGATGTTCCGCCTGTAGTT
Itga6	NM_053725.2	AGAGGAGGGTGTAGGAAAGAA CCTGGGTGTAGTCAGTCTCATA
Itga7	NM_030842.1	GTCAGTCACTGCCTAACTTCTC ATGAAGCCAGCAACCTACTC
Itgb1	NM_017022.2	TGACACTGCTGGTGCTAATG TAGTCCTGGCCACTCTGTAA
Itgb4	NM_013180.2	CTGCTTGCCAAACACAACATTA CCAGAGAGGAGACAGGGAAATA

Table 8. PCR primer (rat)

Antibodies table

Category	Antibody	Isotype	Manufacturer	Category Number
Polyclonal	Itga3	Rabbit	Thermo-Fisher	BS-2093R
Monoclonal	Itga6	Rabbit	Thermo-Fisher	MA5-41025
Polyclonal	Itga7	Rabbit	Thermo-Fisher	**BS-1816R**
Monoclonal	Itgb1	Rabbit	Thermo-Fisher	**MA5-31981**
Polyclonal	Itgb4	Rabbit	Thermo-Fisher	**PA5-79540**
Polyclonal	FAK	Rabbit	Thermo-Fisher	**AHO0502**
Monoclonal	Phospho-FAK	Rabbit	Thermo-Fisher	**44-625G**
Polyclonal	Talin	Rabbit	Thermo-Fisher	**PA5-82162**
Monoclonal	Vinculin	Mouse	Thermo-Fisher	**14-9777-82**
Monoclonal	Phalloidin	Rabbit	Thermo-Fisher	**A12379**

Table 9. List of antibodies

Primer efficiency (human)

Integrin alpha 3

Ct value	cDNA quantity	Log (cDNA)
21.76	1.0000	0.00
24.34	0.1000	-1.00
27.90	0.0100	-2.00
30.66	0.0010	-3.00
33.61	0.0001	-4.00

Dilution Factor	10

Results	
Slope	-3.002
R Squared	0.9981
Amplification factor (E]	2.15
Efficiency (%)	115.33
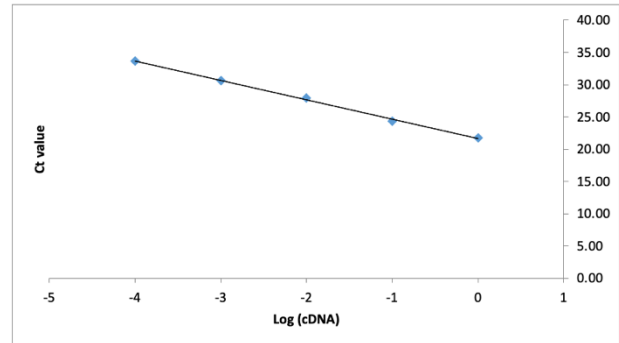
Integrin alpha 6

Ct value	cDNA quantity	Log (cDNA)
15.20	1.0000	0.00
18.19	0.1000	-1.00
21.09	0.0100	-2.00
24.38	0.0010	-3.00
27.47	0.0001	-4.00

Dilution Factor	10

Results	
Slope	-3.073
R Squared	0.9996
Amplification factor (E]	2.12
Efficiency (%)	111.55
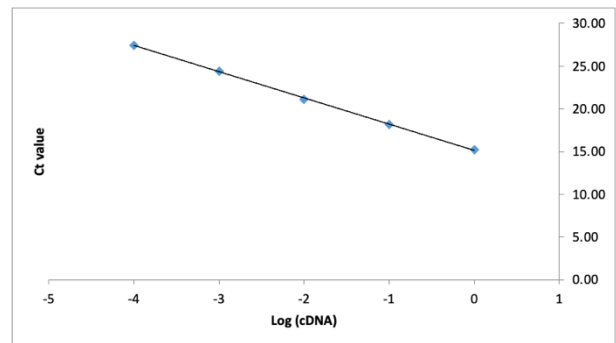
Integrin alpha 7

Ct value	cDNA quantity	Log (cDNA)
24.48	1.0000	0.00
27.34	0.1000	-1.00
30.66	0.0100	-2.00
33.78	0.0010	-3.00
36.77	0.0001	-4.00

Dilution Factor	10

Results	
Slope	-3.102
R Squared	0.9996
Amplification factor (E]	2.10
Efficiency (%)	110.07
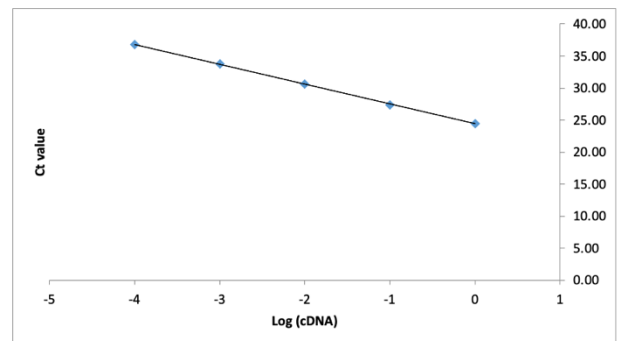
Integrin beta 1

Ct value	cDNA quantity	Log (cDNA)
17.99	1.0000	0.00
21.85	0.1000	-1.00
24.78	0.0100	-2.00
27.56	0.0010	-3.00
31.44	0.0001	-4.00

Dilution Factor	10

Results	
Slope	-3.261
R Squared	0.9961
Amplification factor (E]	2.03
Efficiency (%)	102.61
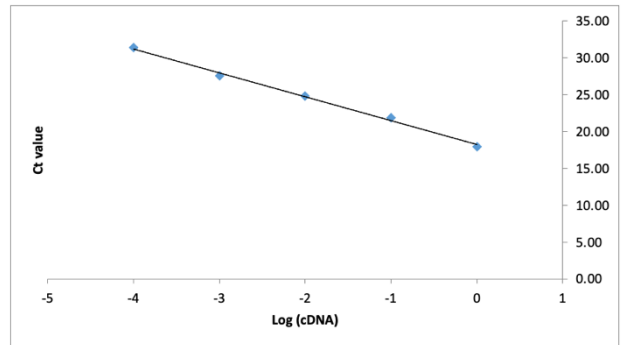
Integrin beta 4

Ct value	cDNA quantity	Log (cDNA)
19.57	1.0000	0.00
22.71	0.1000	-1.00
26.29	0.0100	-2.00
29.40	0.0010	-3.00
32.55	0.0001	-4.00

Dilution Factor	10

Results	
Slope	-3.265
R Squared	0.9994
Amplification factor (E]	2.02
Efficiency (%)	102.43
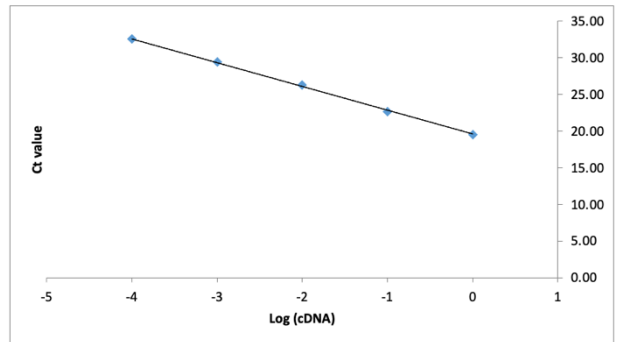
GAPDH

Ct value	cDNA quantity	Log (cDNA)
11.33	1.0000	0.00
14.15	0.1000	-1.00
17.13	0.0100	-2.00
20.57	0.0010	-3.00
23.94	0.0001	-4.00

Dilution Factor	10

Results	
Slope	-3.164
R Squared	0.9981
Amplification factor (E]	2.07
Efficiency (%)	107.04
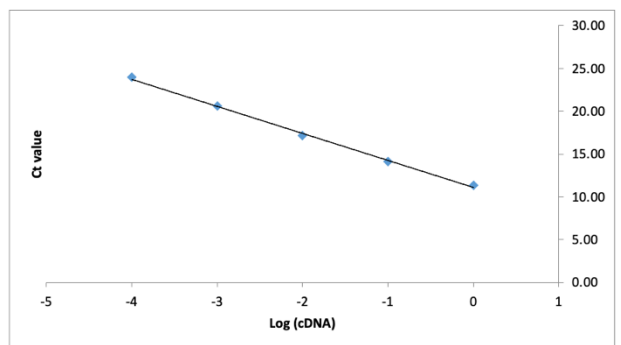
Figure 68. Primer efficiency

152

Primer efficiency (rat)

Integrin alpha 3

Ct value	cDNA quantity	Log (cDNA)
31.95	1.0000	0.00
35.26	0.1000	-1.00
38.87	0.0100	-2.00
41.59	0.0010	-3.00
44.45	0.0001	-4.00

Dilution Factor	10

Results	
Slope	-3.133
R Squared	0.9969
Amplification factor (E]	2.09
Efficiency (%)	108.54
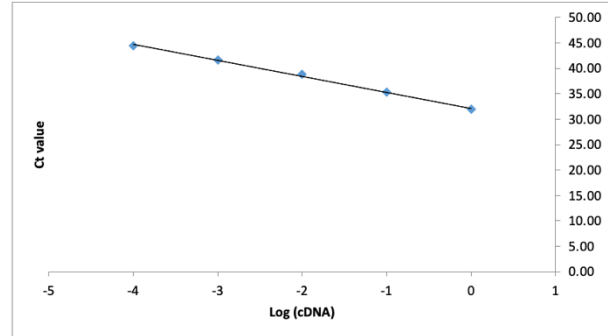
Integrin alpha 6

Ct value	cDNA quantity	Log (cDNA)
18.50	1.0000	0.00
21.43	0.1000	-1.00
24.83	0.0100	-2.00
28.94	0.0010	-3.00
31.31	0.0001	-4.00

Dilution Factor	10

Results	
Slope	-3.313
R Squared	0.9945
Amplification factor (E]	2.00
Efficiency (%)	100.37
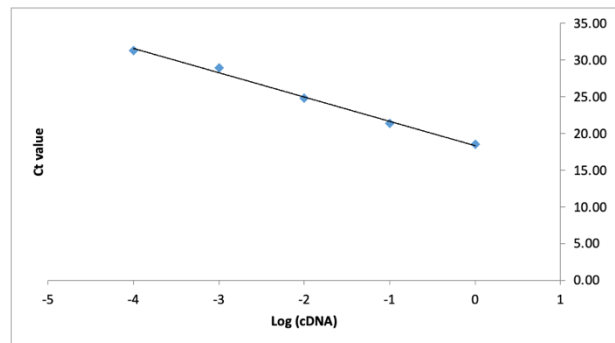
Integrin alpha 7

Ct value	cDNA quantity	Log (cDNA)
28.58	1.0000	0.00
31.27	0.1000	-1.00
34.48	0.0100	-2.00
37.99	0.0010	-3.00
40.32	0.0001	-4.00

Dilution Factor	10

Results	
Slope	-3.02
R Squared	0.9965
Amplification factor (E]	2.14
Efficiency (%)	114.35
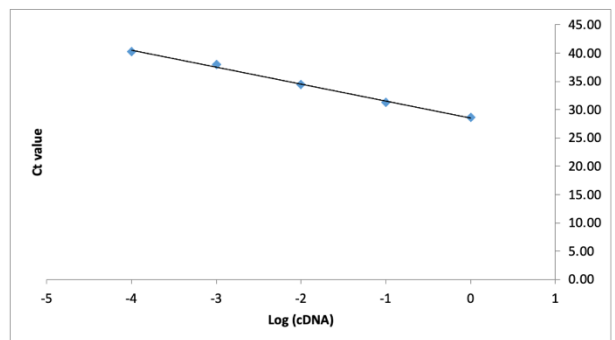
Integrin beta 1

Ct value	cDNA quantity	Log (cDNA)
17.45	1.0000	0.00
20.31	0.1000	-1.00
23.46	0.0100	-2.00
27.40	0.0010	-3.00
30.20	0.0001	-4.00

Dilution Factor	10

Results

Slope	-3.259
R Squared	0.9970
Amplification factor (E]	2.03
Efficiency (%)	102.69
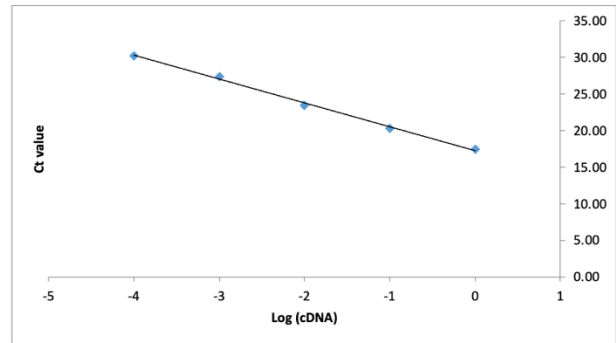
Integrin beta 4

Ct value	cDNA quantity	Log (cDNA)
25.89	1.0000	0.00
28.65	0.1000	-1.00
31.85	0.0100	-2.00
34.67	0.0010	-3.00
37.91	0.0001	-4.00

Dilution Factor	10

Results

Slope	-3.006
R Squared	0.9993
Amplification factor (E]	2.15
Efficiency (%)	115.11
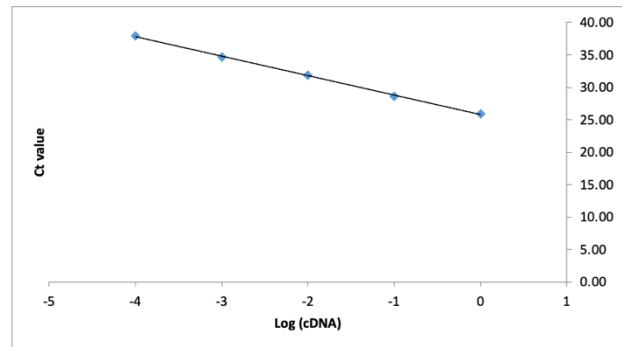
GAPDH

Ct value	cDNA quantity	Log (cDNA)
13.10	1.0000	0.00
15.98	0.1000	-1.00
18.90	0.0100	-2.00
22.49	0.0010	-3.00
25.76	0.0001	-4.00

Dilution Factor	10

Results

Slope	-3.183
R Squared	0.9980
Amplification factor (E]	2.06
Efficiency (%)	106.14
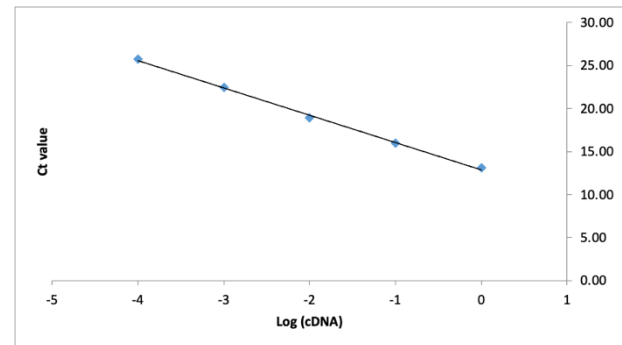
Primer efficiency PHY-RIND-EDSB

RIND EDSB

Ct value	cDNA quantity	Log (cDNA)
22.36	1.0000	0.00
25.44	0.1000	-1.00
28.61	0.0100	-2.00
31.64	0.0010	-3.00
34.55	0.0001	-4.00

Dilution Factor	10

Results

Slope	-3.058
R Squared	0.9998
Amplification factor (E)	2.12
Efficiency (%)	112.33
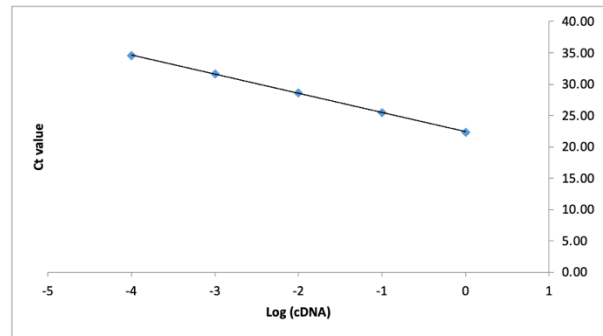
VITA

NAME	Jiraroch Meevassana
DATE OF BIRTH	11 Aug 1980
PLACE OF BIRTH	Thailand
INSTITUTIONS ATTENDED	Chulalongkorn University
HOME ADDRESS	111/276 Room 276 The Bangkok Condominium Core D2 Sathon Road Yannawa, Sathon 10120
PUBLICATION	1. MEEVASSANA, J., SERIRODOM, S., PRABSATTRU, P., BOONSONGSERM, P., KAMOLRATANAKUL, S., SIRITIENTONG, T., MUTIRANGURA, A. & ANGSPATT, A. 2021. Alu repetitive sequence CpG methylation changes in burn scars. Burns.

จุฬาลงกรณ์มหาวิทยาลัย
CHULALONGKORN UNIVERSITY